Laser-Assisted Fast Prototyping of Microdevices for the Microfluidic Manipulation of Liquid and Cells

Kerui Xu
Beijing, China

M.S., University of Virginia, 2015
B.S., Peking University, 2009

A Dissertation presented to the Graduate Faculty
of the University of Virginia in Candidacy for the Degree of
Doctor of Philosophy

Department of Chemistry

University of Virginia
August, 2015

_____

_____

_____

_____

_____

This late dissertation is dedicated to the memory of my beloved mother, Ren, Zhaohong, who passed away during the writing of this work, on March 17th, 2015, exactly two months before my planned graduation with the degree of Doctor of Philosophy, the moment that she has eagerly expected to see for the entire last six years of her life but unfortunately will never make it. I wish that she could still be alive today to witness my graduation.

I have promised to make my mother proud by the achievement of this monumental academic goal and I hope I have fulfilled the promise. However I can't find any way to let my mother know nor express my gratitude to her any more, for her consistent support, sacrifice and love in the past 28 years of my life. Completion of the dissertation and the degree of Ph.D., although still incompetent to what she had done for me, is currently the best way I can find to honor her and her unconditional love.

Abstract

Microfabrication is an everlasting topic in the evolution of the microfluidic communities. Being fast, automated, material-versatile, and clean-room-free, laser-assisted fabrication and prototyping has drawn increasing attention in the manufacturing of microdevices and become more and more appealing to innovators interested in the commercialization of lab-on-a-chip products. In this dissertation, the power of laser assisted fabrication is exploited in the fast prototyping of various types of microdevices that enables sophisticated manipulation of liquid or cells.

An introduction of the principles, procedures and recent applications of laser assisted fabrication is presented in Chapter 1. In Chapter 2 a novel, scanner-based profiling method is described for the examination of laser ablated microstructures in PDMS and polymers. In Chapter 3, a one-way check valve is created through laser-assisted fabrication and serves as the key component of passive flow control in a finger-driven microdevice that enables precise metering and delivery of multiple reagents. In Chapter 4 the acoustic differential extraction (ADE) is reported, in which sperm cells are separated from mock sexual assault samples by ultrasonic standing waves generated in a laser-ablated glass-PDMS-glass microdevice. Laser-ablated check valves are integrated onto the microdevice to control the on-chip flow switching in the multiple steps of sperm extraction including sample infusion, washing and elution. The power of laser is further extended to glass in Chapter 5, in which the surface of glass, after being cleaned by laser beams, shows remarkable hydrophilicity that enables the direct retaining and partitioning of aqueous liquid into droplet arrays by simple action of dipping-and-pulling. Suspension of cells can

be easily arrayed by this process for high-throughput bioassays. Finally, concluding remarks and future directions are outlined in Chapter 6.

Table of Contents

List of Figures

PAPERS RESULTING FROM THIS THESIS

Kerui Xu, Matthew R. Begley and James P. Landers, Simultaneous Metering and Dispensing of Multiple Reagents on Passively Controlled Microdevice Solely by Finger Pressing, *Lab on a chip*, 2015,**15**, 867-876

Kerui Xu, Xiaopu Wang, Roseanne M. Ford and James P. Landers, Self-partitioned Droplet Array on Laser-patterned Superhydrophilic Glass Surface for Wall-less, Cell-array-based Bioassay Development, for submission to *Analytical Chemistry*

Kerui Xu, Qian Liu, James P. Landers, The μSCAPE System: 3-Dimensional Profiling of Microfluidic Architectural Features Using a Flatbed Scanner, for submission to *Nature Scientific Reports*

Kerui Xu, Brian L. Poe, Jenny A. Lounsbury, and James, P. Landers, Bead-assisted Acoustic Differential Extraction of Sperm Cells in Dilute Samples for Potential Forensic Analyses, for submission to *Analytical Chemistry*

Chapter 1.Introduction

1.1 Overview

As one of the most critical limiting factors in the commercialization of lab-on-chip devices[1], microfabrication technology is an ever-evolving topic in the field of microfluidics since the first report of the microchip-based chemical analysis system[2]. Starting from the photolithography-based wet etching in glass or silicon[3], microfabrication was initially confined in clean room environment and hands of skillful experts, who keeps extreme cautiousness on expensive photoresist-coated wafers as well as the highly corrosive and environmentally hazardous chemicals used in the microfabrication. Ever since then great efforts and progresses have been made to liberate microfabrication and make it better accepted for the production of microdevices that solve practical problems in a real world. Revolutions on microfabrication techniques have happened in almost every aspects that lead the microfabrication technology onto a less demanding and cost-effect path.

Milestones on this path include molding in poly-dimethylsiloxane (PDMS)[4], which makes the reproduction of the microdevices more convenient and opened the door of microfabrication to an elastic, multifunctional polymer which becomes a leading role in the subsequent development of microfluidics. Heat-embossing and injection molding[5], [6] which enables the low-cost, mass production of thermoplastic microdevices. Laser ablation[7] and direct printing [8][9], which provides convenient prototyping tools for the microfabrication in the initial developing phase of microfluidic devices. Each of these microfabrication techniques has its own specific advantages and disadvantages, however

the major trend of the development of microfabrication is from highly-cost substrates towards affordable and disposable substrates, from mask-required, multiple-step process towards direct, single-step process. As a representative of direct and mask-less fabrication techniques, CO_2 laser ablation has been widely used in the micromachining of a broad range of polymers[10], [11]. The work in this dissertation reports various types of CO_2 laser-fabricated PDMS or glass devices and their related applications in microfluidic flow control, cell separation and high through-put bioassay

1.2 Comparison of the commonly used fabrication methods

To better understand the pros and cons of laser micromachining, in this section in addition to the details of laser ablation process, three other commonly used fabrication techniques are compared with laser ablation: (1) wet etching in glass or silicon, (2) molding of polymeric materials and (3) direct printing by an inkjet printer or a 3D printer.

Table 1-1 shows the comparison among major fabrication techniques in terms of applicable material, time consumption, material cost, labor/skill required, automation level and quality/resolution. These features are selected because of their close relevance in the fast prototyping of microdevices. In general, laser ablation has obvious advantages in the fast prototyping of microdevices with average qualities. Direct printing is also suitable for prototyping but the quality of the generated microdevice is relatively low compared with other methods. Molding, especially the molding based fabrication of thermoplastics, is desired in the mass production stage when the design of the microdevices has been settled down, but not so desirable in prototyping stage because that in companion of every change of the design a new mold needs to be fabricated which is less desired in the prototyping

stage. Wet etching is the least desirable methods for prototyping phase mainly because of its relatively high consumption of time, requirement for labor/skill, material cost. While presenting the highest quality, it still has some market within laboratory when super-delicate microstructures are needed.

	Applicable materials	Time consumption (from new design to actual device)	Material /chemical cost	Labor/skill requirement (from new design to actual device)	Automation level	Quality/resolution
Wet etching	*Glass, silicon*	*Hours*	*High*	*High*	*Low*	*High*
Molding	*PDMS, hydrogel,*	*Hours*	*Low*	*High*	*Low*	*High*
	Thermoplastics	*Hours*	*Low*	*Medium*	*High*	*High*
Direct printing	*Resin, wax, adjusted liquid solution*	*Minutes*	*Medium*	*Low*	*High*	*Low*
CO_2 Laser ablation	*Glass. PDMS, thermoplastics*	*Minutes*	*Low*	*Low*	*High*	*Medium*

Table 1-1. The comparison between the four major fabrication methods in terms of their desirability in fast prototyping (red: undesired, yellow: average, green: desired)

1.2.1 Wet Etching

Wet etching in glass or silicon is the earliest fabrication techniques in the community of microfluidics[3]. For wet etching in glass and silicon, the typical procedures are shown in **Figure 1-1**A[12] and **Figure 1-1**B[3], respectively. The whole procedure of etching requires multiple steps including exposure, baking, developing, chrome etching, substrate etching and removal of unexposed photoresist, which usually takes about 1 to 2 hours for each wafer. In addition, the whole procedure has to be done in a cleanroom to avoid contamination and defects of the micro structures. The multi-step fabrication procedure makes the photolithography based wet etching rather tedious and the reproduction of each batch of new microdevices requires the repeating of the whole procedure.

In the early era of microfluidics, most of the microdevices were fabricated through wet etching. Two representative applications of the wet-etched microdevices are (1) microchip electrophoresis in HF-etched glass channels and (2) acoustophoresis in HF/KOH etched silicon channels

Due to its unique surface properties that enable the establishment of electroosmotic flow (EOF), it is quite natural that the earliest application of the glass microdevices is electrophoresis. The first glass microchip based electrophoresis was reported by Manz et al. in 1992 showing the successful separation of two fluorescent dyes[13], [14], and one year later, separation of three fluorescently labeled amino acids by microchip electrophoresis was reported by the same research group[15]. In 1994 Mathies group reported the separation and resolution of DNA fragments ranging between 70-1000 base

pairs[16] which opened the door of high-resolution and high-through put DNA sequencing in the following years[17]–[19]. The technology of micro-chip electrophoresis based DNA detection and sequencing were rapidly developed thereafter to address problems in various fields from clinical diagnosis[20], [21] to biodefense detection[22]. Other biomacromolecules such as peptides can also be separated by combined micellar electrokinetic chromatography (MEKC) and capillary electrophoresis (CE) using glass microdevices[23]–[25].

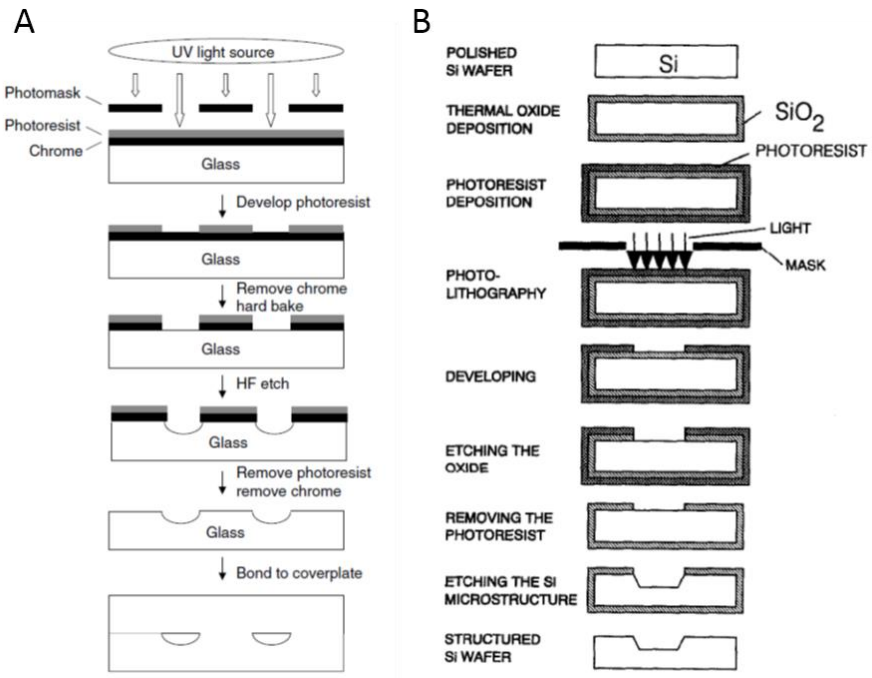

Figure 1-1 . Diagrams showing the photolithography and etching of glass(A) [12] *and silicon(B)* [14]*microdevice*

The common scale of the structures in glass usually ranges from tens of micro meters to hundreds of micrometers, and due to the isotropic etching process, the aspect ratio (depth : width) of etched structures is limited below 1, while in silicon because of the

anisotropic etching process microstructures with much higher aspect ratios (>1) can be fabricated, and the dimensions of the etched microstructures can be down to a few micrometers. One of the representative applications that relies on silicon microdevices is acoustophoresis, in which particles are focused by horizontal ultrasonic standing waves between the walls of the microfluidic channel (**Figure 1-2**). The perfectly vertical walls of the etched silicon channels ensures the establishment of the acoustic standing waves in horizontal directions and the particles be focused in the center stream.

The separation ability of acoustophoresis provides a powerful alternative to conventional methods such as centrifugation in clinical applications for the isolation of cells in whole blood, in that it doesn't impose strong shear force that may cause hemolysis[26], and its automated, on-chip work flow may seamlessly be integrated with other sequential treatments. A good example of the application of acoustophoresis in clinical diagnostics is the purification of the plasma from whole blood sample for the detection of the prostate specific antigen (PSA), an informative biomarker in the diagnosis of prostate cancer. Over 99% of the blood cells was removed by the acoustophoresis with a processing rate of 80 μL/min and the purified plasma could be directly used in the fluorescent detection of PSA. Other applications of acoustophoresis include the successful separation of lipid droplets [27], [28], platelet[29], prostate cancer cells[30] and leukocyte[31] from whole blood samples for clinical purposes.

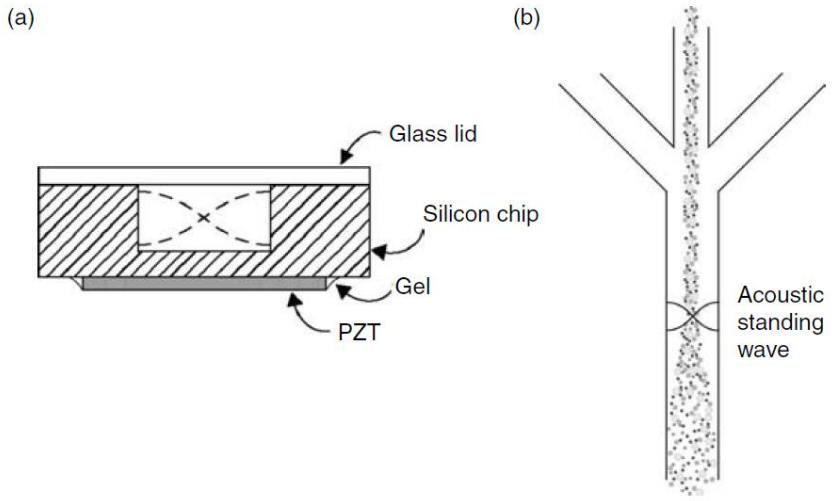

Figure 1-2. The principle of acoustophoresis in etched silicon channels[177] *(A) Cross-section of the acoustophoresis chip showing the ultrasonic standing waves with one resonance node established between two vertical walls. (b) Schematic top view of focusing of the particles by acoustophoresis.*

1.2.2 Molding

Two major types of the molding-based fabrication techniques are introduced in this section: (1) transfer of the feature of the mold by curing of the polymer such as PDMS or hydrogel, and (2) transfer of the feature of the mold by heat embossing or injection mold on thermoplastics.

1.2.2.1 Molding on PDMS and hydrogel

In the making of PDMS microstructures, the master mold is usually made in negative photoresist which cross-links and solidifies after exposed to UV light, such as SU-8 (**Figure 1-3**[32], left part). The features on the master mold are then transferred into PDMS by the curing of the PDMS's monomer (**Figure 1-3**[32], right part). The thickness

or depth of the microstructures are controlled by the thickness of the spin-coated photoresist and usually below tens of micrometers. Although in this procedure, new batch of microdevices can be conveniently reproduced by curing the polymer on the same re-usable master mold, the spin-coating, pre-baking and post-baking add up new burdens on the operation, especially when accurate feature depth is needed. The average time required for the making of master mold is roughly 1~2 hours and for each batch of PDMS curing ~1hour is needed.

The most representative molded PDMS microstructures are various types of check valves. The actively controlled check valves are the most widely used structures for the flow switching in various applications such as pumping and valving in micro total analysis system[31][32], frequency specific passive flow control[35][36], automated logic fluidic control[37]–[39], automated fluidic oscillator[38][39], finger driven microfluidic device[40][41], and integrated microfluidic device for high-throughput genotyping and bioassays[44]–[47]. The molded PDMS valve structures have been widely accepted by the community of microfluidics but the problem of tedious fabrication process and inconvenient change of design (new mask and molds required) still remain as challenges in the prototyping stage of the microfluidic devices. To the contrary, laser-assisted fabrication shows great advantages in the fast prototyping phase and the application of laser-assisted fabrication is demonstrated in the finger driven simultaneous metering and delivery of multiple reagents in Chapter 3 of this dissertation.

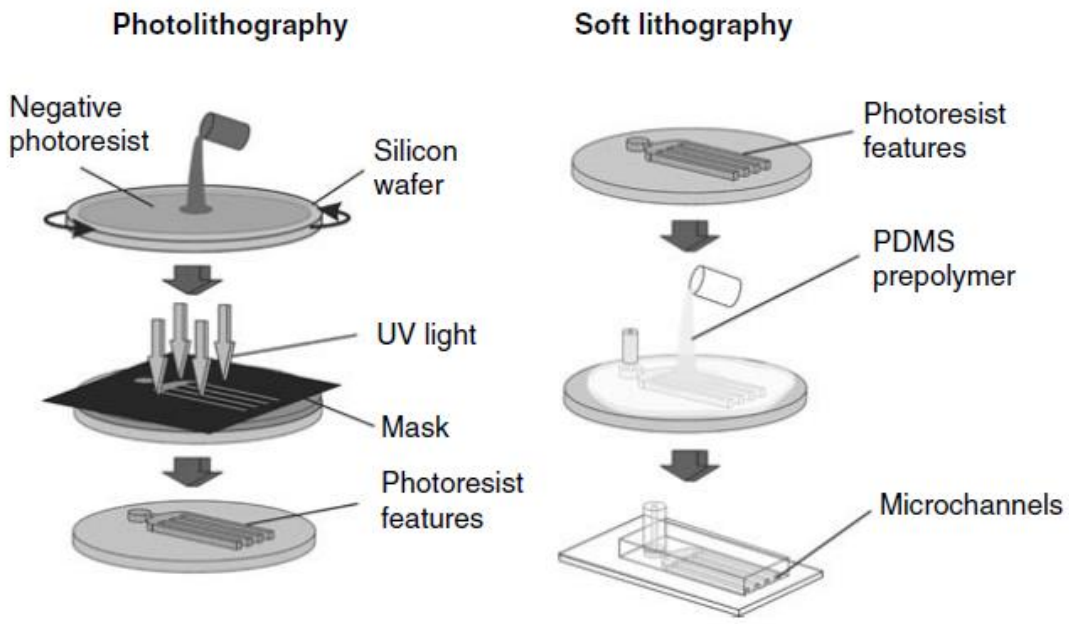

Figure 1-3. Diagram showing the procedures of PDMS molding[32]

Hydrogel is another major type of polymer that can be cured and shaped by molding procedure. The molding procedure is similar with the molding of PDMS except that UV light is used for the activation of the cross-linking of the monomers. So for simple hydrogel structures sometimes only photolithography is needed to directly cure the hydrogel, but for more complicated hydrogel structures, making of a master mold is still required[48]. The spatial resolution of the molding of hydrogel enables the fabrication of nanostructure[49] and multiple subtle variations of the molding strategy can provide a wide range of nanostructures such as nanohair[50], [51], hollow structures[52] and monolithic bridge[53]. Because of its unique biocompatibility, biodegradability, surface grafting ability and stimulus responsiveness, the major application of the hydrogel microstructures lies in the mimic of extracellular matrix (ECM) for biological studies such as cell-cell, cell-environment interactions[54][55], tissue engineering[55]–[58] and drug/cell delivery[59],

in which the hydrogel structures can be fabricated with encapsulated cells using the molding methods[60]–[62].

1.2.2.2 Molding on thermoplastics (hot embossing and injection molding)

In the molding-based fabrication of thermoplastics, there are two major methods: hot embossing[63][64] and injection molding[65]–[67]. The molding of thermoplastic is different from the molding of either PDMS or hydrogel, in that the molding process of the thermoplastic is based on the physical change of the polymer from either glass-transition state (in hot embossing) or semi-liquid state (in injection molding), to solid state through heating and cooling under pressure, while the molding processes of PDMS and hydrogel involve the polymerization of the monomers that is triggered by inducing factors (curing reagent for PDMS and UV radiation for hydrogel). Therefore the molding based fabrication of thermoplastic is relatively simpler without the steps needed in polymerization. The basic procedures of the hot embossing and injection molding are listed below and shown in Figure 1-4

In hot embossing, there are three fundamental steps[65]:

(1) The polymer substrate (wafer or sheet material) and the mold are both heated in vacuum to a temperature just above the glass transition temperature.
(2) The mold is pressed into the polymer substrate by certain level of pressure that depends on design, polymer material and the mold material
(3) Cooling and demolding

And in injection molding, the fabrication process mainly contains[65]:

(1) Plasticization of the polymer into a viscous, semi-flowing state by heating, and placement of the mold insert in the molding chamber.

(2) The molding chamber is clamped and vacuumized.

(3) Melted polymer are injected into the vacuumized molding chamber until filled up.

(4) Cooling and demolding.

Each of these two procedures has its own specific advantages and drawbacks[66]. The major difference is that the hot embossing process allows the realization of small to medium-scale series of higher quality of microstructures, while injection molding process is more suitable in larger scale of production (>1000 pieces) but with lower qualities.

The basic procedure of the molding based fabrication is applicable to most of the available thermoplastics[63][68] and result in enormous microdevices and related applications[69]–[71]. Here we only selected the molded thermoplastic microdevices that are related with the analysis of biomacromolcules and give a brief summary of their applications: (1) electrophoretic separation of biomacromolecules such as DNA[5][72], polysaccharide[73], protein and peptide[74]–[76]; (2) solid phase extraction (SPE) of DNA[77] and RNA[78]; (3) polymerase chain reaction (PCR) for the amplification of single nucleotide polymophorism (SNP)[79], tumor suppressing gene[80] and cancer marker gene[81]; (4) Electrospray device in mass spectrometry[82], [83]; and (5) microfluidic immunoassay assays[84]–[86].

The hot embossing and injection molding processes have their significant advantages over other methods in that it is highly automated and requires no hazardous chemical. However because during the fabrication process the mold has to sustain extreme

conditions of high temperature and pressure, in order to keep it durable and reusable from batch to batch the mold is usually made from metal to avoid deformation or abrasion [63][87]. The cost of the mold is relatively higher than photoresist mold. Therefore the hot-embossing fabrication process is more suitable in the phase of mass-production rather than the stage of prototyping. For the microdevices that are approaching or have already entered the arena of real world applications, injection molding or hot embossing are the most favorable fabrication method. This trend is self-evident by the injection molded or hot embossed, almost-productized microdevices that are increasingly emerging in recent years, with the capacity of handling near-practical analytical tasks such as virus detection[88], bacterial detection[89] and forensic genotyping[90], [91].

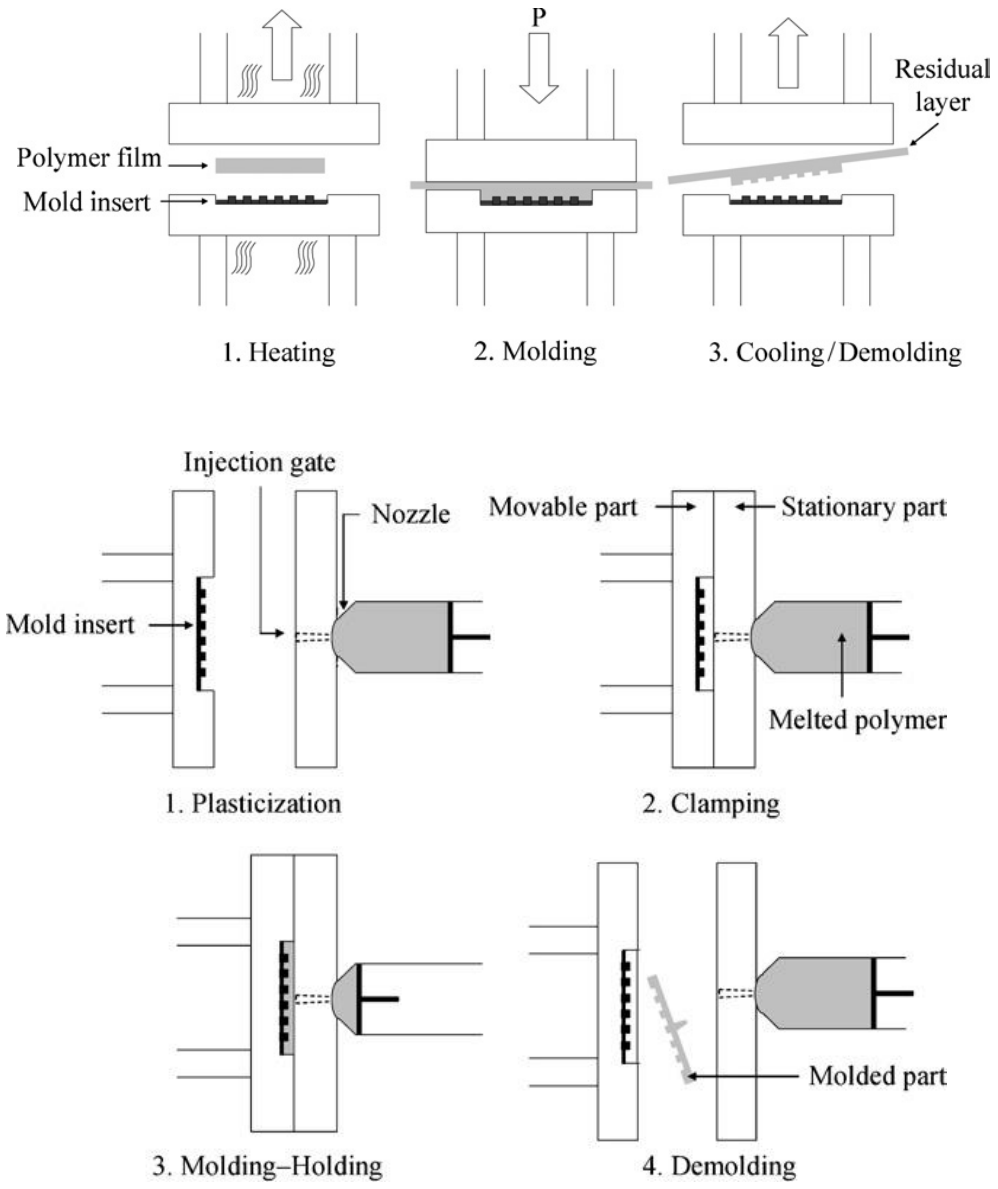

Figure 1-4[65]. *Schematics of procedures of molding based fabrication on thermoplastics: hot embossing (top) and injection molding (bottom)*

1.2.3 Inkjet printing and 3D printing

Inkjet printing and 3D printing are not novel technologies, but only until recent years they are beginning to be used in the fabrication of microfluidic devices[92].

Compared with other fabrication methods, the most distinct feature of inkjet printing and 3D printing is their cost effectiveness, which comes from two aspects: (1) they don't require any masks or molds in the fabrication and all features are directly deposited onto the substrate; (2) they are "additive deposition methods" rather than "subtractive" methods which means the microstructures are generated by the accumulation of materials from scratch rather than the "left-over" parts after removal of undesired portion from the raw material through etching or laser ablation. There is almost no waste of the material in the additive deposition process compared with subtractive methods. The advantage becomes rather significant when the material of the target microstructure is precious, e.g., when printing gold electrode[93], [94] or antibody[95], [96] as the sensing part of the microdevice.

However, the general methodology of the direct printing still suffer from obvious problems at current stage: (1) the resolution of either the ink printing or the 3D printing is around the level of 10-100 μm which affects the quality and the performance of the printed microdevices, and (2) strict selection and preparation of the printed materials in inkjet printing. An Inkjet printer can print most of the solutions of the needed materials or reagents[92] but requires careful adjustment of the viscosity[97], [98] or surface tension[99] of the solution, by spiking additives into the solution but sometimes the surfactant-based additive will affect the bioactivity of the printed reagents[100]. (3) In 3D printing technology the printable material in most commonly used set-up are still limited to resins or wax at current stage.

The most widely reported inkjet-printing fabricated microdevice is paper-based microfluidic devices[101]. Wax can be printed though a modified printer (**Figure 1-5**) on

to filter paper and, after baking, outlines the hydrophobic border of the channels to confine and guide the flow in designed course[102]–[104]. The printed paper-based microfluidic devices, due to their advantages in being cost-effective, highly portable, and truly disposable, have shown unique values in point-of-care (PoC) diagnostics. Examination of the level of glucose and protein[8], [105], lactate and uric acid[106] in artificial urine, liver functions related biomarkers[107], lead concentrations[108] have been proved successful. Other applications such as liquid molding for PDMS fabrication[109][110] and fluidic diode[111] have also been reported.

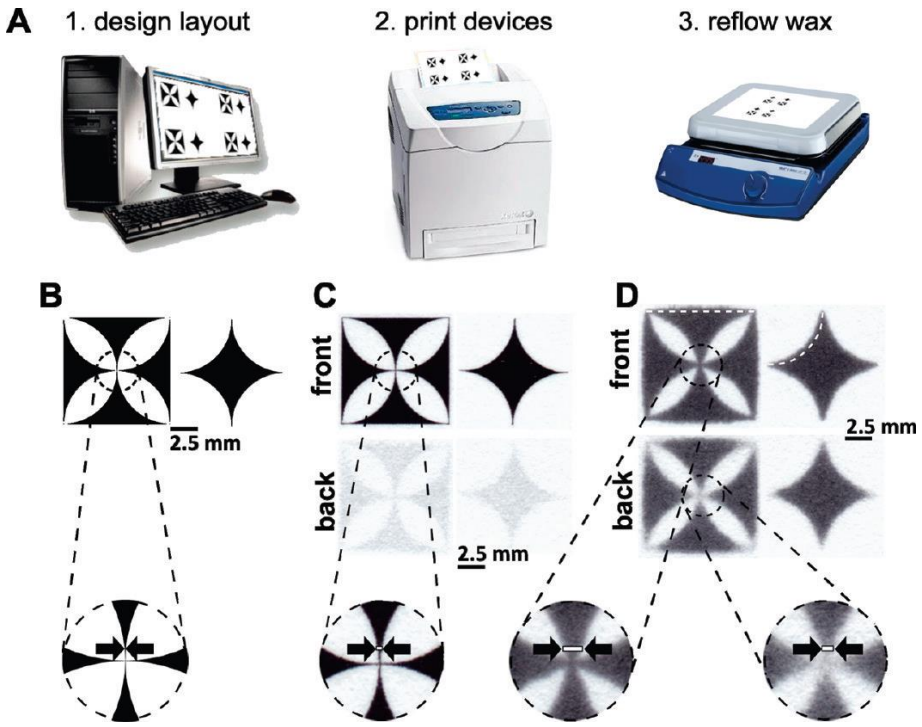

Figure 1-5[103]. *The fabrication procedure of the paper-based microfluidic device using an inkjet printer followed by baking*

Using the same idea of the inkjet printer based deposition, toner can be directly patterned on polyester film[112] for microchip electrophoresis[113], [114], DNA extraction and PCR[115]. And by exploiting the hydrophobicity of toner layer Ouyang et

al. have reported a toner based hydrophobic valve than can be directly printed on the polyester film in a polyester-toner (PeT) centrifugal microdevice for the basic metering and delivery of aqueous liquid(Figure 1-6) [116]. The burst pressure of the hydrophobic valve can be conveniently adjusted by the greyscale of the toner printed in the valve. The determination of the level of the white blood cells in whole blood has been demonstrated using the centrifugal microfluidic system [117].

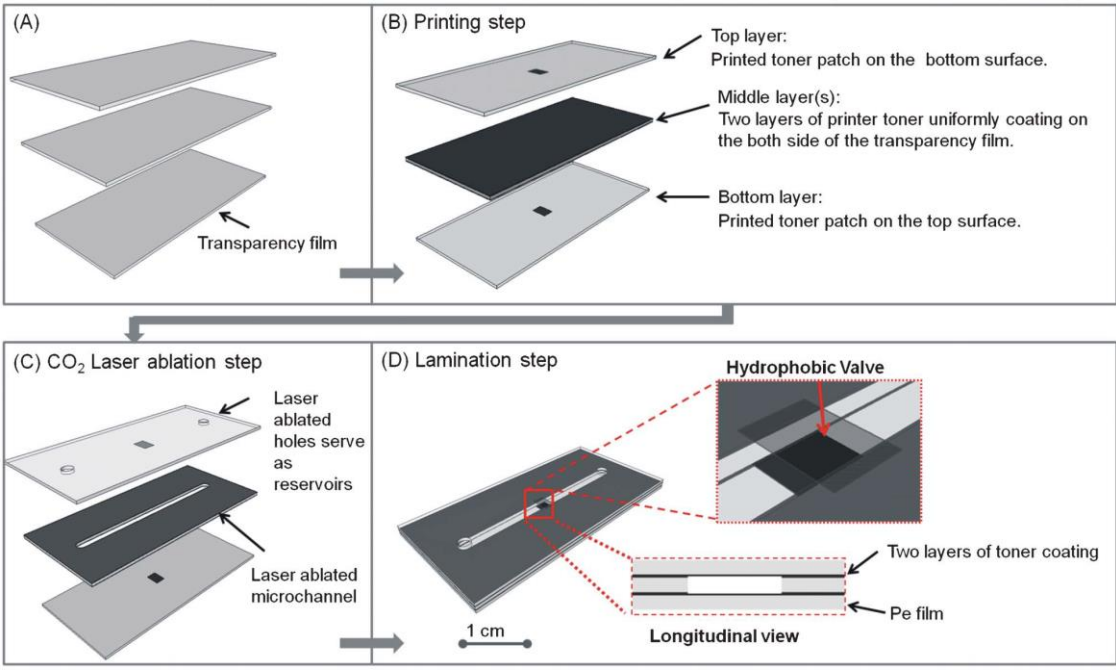

Figure 1-6[116]. *Inkjet-printed toner patch on polyester film as hydrophobic valve.*

Compared with inkjet printing which mainly construct features confined in a 2D plane, 3D printing technology has opened the door to an additional dimension in the vertical direction, which enables the direct fabrication of much more complicated micro-structures[118]. However due to the relatively low resolution and limited selection of material (resin or wax)[119], current examples of 3D printed microdevice are mostly focusing on the fabrication of mold [120][121], check valves[122], channel networks [123]

[124], microfluidic interfacing component[124]–[126] and cell separation devices based on hydrodynamic effects [127].

Although the inkjet printing and 3D printing has been proved successful in the applications shown above, the restricted selection of printed material/reagent makes the direct printing method less powerful in the prototyping stage.

1.2.4 CO_2 Laser ablation

As another representative technology of mask-free and chemical-free fabrication methods CO_2 laser ablation has many advantages for fast prototyping[119]. It has the same pros of direct printing and requires no masks, molds nor chemical in fabrication while being applicable to a wide range of materials including glass, PDMS, paper and most of the thermoplastics, which is highly suitable in the prototyping stage. The instrumentation of the CO_2 laser system composes of several major components (**Figure 1-7**[128]):

(1) A laser head with optics for the focusing of laser beam

(2) A step-motor system that controls the motion of laser head in X-Y plane

(3) Laser source

(4) A static stage for the placement of substrate

(5) User interfacing and other supporting parts

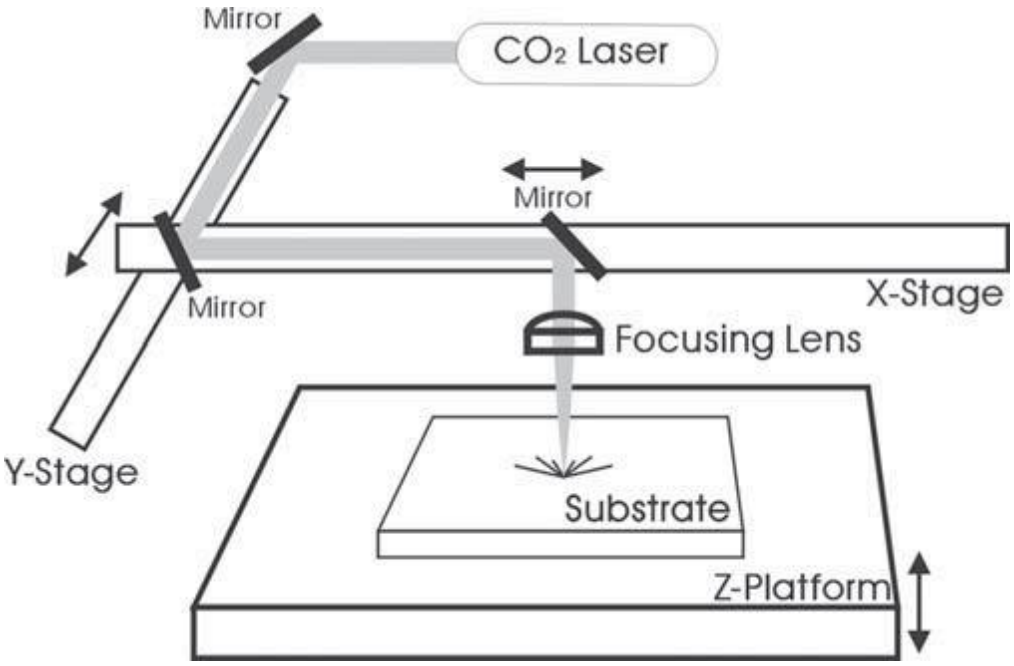

Figure 1-7. Configuration of a direct-write laser machining system with an X-Y stage[128]

The features to be ablated can be designed in a commercial graphic design software (CorelDRAW) and directly transferred into the user interface of the laser system. The wavelength of the CO_2 laser beam is usually ~10 μm which is in the infrared region, so the interaction between the material and the laser beam is governed by heat effect. The temperature at the focal point is high enough for most of the thermoplastic to melt or dissociate and evaporate, providing a convenient subtractive fabrication method. The theoretical limit of the resolution of the laser beam is the half length of the wavelength which is around 5 μm, but due to the diffraction of set of optics use in the laser system the minimum diameter of the beam spot is around 25 μm[129].

The most outstanding advantage of CO_2 laser assisted fabrication compared with other methods is the wide range of materials that it can be applied on. Major types of the

materials that have been used in laser-assisted fabrication are: Glass[130]–[135], PDMS[129], [136]–[141], most of the thermoplastics including but not limited to PMMA[141]–[150], polystyrene[141][151] and polycarbonate[152]; polyester[115]–[117], filter paper[153]–[160], wax[161], [162]. It is noteworthy that these laser-ablated and prototyped microfluidic devices have provided platforms for almost every step in DNA analysis starting from cell lysis[163], DNA extraction and purification[149], PCR[144]–[146] and detection either by electrophoresis[150] or the label-free 'pinwheel' effect[117], [147], [148]. Laser-fabricated microfluidic devices have also been applied in the prototyping of other microdevices for applications such as pumping[164], [165], surface tension valving[116], molding[141][141], passive fluidic mixing[164], droplet-related study and applications[151], [161], [167]–[169], etc.

The laser ablated features, depending on the substrate materials, show two major characteristics: (1) the cross-section of the ablation stroke is usually cone shaped or Gaussian curve-shaped[7], [170] which is due to the Gaussian beam of the laser focus. (2) The ablated surfaces are usually rough[129], [131], [142], [171] and sometimes comes with cracking[172] or ashes[129], which requires additional post-treatment to smooth[128], [142] or protection[131]–[134] during the fabrication. Although the feature's quality of laser-ablation is relatively lower than conventional wet etching or molding, with proper treatment or protection the advantages of time-saving, clean room-free and versatility in materials still outweigh the quality issues in the prototyping phase of the microdevices.

1.3 Description of the goal of research and concluding remarks

Even though laser-ablation facilitates the fast prototyping of microdevices, the examination (usually by confocal microscopy[173], stylus profilometry[174], scanning white-light interferometry (SWLI)[175] etc.) of these structures still remains inconvenient with relatively complicated operation procedures, expensive instrumentation and limited field of view (FOV). In this dissertation, alternative low-cost profiling method has been developed using a conventional office scanner and dye solution that achieves resolution of micrometer level. The principle and protocol of this method, as well as the examples of the examination on laser-ablated microstructures are detailed in Chapter 2.

Because of the nature of the subtractive fabrication process of laser ablation, majority of the laser ablated microstructures are channels, holes or wells/chambers, and most of the microdevices listed in previous paragraphs exploit the usage of those hollow spaces. The unremoved parts that remain after the laser ablation rarely play the key role in the microdevices. In this dissertation, the remaining part of a laser-ablated PDMS film serves as a flap membrane, a critical structure in a conventional check valve[176] or fluidic diode[41] which is usually fabricated by tedious soft lithography. The applications of the laser-ablated valve structures in the context of the prototyping of finger-driven microfluidic device and integrated microdevice for acoustic differential extraction are detailed in Chapter 3 and Chapter 4, respectively.

In addition, the application of CO_2 laser on glass mainly focuses on the ablation into the bulk of the material[130]–[135] but rarely touches the surface treatment. The heat effect of the CO_2 laser, if adjusted properly, can be a powerful tool in the surface

modification of the glass surface. In Chapter 5, CO_2 laser beam is used to clean out superhydrophilic patterns on the surface of glass and enables self-partitioning of aqueous solution.

In summary, the following chapters focus on the development of novel examination methods for typical laser ablated micro-structures and the prototyping of laser ablated/treated PDMS or glass microdevices for various applications. In Chapter 2 a flatbed scanner based 3D profilometry is developed to conveniently inspect laser-ablated microstructures. In Chapter 3 a laser-ablated glass-PDMS-glass one-way check valves are created and applied to a finger driven liquid handling microdevices. In Chapter 4, a laser-ablated, integrated on-chip-valve-controlled glass-PDMS-glass microdevice is prototyped and developed for the acoustic trapping of sperm cells, serving as a potential tool for the DNA extraction in the sexual assault evidence. In Chapter 5, superhydrophilic glass patterns are created by laser treatment and applied in the self-assembling of liquid droplet arrays for the development of high through-put bioassay. Concluding remarks and future perspective are outlined in Chapter 6.

1.4 References

[1] G. M. Whitesides, "The origins and the future of microfluidics.," *Nature*, vol. 442, no. 7101, pp. 368–373, 2006.

[2] D. Harrison, K. Fluri, and K. Seiler, "Micromachining a miniaturized capillary electrophoresis-based chemical analysis system on a chip," *Science.*, vol. 261, no. 5123, pp. 895–897, 1993.

[3] A. Manz and D. Harrison, “Planar chips technology for miniaturization and integration of separation techniques into monitoring systems: capillary electrophoresis on a chip,” *J. Chromatogr. A*, vol. 593, pp. 253–258, 1992.

[4] D. Duffy and J. McDonald, “Rapid prototyping of microfluidic systems in poly (dimethylsiloxane),” *Anal. Chem.*, vol. 70, no. 23, pp. 4974–4984, 1998.

[5] G. Lee, S. Chen, and G. Huang, “Microfabricated plastic chips by hot embossing methods and their applications for DNA separation and detection,” *Sensors Actuators B Chem.*, vol. 75, pp. 142–148, 2001.

[6] Y. Juang, L. Lee, and K. Koelling, “Hot embossing in microfabrication. Part I: Experimental,” *Polym. Eng. Sci.*, vol. 42, no. 3, pp. 539–550, 2002.

[7] H. Klank, J. P. Kutter, and O. Geschke, “CO2-laser micromachining and back-end processing for rapid production of PMMA-based microfluidic systems.,” *Lab Chip*, vol. 2, no. 4, pp. 242–6, Nov. 2002.

[8] A. W. Martinez, S. T. Phillips, M. J. Butte, and G. M. Whitesides, “Patterned paper as a platform for inexpensive, low-volume, portable bioassays.,” *Angew. Chem. Int. Ed. Engl.*, vol. 46, no. 8, pp. 1318–20, Jan. 2007.

[9] C. M. B. Ho, S. H. G. Ng, K. H. H. Li, and Y.-J. Yoon, “3D Printed Microfluidics for Biological Applications,” *Lab Chip*, no. May, 2015.

[10] C. G. Khan Malek, “Laser processing for bio-microfluidics applications (part I).,” *Anal. Bioanal. Chem.*, vol. 385, no. 8, pp. 1351–61, Aug. 2006.

[11] C. G. Khan Malek, “Laser processing for bio-microfluidics applications (part II).,” *Anal. Bioanal. Chem.*, vol. 385, no. 8, pp. 1362–9, Aug. 2006.

[12] L. A. Legendre, J. F. Ferrance, and J. P. Landers, “Microfluidic devices for eletrophoretic separations: Fabrication and Use,” in *Handbook of Capillary and Microchip Electrophoresis and Associated Microtechniques*, 3rd ed., J. P. Landers, Ed. Boca Raton, FL, USA: CRC Press, Inc., 2008, p. 339.

[13] D. J. Harrison, A. Manz, Z. Fan, H. Luedi, and H. M. Widmer, “Capillary electrophoresis and sample injection systems integrated on a planar glass chip,” *Anal. Chem.*, vol. 64, no. 20, pp. 1926–1932, 1992.

[14] A. Manz, D. J. Harrison, E. M. J. Verpoorte, J. C. Fettinger, A. Paulus, H. Lüdi, and H. M. Widmer, “Planar chips technology for miniaturization and integration of separation techniques into monitoring systemsCapillary electrophoresis on a chip,” *J. Chromatogr. A*, vol. 593, no. 1–2, pp. 253–258, 1992.

[15] K. Seiler, D. J. Harrison, and A. Manz, “Planar Glass Chips for Capillary Electrophoresis: Repetitive Sample Injection, Quantitation, and Separation Efficiency,” *Anal. Chem.*, vol. 65, no. 12, pp. 1481–1488, 1993.

[16] A. T. Woolley and R. A. Mathies, “Ultra-high-speed DNA fragment separations using microfabricated capillary array electrophoresis chips.,” *Proc. Natl. Acad. Sci. U. S. A.*, vol. 91, no. 24, pp. 11348–11352, 1994.

[17] B. M. Paegel, C. A. Emrich, G. J. Wedemayer, J. R. Scherer, and R. A. Mathies, “High throughput DNA sequencing with a microfabricated 96-lane capillary array electrophoresis bioprocessor.,” *Proc. Natl. Acad. Sci. U. S. A.*, vol. 99, no. 2, pp. 574–579, 2002.

[18] A. T. Woolley and R. A. Mathies, “Ultra-high-speed DNA sequencing using capillary electrophoresis chips.,” *Anal. Chem.*, vol. 67, no. 20, pp. 3676–3680, 1995.

[19] S. Liu, H. Ren, Q. Gao, D. J. Roach, R. T. Loder, T. M. Armstrong, Q. Mao, I. Blaga, D. L. Barker, and S. B. Jovanovich, “Automated parallel DNA sequencing on multiple channel microchips.,” *Proc. Natl. Acad. Sci. U. S. A.*, vol. 97, no. 10, pp. 5369–5374, 2000.

[20] C. N. Hestekin, J. P. Jakupciak, T. N. Chiesl, C. W. Kan, C. D. O’Connell, and A. E. Barron, “An optimized microchip electrophoresis system for mutation detection by tandem SSCP and heteroduplex analysis for p53 gene exons 5-9,” *Electrophoresis*, vol. 27, no. 19, pp. 3823–3835, 2006.

[21] H. Tian, A. Jaquins-Gerstl, N. Munro, M. Trucco, L. C. Brody, and J. P. Landers, “Single-strand conformation polymorphism analysis by capillary and microchip electrophoresis: a fast, simple method for detection of common mutations in BRCA1 and BRCA2.,” *Genomics*, vol. 63, no. 1, pp. 25–34, 2000.

[22] J. M. Karlinsey and J. P. Landers, “Multicolor fluorescence detection on an electrophoretic microdevice using an acoustooptic tunable filter,” *Anal. Chem.*, vol. 78, no. 15, pp. 5590–5596, 2006.

[23] N. Gottschlich, S. C. Jacobson, C. T. Culbertson, and J. M. Ramsey, “Two-Dimensional Electrochromatography / Capillary Electrophoresis on a Microchip,” *Anal. Chem.*, vol. 73, no. 11, pp. 2669–2674, 2008.

[24] J. D. Ramsey, S. C. Jacobson, C. T. Culbertson, and J. M. Ramsey, “High-Efficiency, Two-Dimensional Separations of Protein Digests on Microfluidic Devices,” *Anal. Chem.*, vol. 75, no. 7, pp. 3758–3764, 2008.

[25] R. D. Rocklin, R. S. Ramsey, and J. M. Ramsey, "A microfabricated fluidic device for performing two-dimensional liquid-phase separations," *Anal. Chem.*, vol. 72, no. 21, pp. 5244–5249, 2000.

[26] H. Jönsson, C. Holm, A. Nilsson, F. Petersson, P. Johnsson, and T. Laurell, "Particle separation using ultrasound can radically reduce embolic load to brain after cardiac surgery.," *Ann. Thorac. Surg.*, vol. 78, no. 5, pp. 1572–7, Nov. 2004.

[27] F. Petersson, A. Nilsson, C. Holm, H. Jonsson, and T. Laurell, "Continuous separation of lipid particles from erythrocytes by means of laminar flow and acoustic standing wave forces.," *Lab Chip*, vol. 5, no. 1, pp. 20–22, 2005.

[28] F. Petersson, A. Nilsson, C. Holm, H. Jonsson, and T. Laurell, "Separation of lipids from blood utilizing ultrasonic standing waves in microfluidic channels.," *Analyst*, vol. 129, no. 10, pp. 938–943, 2004.

[29] J. Nam, H. Lim, D. Kim, and S. Shin, "Separation of platelets from whole blood using standing surface acoustic waves in a microchannel.," *Lab Chip*, vol. 11, no. 19, pp. 3361–3364, 2011.

[30] P. Augustsson, C. Magnusson, M. Nordin, H. Lilja, and T. Laurell, "Microfluidic, Label-Free Enrichment of Prostate Cancer Cells in Blood Based on Acoustophoresis," *Anal. Chem.*, vol. 84, pp. 7954–7962, 2012.

[31] F. Petersson, L. Åberg, A. M. Swärd-Nilsson, and T. Laurell, "Free flow acoustophoresis: Microfluidic-based mode of particle and cell separation," *Anal. Chem.*, vol. 79, no. 14, pp. 5117–5123, 2007.

[32] K. Thomas and D. Beebe, "Cell manipulation at the micro scale," in *Handbook of Capillary and Microchip Electrophoresis and Associated Microtechniques*, 3rd ed., J. P. Landers, Ed. Boca Raton, FL, USA: CRC Press, Inc., 2008, p. 982.

[33] E. T. Lagally, J. R. Scherer, R. G. Blazej, N. M. Toriello, B. A. Diep, M. Ramchandani, G. F. Sensabaugh, L. W. Riley, and R. A. Mathies, "Integrated portable genetic analysis microsystem for pathogen/infectious disease detection.," *Anal. Chem.*, vol. 76, no. 11, pp. 3162–70, Jun. 2004.

[34] C. J. Easley, J. M. Karlinsey, J. M. Bienvenue, L. A. Legendre, M. G. Roper, S. H. Feldman, M. A. Hughes, E. L. Hewlett, T. J. Merkel, J. P. Ferrance, and J. P. Landers, "A fully integrated microfluidic genetic analysis system with sample-in-answer-out capability.," *Proc. Natl. Acad. Sci. U. S. A.*, vol. 103, no. 51, pp. 19272–7, Dec. 2006.

[35] D. C. Leslie, C. J. Easley, E. Seker, J. M. Karlinsey, M. Utz, M. R. Begley, and J. P. Landers, "Frequency-specific flow control in microfluidic circuits with passive elastomeric features," *Nat. Phys.*, vol. 5, no. 3, pp. 231–235, Feb. 2009.

[36] R. R. Collino, N. Reilly-Shapiro, B. Foresman, K. Xu, M. Utz, J. P. Landers, and M. R. Begley, "Flow switching in microfluidic networks using passive features and frequency tuning.," *Lab Chip*, vol. 13, no. 18, pp. 3668–74, 2013.

[37] H. Takao, M. Ishida, and K. Sawada, "A pneumatically actuated full in-channel microvalve with MOSFET-like function in fluid channel networks," *J. Microelectromechanical Syst.*, vol. 11, no. 5, pp. 421–426, 2002.

[38] W. H. Grover, R. H. C. Ivester, E. C. Jensen, and R. A. Mathies, "Development and multiplexed control of latching pneumatic valves using microfluidic logical structures.," *Lab Chip*, vol. 6, no. 5, pp. 623–31, May 2006.

[39] M. Rhee and M. a Burns, "Microfluidic pneumatic logic circuits and digital pneumatic microprocessors for integrated microfluidic systems.," *Lab Chip*, vol. 9, no. 21, pp. 3131–43, Nov. 2009.

[40] S.-J. Kim, R. Yokokawa, S. C. Lesher-Perez, and S. Takayama, "Constant flow-driven microfluidic oscillator for different duty cycles.," *Anal. Chem.*, vol. 84, no. 2, pp. 1152–6, Jan. 2012.

[41] B. Mosadegh, C.-H. Kuo, Y.-C. Tung, Y.-S. Torisawa, T. Bersano-Begey, H. Tavana, and S. Takayama, "Integrated Elastomeric Components for Autonomous Regulation of Sequential and Oscillatory Flow Switching in Microfluidic Devices.," *Nat. Phys.*, vol. 6, no. 6, pp. 433–437, Jun. 2010.

[42] K. Iwai, K. C. Shih, X. Lin, T. A. Brubaker, R. D. Sochol, and L. Lin, "Lab on a Chip multilayer soft lithography and injection," *Lab Chip*, pp. 3790–3799, 2014.

[43] W. Li, T. Chen, Z. Chen, P. Fei, Z. Yu, Y. Pang, and Y. Huang, "Squeeze-chip: A finger controlled microfluidic flow network device and its application to biochemical assays," *Lab Chip*, vol. 12, no. 9, 2012.

[44] T. Thorsen, S. J. Maerkl, and S. R. Quake, "Microfluidic large-scale integration.," *Science.*, vol. 298, no. 5593, pp. 580–4, Oct. 2002.

[45] C. L. Hansen, E. Skordalakes, J. M. Berger, and S. R. Quake, "A robust and scalable microfluidic metering method that allows protein crystal growth by free interface diffusion.," *Proc. Natl. Acad. Sci. U. S. A.*, vol. 99, no. 26, pp. 16531–6, Dec. 2002.

[46] J. Wang, H. C. Fan, B. Behr, and S. R. Quake, "Genome-wide single-cell analysis of recombination activity and de novo mutation rates in human sperm.," *Cell*, vol. 150, no. 2, pp. 402–12, Jul. 2012.

[47] E. A. Ottesen, J. W. Hong, S. R. Quake, and J. R. Leadbetter, "Microfluidic digital PCR enables multigene analysis of individual environmental bacteria.," *Science.*, vol. 314, no. 5804, pp. 1464–7, Dec. 2006.

[48] D. H. Kang, S. M. Kim, B. Lee, H. Yoon, and K.-Y. Suh, "Stimuli-responsive hydrogel patterns for smart microfluidics and microarrays.," *Analyst*, vol. 138, no. 21, pp. 6230–42, 2013.

[49] M. Ye, J. X. Li, J. Li, W. Li, B. R. Lu, G. Huang, Y. Mei, Y. Chen, and R. Liu, "Humido-responsive nanostructures prepared by nanoimprinting," *Microelectron. Eng.*, vol. 98, pp. 634–637, 2012.

[50] H. E. Jeong, S. H. Lee, P. Kim, and K. Y. Suh, "Stretched polymer nanohairs by nanodrawing," *Nano Lett.*, vol. 6, no. 7, pp. 1508–1513, 2006.

[51] H. E. Jeong, J.-K. Lee, H. N. Kim, S. H. Moon, and K. Y. Suh, "A nontransferring dry adhesive with hierarchical polymer nanohairs.," *Proc. Natl. Acad. Sci. U. S. A.*, vol. 106, no. 14, pp. 5639–5644, 2009.

[52] H. E. Jeong, R. Kwak, J. K. Kim, and K. Y. Suh, "Generation and self-replication of monolithic, dual-scale polymer structures by two-step capillary-force lithography," *Small*, vol. 4, no. 11, pp. 1913–1918, 2008.

[53] R. Kwak, H. E. Jeong, and K. Y. Suh, "Fabrication of monolithic bridge structures by vacuum-assisted capillary-force lithography," *Small*, vol. 5, no. 7, pp. 790–794, 2009.

[54] K. Y. Suh, M. C. Park, and P. Kim, "Capillary force lithography: A versatile tool for structured biomaterials interface towards cell and tissue engineering," *Adv. Funct. Mater.*, vol. 19, no. 17, pp. 2699–2712, 2009.

[55] A. P. Wong, R. Perez-Castillejos, J. C. Love, and G. M. Whitesides, "Partitioning Microfluidic Channels with Hydrogel to Construct Tunable 3-D Cellular Microenvironments," *Biomaterials*, vol. 29, no. 12, pp. 1853–1861, 2008.

[56] X. (James) Li, A. V. Valadez, P. Zuo, and Z. Nie, "Microfluidic 3D cell culture: potential application for tissue- based bioassays," *Bioanalysis*, vol. 4, no. 12, pp. 1509–1525, 2012.

[57] A. Khademhosseini and R. Langer, "Microengineered hydrogels for tissue engineering," *Biomaterials*, vol. 28, no. 34, pp. 5087–5092, 2007.

[58] B. G. Chung, K.-H. Lee, A. Khademhosseini, and S.-H. Lee, "Microfluidic fabrication of microengineered hydrogels and their application in tissue engineering," *Lab Chip*, vol. 12, no. 1, p. 45, 2012.

[59] T. Garg, S. Singh, and A. Goyal, “Stimuli-sensitive hydrogels: an excellent carrier for drug and cell delivery,” *Crit. Rev. Ther. Drug Carr. Syst.*, vol. 30, no. 5, pp. 369–409, 2013.

[60] S. Mazzitelli, L. Capretto, F. Quinci, R. Piva, and C. Nastruzzi, “Preparation of cell-encapsulation devices in confined microenvironment,” *Adv. Drug Deliv. Rev.*, vol. 65, no. 11–12, pp. 1533–1555, 2013.

[61] E. Cukierman, R. Pankov, and K. M. Yamada, “Cell interactions with three-dimensional matrices,” *Curr. Opin. Cell Biol.*, vol. 14, no. 5, pp. 633–639, 2002.

[62] Y. Shin, S. Han, J. S. Jeon, K. Yamamoto, I. K. Zervantonakis, R. Sudo, R. D. Kamm, and S. Chung, “Microfluidic assay for simultaneous culture of multiple cell types on surfaces or within hydrogels,” *Nat. Protoc.*, vol. 7, no. 7, pp. 1247–1259, 2012.

[63] L. Peng, Y. Deng, P. Yi, and X. Lai, “Micro hot embossing of thermoplastic polymers: a review,” *J. Micromechanics Microengineering*, vol. 24, no. 1, p. 13001–, 2014.

[64] H. Becker and U. Heim, “Hot embossing as a method for the fabrication of polymer high aspect ratio structures,” *Sensors Actuators, A Phys.*, vol. 83, no. 1, pp. 130–135, 2000.

[65] J. Giboz, T. Copponnex, and P. Mélé, “Microinjection molding of thermoplastic polymers: a review,” *J. Micromechanics Microengineering*, vol. 17, no. 6, pp. R96–R109, 2007.

[66] M. Heckele and W. K. Schomburg, “Review on micro molding of thermoplastic polymers,” *J. Micromechanics Microengineering*, vol. 14, no. 3, pp. R1–R14, 2003.

[67] U. M. Attia, S. Marson, and J. R. Alcock, “Micro-injection moulding of polymer microfluidic devices,” *Microfluid. Nanofluidics*, vol. 7, no. 1, pp. 1–28, 2009.

[68] H. Becker and C. Gärtner, “Polymer microfabrication technologies for microfluidic systems.,” *Anal. Bioanal. Chem.*, vol. 390, no. 1, pp. 89–111, Jan. 2008.

[69] A. Alrifaiy, O. A. Lindahl, and K. Ramser, “Polymer-based microfluidic devices for pharmacy, biology and tissue engineering,” *Polymers (Basel).*, vol. 4, no. 3, pp. 1349–1398, 2012.

[70] Y. Chen, L. Zhang, and G. Chen, “Fabrication, modification, and application of poly(methyl methacrylate) microfluidic chips,” *Electrophoresis*, vol. 29, no. 9, pp. 1801–1814, 2008.

[71] P. S. Nunes, P. D. Ohlsson, O. Ordeig, and J. P. Kutter, "Cyclic olefin polymers: Emerging materials for lab-on-a-chip applications," *Microfluid. Nanofluidics*, vol. 9, no. 2–3, pp. 145–161, 2010.

[72] R. Liedert, L. K. Amundsen, A. Hokkanen, M. Mäki, A. Aittakorpi, M. Pakanen, J. R. Scherer, R. A. Mathies, M. Kurkinen, S. Uusitalo, L. Hakalahti, T. K. Nevanen, H. Siitari, and H. Söderlund, "Disposable roll-to-roll hot embossed electrophoresis chip for detection of antibiotic resistance gene mecA in bacteria," *Lab on a Chip*, vol. 12, no. 2. p. 333, 2012.

[73] F. Dang, K. Kakehi, K. Nakajima, Y. Shinohara, M. Ishikawa, N. Kaji, M. Tokeshi, and Y. Baba, "Rapid analysis of oligosaccharides derived from glycoproteins by microchip electrophoresis," *J. Chromatogr. A*, vol. 1109, no. 2, pp. 138–143, 2006.

[74] J. Liu, T. Pan, A. T. Woolley, and M. L. Lee, "Surface-modified poly(methyl methacrylate) capillary electrophoresis microchips for protein and peptide analysis," *Anal. Chem.*, vol. 76, no. 23, pp. 6948–6955, 2005.

[75] A. E. Herr, J. I. Molho, K. A. Drouvalakis, J. C. Mikkelsen, P. J. Utz, J. G. Santiago, and T. W. Kenny, "On-chip coupling of isoelectric focusing and free solution electrophoresis for multidimensional separations," *Anal. Chem.*, vol. 75, no. 5, pp. 1180–1187, 2003.

[76] H. Shadpour and S. A. Soper, "Two-dimensional electrophoretic separation of proteins using poly(methyl methacrylate) microchips," *Anal. Chem.*, vol. 78, no. 11, pp. 3519–3527, 2006.

[77] D. S. W. Park, M. L. Hupert, M. A. Witek, B. H. You, P. Datta, J. Guy, J. B. Lee, S. a. Soper, D. E. Nikitopoulos, and M. C. Murphy, "A titer plate-based polymer microfluidic platform for high throughput nucleic acid purification," *Biomed. Microdevices*, vol. 10, no. 1, pp. 21–33, 2008.

[78] S. R. Nugen, P. J. Asiello, and A. J. Baeumner, "Design and fabrication of a microfluidic device for near-single cell mRNA isolation using a copper hot embossing master," *Microsyst. Technol.*, vol. 15, no. 3, pp. 477–483, 2009.

[79] S. L. Marasso, D. Mombello, M. Cocuzza, D. Casalena, I. Ferrante, A. Nesca, P. Poiklik, K. Rekker, A. Aaspollu, S. Ferrero, and C. F. Pirri, "A polymer Lab-on-a-Chip for genetic analysis using the arrayed primer extension on microarray chips," *Biomed. Microdevices*, vol. 16, no. 5, pp. 661–670, 2014.

[80] D.-S. Lee, S. H. Park, H. Yang, K.-H. Chung, T. H. Yoon, S.-J. Kim, K. Kim, and Y. T. Kim, "Bulk-micromachined submicroliter-volume PCR chip with very rapid thermal response and low power consumption.," *Lab Chip*, vol. 4, no. 4, pp. 401–407, 2004.

[81] A. Gulliksen, L. A. Solli, K. S. Drese, O. Sörensen, F. Karlsen, H. Rogne, E. Hovig, and R. Sirevåg, "Parallel nanoliter detection of cancer markers using polymer microchips.," *Lab Chip*, vol. 5, no. 4, pp. 416–420, 2005.

[82] J. Kameoka, R. Orth, B. Ilic, D. Czaplewski, T. Wachs, and H. G. Craighead, "An electrospray ionization source for integration with microfluidics," *Anal. Chem.*, vol. 74, no. 22, pp. 5897–5901, 2002.

[83] J. Liu, K. W. Ro, R. Nayak, and D. R. Knapp, "Monolithic column plastic microfluidic device for peptide analysis using electrospray from a channel opening on the edge of the device," *Int. J. Mass Spectrom.*, vol. 259, no. 1–3, pp. 65–72, 2007.

[84] F. Darain, K. L. Gan, and S. C. Tjin, "Antibody immobilization on to polystyrene substrate - On-chip immunoassay for horse IgG based on fluorescence," *Biomed. Microdevices*, vol. 11, no. 3, pp. 653–661, 2009.

[85] C. Jönsson, M. Aronsson, G. Rundström, C. Pettersson, I. Mendel-Hartvig, J. Bakker, E. Martinsson, B. Liedberg, B. MacCraith, O. Ohman, and J. Melin, "Silane-dextran chemistry on lateral flow polymer chips for immunoassays.," *Lab Chip*, vol. 8, no. 7, pp. 1191–1197, 2008.

[86] H. Wang, S. Meng, K. Guo, Y. Liu, P. Yang, W. Zhong, and B. Liu, "Microfluidic immunosensor based on stable antibody-patterned surface in PMMA microchip," *Electrochem. commun.*, vol. 10, no. 3, pp. 447–450, 2008.

[87] M. B. Esch, S. Kapur, G. Irizarry, and V. Genova, "Influence of master fabrication techniques on the characteristics of embossed microfluidic channels.," *Lab Chip*, vol. 3, no. 2, pp. 121–127, 2003.

[88] A. Gulliksen, H. Keegan, C. Martin, J. O'Leary, L. A. Solli, I. M. Falang, P. Grnn, A. Karlgrd, M. M. Mielnik, I. R. Johansen, T. R. Tofteberg, T. Baier, R. Gransee, K. Drese, T. Hansen-Hagge, L. Riegger, P. Koltay, R. Zengerle, F. Karlsen, D. Ausen, and L. Furuberg, "Towards a sample-in, answer-out point-of-care platform for nucleic acid extraction and amplification: Using an HPV E6/E7 mRNA model system," *J. Oncol.*, vol. 2012, 2012.

[89] G. Czilwik, T. Messinger, O. Strohmeier, S. Wadle, F. von Stetten, N. Paust, G. Roth, R. Zengerle, P. Saarinen, J. Niittymaki, K. McAllister, O. Sheils, J. J. O'Leary, and D. Mark, "Rapid molecular infectious disease diagnostics on a fully automated centrifugal-microfluidic LabDisk system using highly sensitive nested PCR with integrated sample preparation," *Lab Chip*, vol. In press, 2015.

[90] D. Le Roux, B. E. Root, J. A. Hickey, O. N. Scott, A. Tsuei, J. Li, D. J. Saul, L. Chassagne, J. P. Landers, and P. de Mazancourt, "An integrated sample-in-answer-

out microfluidic chip for rapid human identification by STR analysis," *Lab Chip*, vol. 14, no. 22, pp. 4415–4425, 2014.

[91] D. Le Roux, B. E. Root, C. R. Reedy, J. A. Hickey, O. N. Scott, J. M. Bienvenue, J. P. Landers, L. Chassagne, and P. de Mazancourt, "DNA Analysis Using an Integrated Microchip for Multiplex PCR Amplification and Electrophoresis for Reference Samples," *Anal. Chem.*, vol. 86, no. 16, pp. 8192–8199, 2014.

[92] N. Komuro, S. Takaki, K. Suzuki, and D. Citterio, "Inkjet printed (bio)chemical sensing devices," *Anal. Bioanal. Chem.*, vol. 405, no. 17, pp. 5785–5805, 2013.

[93] G. C. Jensen, C. E. Krause, G. A. Sotzing, and J. F. Rusling, "Inkjet-printed gold nanoparticle electrochemical arrays on plastic. Application to immunodetection of a cancer biomarker protein.," *Phys. Chem. Chem. Phys.*, vol. 13, no. 11, pp. 4888–4894, 2011.

[94] C. Hu, X. Bai, Y. Wang, W. Jin, X. Zhang, and S. Hu, "Inkjet printing of nanoporous gold electrode arrays on cellulose membranes for high-sensitive paper-like electrochemical oxygen sensors using ionic liquid electrolytes," *Anal. Chem.*, vol. 84, no. 8, pp. 3745–3750, 2012.

[95] R. S. J. Alkasir, M. Ornatska, and S. Andreescu, "Colorimetric paper bioassay for the detection of phenolic compounds," *Anal. Chem.*, vol. 84, no. 22, pp. 9729–9737, 2012.

[96] S. Su, M. M. Ali, C. D. M. Filipe, Y. Li, and R. Pelton, "Microgel-based inks for paper-supported biosensing applications," *Biomacromolecules*, vol. 9, no. 3, pp. 935–941, 2008.

[97] H. Kwon, F. Samain, and E. T. Kool, "Fluorescent DNAs printed on paper: sensing food spoilage and ripening in the vapor phase," *Chem. Sci.*, vol. 3, no. 8, p. 2542, 2012.

[98] M. Yang, L. Li, S. Zhang, G. Li, and H. Zhao, "Preparation, characterisation and sensing application of inkjet-printed nanostructured TiO2 photoanode," *Sensors Actuators, B Chem.*, vol. 147, no. 2, pp. 622–628, 2010.

[99] B. Yoon, H. Shin, O. Yarimaga, D.-Y. Ham, J. Kim, I. S. Park, and J.-M. Kim, "An inkjet-printable microemulsion system for colorimetric polydiacetylene supramolecules on paper substrates," *Journal of Materials Chemistry*, vol. 22, no. 17. p. 8680, 2012.

[100] S. Di Risio and N. Yan, "Piezoelectric ink-jet printing of horseradish peroxidase: Effect of ink viscosity modifiers on activity," *Macromol. Rapid Commun.*, vol. 28, no. 18–19, pp. 1934–1940, 2007.

[101] D. M. Cate, J. A. Adkins, J. Mettakoonpitak, and C. S. Henry, “Recent Developments in Paper-Based Micro fluidic Devices,” *Anal. Chem.*, vol. 87, pp. 19–41, 2015.

[102] R. Lu, W. Shi, L. Jiang, J. Qin, and B. Lin, “Rapid prototyping of paper-based microfluidics with wax for low-cost, portable bioassay,” *Electrophoresis*, vol. 30, no. 9, pp. 1497–1500, 2009.

[103] E. Carrilho, A. W. Martinez, and G. M. Whitesides, “Understanding wax printing: a simple micropatterning process for paper-based microfluidics.,” *Anal. Chem.*, vol. 81, no. 16, pp. 7091–5, Aug. 2009.

[104] C. Renault, J. Koehne, A. J. Ricco, and R. M. Crooks, “Three-dimensional wax patterning of paper fluidic devices,” *Langmuir*, vol. 30, no. 23, pp. 7030–7036, 2014.

[105] A. W. Martinez, S. T. Phillips, E. Carrilho, S. W. Thomas, H. Sindi, and G. M. Whitesides, “Simple telemedicine for developing regions: camera phones and paper-based microfluidic devices for real-time, off-site diagnosis.,” *Anal. Chem.*, vol. 80, no. 10, pp. 3699–707, May 2008.

[106] X. Li and X. Liu, “Fabrication of three-dimensional microfluidic channels in a single layer of cellulose paper,” *Microfluid. Nanofluidics*, pp. 1–9, 2014.

[107] S. J. Vella, P. Beattie, R. Cademartiri, A. Laromaine, A. W. Martinez, S. T. Phillips, K. A. Mirica, and G. M. Whitesides, “Measuring markers of liver function using a micropatterned paper device designed for blood from a fingerstick.,” *Anal. Chem.*, vol. 84, no. 6, pp. 2883–91, Mar. 2012.

[108] P. J. Bracher, M. Gupta, and G. M. Whitesides, “Patterning precipitates of reactions in paper,” *J. Mater. Chem.*, vol. 20, no. 24, p. 5117, 2010.

[109] Y. Lu, B. Lin, and J. Qin, “Patterned paper as a low-cost, flexible substrate for rapid prototyping of PDMS microdevices via ‘liquid molding’.,” *Anal. Chem.*, vol. 83, no. 5, pp. 1830–5, Mar. 2011.

[110] X. Liu, Q. Wang, J. Qin, and B. Lin, “A facile ‘liquid-molding’ method to fabricate PDMS microdevices with 3-dimensional channel topography.,” *Lab Chip*, vol. 9, no. 9, pp. 1200–5, May 2009.

[111] H. Chen, J. Cogswell, C. Anagnostopoulos, and M. Faghri, “A fluidic diode, valves, and a sequential-loading circuit fabricated on layered paper,” *Lab Chip*, vol. 12, no. 16, p. 2909, 2012.

[112] C. L. do Lago, “A dry process for production of microfluidic devices based on the lamination of laser-printed polyester films,” *Anal. Chem.*, vol. 75, no. 15, pp. 3853–3858, 2003.

[113] W. K. Tomazelli Coltro, J. A. Fracassi da Silva, H. D. Torres da Silva, E. M. Richter, R. Furlan, L. Angnes, C. L. do Lago, L. H. Mazo, and E. Carrilho, “Electrophoresis microchip fabricated by a direct-printing process with end-channel amperometric detection.,” *Electrophoresis*, vol. 25, no. 21–22, pp. 3832–9, Nov. 2004.

[114] G. R. M. Duarte, W. K. T. Coltro, J. C. Borba, C. W. Price, J. P. Landers, and E. Carrilho, “Disposable polyester–toner electrophoresis microchips for DNA analysis,” *The Analyst*, vol. 137, no. 11. p. 2692, 2012.

[115] G. R. M. Duarte, C. W. Price, B. H. Augustine, E. Carrilho, and J. P. Landers, “Dynamic solid phase DNA extraction and PCR amplification in polyester-toner based microchip.,” *Anal. Chem.*, vol. 83, no. 13, pp. 5182–9, Jul. 2011.

[116] Y. Ouyang, S. Wang, J. Li, P. S. Riehl, M. Begley, and J. P. Landers, “Rapid patterning of ‘tunable’ hydrophobic valves on disposable microchips by laser printer lithography.,” *Lab Chip*, vol. 13, no. 9, pp. 1762–71, May 2013.

[117] B. L. Thompson, Y. Ouyang, G. R. M. Duarte, E. Carrilho, S. T. Krauss, and J. P. Landers, “Inexpensive, rapid prototyping of microfluidic devices using overhead transparencies and a laser print, cut and laminate fabrication method.,” *Nat. Protoc.*, vol. 10, no. 6, pp. 875–86, Jun. 2015.

[118] R. Walczak and K. Adamski, “Inkjet 3D printing of microfluidic structures—on the selection of the printer towards printing your own microfluidic chips,” *J. Micromechanics Microengineering*, vol. 25, no. 8, p. 085013, 2015.

[119] A. Waldbaur, H. Rapp, K. Länge, and B. E. Rapp, “Let there be chip—towards rapid prototyping of microfluidic devices: one-step manufacturing processes,” *Anal. Methods*, vol. 3, no. 12, p. 2681, 2011.

[120] H. N. Chan, Y. Chen, Y. Shu, Y. Chen, Q. Tian, and H. Wu, “Direct, one-step molding of 3D-printed structures for convenient fabrication of truly 3D PDMS microfluidic chips,” *Microfluid. Nanofluidics*, vol. 19, pp. 9–18, 2015.

[121] G. Maltezos, E. Garcia, G. Hanrahan, F. A. Gomez, S. Vyawahare, R. M. van Dam, Y. Chen, and A. Scherer, “Design and fabrication of chemically robust three-dimensional microfluidic valves.,” *Lab Chip*, vol. 7, no. 9, pp. 1209–1211, 2007.

[122] G. Comina, A. Suska, and D. Filippini, “3D Printed Unibody Lab-on-a-Chip: Features Survey and Check-Valves Integration,” *Micromachines*, vol. 6, no. 4, pp. 437–451, 2015.

[123] M. Mehling, T. Frank, C. Albayrak, and S. Tay, “3D-Printed Microfluidic Automation,” *Lab Chip*, vol. 15, pp. 1276–1283, 2015.

[124] A. I. Shallan, P. Smejkal, M. Corban, R. M. Guijt, and M. C. Breadmore, “Cost-effective three-dimensional printing of visibly transparent microchips within minutes,” *Anal. Chem.*, vol. 86, no. 6, pp. 3124–3130, 2014.

[125] S. A. N. Gowers, V. F. Curto, C. A. Seneci, C. Wang, S. Anastasova, P. Vadgama, G.-Z. Yang, and M. G. Boutelle, “3D printed microfluidic device with integrated biosensors for online analysis of subcutaneous human microdialysate,” *Anal. Chem.*, no. in press, 2015.

[126] J. L. Erkal, A. Selimovic, B. C. Gross, S. Y. Lockwood, E. L. Walton, S. McNamara, R. S. Martin, and D. M. Spence, “3D printed microfluidic devices with integrated versatile and reusable electrodes.,” *Lab Chip*, vol. 14, no. 12, pp. 2023–32, 2014.

[127] W. Lee, D. Kwon, W. Choi, G. Y. Jung, and S. Jeon, “3D-Printed Microfluidic Device for the Detection of Pathogenic Bacteria Using Size-based Separation in Helical Channel with Trapezoid Cross-Section,” *Sci. Rep.*, vol. 5, p. 7717, 2015.

[128] J. Cheng, C. Wei, K. Hsu, and T. Young, “Direct-write laser micromachining and universal surface modification of PMMA for device development,” *Sensors Actuators, B Chem.*, vol. 99, no. 1, pp. 186–196, 2004.

[129] H.-B. Liu and H.-Q. Gong, “Templateless prototyping of polydimethylsiloxane microfluidic structures using a pulsed CO2 laser,” *J. Micromechanics Microengineering*, vol. 19, no. 3, pp. 37002–37010, Mar. 2009.

[130] S. Nisar, L. Li, and M. A. Sheikh, “Laser glass cutting techniques—A review,” *J. Laser Appl.*, vol. 25, no. 4, p. 042010, 2013.

[131] L.-M. Fu, W.-J. Ju, R.-J. Yang, and Y.-N. Wang, “Rapid prototyping of glass-based microfluidic chips utilizing two-pass defocused CO2 laser beam method,” *Microfluid. Nanofluidics*, vol. 14, no. 3–4, pp. 479–487, Oct. 2012.

[132] C. K. Chung, S. L. Lin, H. Y. Wang, T. K. Tan, K. Z. Tu, and H. F. Lung, “Fabrication and simulation of glass micromachining using CO2 laser processing with PDMS protection,” *Appl. Phys. A*, vol. 113, no. 2, pp. 501–507, Jan. 2013.

[133] C. K. Chung and S. L. Lin, “CO2 laser micromachined crackless through holes of Pyrex 7740 glass,” *Int. J. Mach. Tools Manuf.*, vol. 50, no. 11, pp. 961–968, 2010.

[134] C. K. Chung, H. C. Chang, T. R. Shih, S. L. Lin, E. J. Hsiao, Y. S. Chen, E. C. Chang, C. C. Chen, and C. C. Lin, "Water-assisted CO2 laser ablated glass and modified thermal bonding for capillary-driven bio-fluidic application.," *Biomed. Microdevices*, vol. 12, no. 1, pp. 107–14, Feb. 2010.

[135] C. A. Baker, R. Bulloch, and M. G. Roper, "Comparison of separation performance of laser-ablated and wet-etched microfluidic devices.," *Anal. Bioanal. Chem.*, vol. 399, no. 4, pp. 1473–9, Feb. 2011.

[136] S. Xing, R. S. Harake, and T. Pan, "Droplet-driven transports on superhydrophobic-patterned surface microfluidics.," *Lab Chip*, vol. 11, no. 21, pp. 3642–8, Dec. 2011.

[137] A. Chen and T. Pan, "Three-dimensional fit-to-flow microfluidic assembly.," *Biomicrofluidics*, vol. 5, no. 4, pp. 46505–465059, Dec. 2011.

[138] B. A. Fogarty, K. E. Heppert, T. J. Cory, K. R. Hulbutta, R. S. Martin, and S. M. Lunte, "Rapid fabrication of poly(dimethylsiloxane)-based microchip capillary electrophoresis devices using CO2 laser ablation.," *Analyst*, vol. 130, no. 6, pp. 924–30, Jun. 2005.

[139] J. Huft, D. J. Da Costa, D. Walker, and C. L. Hansen, "Three-dimensional large-scale microfluidic integration by laser ablation of interlayer connections.," *Lab Chip*, vol. 10, no. 18, pp. 2358–65, Sep. 2010.

[140] M. Li, S. Li, J. Wu, W. Wen, W. Li, and G. Alici, "A simple and cost-effective method for fabrication of integrated electronic-microfluidic devices using a laser-patterned PDMS layer," *Microfluid. Nanofluidics*, vol. 12, no. 5, pp. 751–760, Dec. 2011.

[141] T. Y. Tu, Z. Wang, J. Bai, W. Sun, W. K. Peng, R. Y. J. Huang, J. P. Thiery, and R. D. Kamm, "Rapid prototyping of concave microwells for the formation of 3D multicellular cancer aggregates for drug screening," *Adv Heal. Mater*, vol. 3, no. 4, pp. 609–616, 2014.

[142] Z. K. Wang, H. Y. Zheng, R. Y. H. Lim, Z. F. Wang, and Y. C. Lam, "Improving surface smoothness of laser-fabricated microchannels for microfluidic application," *J. Micromechanics Microengineering*, vol. 21, no. 9, p. 095008, Sep. 2011.

[143] M. Riahi, "Fabrication of a passive 3D mixer using CO2 laser ablation of PMMA and PDMS moldings," *Microchem. J.*, vol. 100, pp. 14–20, Jan. 2012.

[144] J. A. Lounsbury and J. P. Landers, "Ultrafast amplification of DNA on plastic microdevices for forensic short tandem repeat analysis," *J. Forensic Sci.*, vol. 58, no. 4, pp. 866–874, 2013.

[145] J. A. Lounsbury, B. L. Poe, M. Do, and J. P. Landers, “Laser-ablated poly(methyl methacrylate) microdevices for sub-microliter DNA amplification suitable for micro-total analysis systems,” *J. Micromechanics Microengineering*, vol. 22, no. 8, p. 085006, Aug. 2012.

[146] D. J. Marchiarullo, A. H. Sklavounos, K. Oh, B. L. Poe, N. S. Barker, and J. P. Landers, “Low-power microwave-mediated heating for microchip-based PCR.,” *Lab Chip*, vol. 13, no. 17, pp. 3417–25, 2013.

[147] D. A. Nelson, B. C. Strachan, H. S. Sloane, J. Li, and J. P. Landers, “Dual-force aggregation of magnetic particles enhances label-free quantification of DNA at the sub-single cell level,” *Anal. Chim. Acta*, vol. 819, pp. 34–41, 2014.

[148] D. C. Leslie, J. Li, B. C. Strachan, M. R. Begley, D. Finkler, L. A. L. Bazydlo, N. S. Barker, D. M. Haverstick, M. Utz, and J. P. Landers, “New detection modality for label-free quantification of DNA in biological samples via superparamagnetic bead aggregation.,” *J. Am. Chem. Soc.*, vol. 134, no. 12, pp. 5689–96, Mar. 2012.

[149] B. C. Strachan, A. V Karlsson, and J. P. Landers, “Volume-Reduction Solid Phase Extraction on a Plastic Microfluidic Device for Forensic Sample Analysis,” *Proc. Micro Total Anal. Syst. Conf.*, pp. 1969–1971, 2012.

[150] E. F. M. Gabriel, W. K. T. Coltro, and C. D. Garcia, “Fast and versatile fabrication of PMMA microchip electrophoretic devices by laser engraving,” *Electrophoresis*, vol. 35, no. 16, pp. 2325–2332, 2014.

[151] H. Li, Y. Fan, R. Kodzius, and I. G. Foulds, “Fabrication of polystyrene microfluidic devices using a pulsed CO2 laser system,” *Microsyst. Technol.*, vol. 18, no. 3, pp. 373–379, Dec. 2011.

[152] H. Qi, T. Chen, L. Yao, and T. Zuo, “Micromachining of microchannel on the polycarbonate substrate with CO2 laser direct-writing ablation,” *Opt. Lasers Eng.*, vol. 47, no. 5, pp. 594–598, 2009.

[153] P. Spicar-Mihalic, B. J. Toley, J. Houghtaling, T. Liang, P. Yager, and E. Fu, “CO2 laser cutting and ablative etching for the fabrication of paper-based devices,” *J. Micromechanics Microengineering*, vol. 23, no. 6, p. 067003, 2013.

[154] S. Ramachandran, E. Fu, B. Lutz, and P. Yager, “Long-term dry storage of an enzyme-based reagent system for ELISA in point-of-care devices.,” *Analyst*, vol. 139, no. 6, pp. 1456–62, 2014.

[155] J. L. Osborn, B. Lutz, E. Fu, P. Kauffman, D. Y. Stevens, and P. Yager, “Microfluidics without pumps: reinventing the T-sensor and H-filter in paper networks.,” *Lab Chip*, vol. 10, no. 20, pp. 2659–2665, 2010.

[156] G. E. Fridley, H. Q. Le, E. Fu, and P. Yager, "Controlled release of dry reagents in porous media for tunable temporal and spatial distribution upon rehydration," *Lab Chip*, vol. 12, no. 21, p. 4321, 2012.

[157] B. J. Toley, J. A. Wang, M. Gupta, J. R. Buser, L. K. Lafleur, B. R. Lutz, E. Fu, and P. Yager, "A versatile valving toolkit for automating fluidic operations in paper microfluidic devices," *Lab Chip*, vol. 15, pp. 1432–1444, 2015.

[158] E. Fu, S. A. Ramsey, P. Kauffman, B. Lutz, and P. Yager, "Transport in two-dimensional paper networks," *Microfluid. Nanofluidics*, vol. 10, no. 1, pp. 29–35, 2011.

[159] P. Kauffman, E. Fu, B. Lutz, and P. Yager, "Visualization and measurement of flow in two-dimensional paper networks.," *Lab Chip*, vol. 10, no. 19, pp. 2614–2617, 2010.

[160] B. R. Lutz, P. Trinh, C. Ball, E. Fu, and P. Yager, "Two-dimensional paper networks: programmable fluidic disconnects for multi-step processes in shaped paper," *Lab Chip*, vol. 11, no. 24, p. 4274, 2011.

[161] Y. Fan, H. Li, Y. Yi, and I. G. Foulds, "Laser micromachined wax-covered plastic paper as both sputter deposition shadow masks and deep-ultraviolet patterning masks for polymethylmethacrylate-based microfluidic systems," *J. Micro/Nanolithography, MEMS, MOEMS*, vol. 12, no. 4, p. 049701, 2013.

[162] G. Chitnis, T. Tan, and B. Ziaie, "Laser-assisted fabrication of batteries on wax paper," *J. Micromechanics Microengineering*, vol. 23, no. 11, p. 114016, 2013.

[163] J. A. Lounsbury, N. Coult, D. C. Miranian, S. M. Cronk, D. M. Haverstick, P. Kinnon, D. J. Saul, and J. P. Landers, "An enzyme-based DNA preparation method for application to forensic biological samples and degraded stains.," *Forensic Sci. Int. Genet.*, vol. 6, no. 5, pp. 607–15, Sep. 2012.

[164] W. Zhang, S. Lin, C. Wang, J. Hu, C. Li, Z. Zhuang, Y. Zhou, R. A. Mathies, and C. J. Yang, "PMMA/PDMS valves and pumps for disposable microfluidics.," *Lab Chip*, vol. 9, no. 21, pp. 3088–94, Nov. 2009.

[165] Y.-C. Hsu and T.-Y. Chen, "Applying Taguchi methods for solvent-assisted PMMA bonding technique for static and dynamic micro-TAS devices.," *Biomed. Microdevices*, vol. 9, no. 4, pp. 513–22, Aug. 2007.

[166] C.-W. Wei, J.-Y. Cheng, and T.-H. Young, "Elucidating in vitro cell-cell interaction using a microfluidic coculture system.," *Biomed. Microdevices*, vol. 8, no. 1, pp. 65–71, Mar. 2006.

[167] G. Pozza, S. Kroesen, G. Bettella, A. Zaltron, M. Esseling, G. Mistura, P. Sartori, E. Chiarello, M. Pierno, C. Denz, and C. Sada, "T-junction droplet generator realised in lithium niobate crystals by laser ablation," *Optofluidics, Microfluid. Nanofluidics*, vol. 1, no. 1, pp. 34–42, Jan. 2014.

[168] C.-H. Yang, K.-S. Huang, and J.-Y. Chang, "Manufacturing monodisperse chitosan microparticles containing ampicillin using a microchannel chip.," *Biomed. Microdevices*, vol. 9, no. 2, pp. 253–9, Apr. 2007.

[169] S. Xing, R. S. Harake, and T. Pan, "Droplet-driven transports on superhydrophobic-patterned surface microfluidics.," *Lab a chip_Suppliment*, vol. 11, no. 21, pp. 3642–8, Nov. 2011.

[170] D. Snakenborg, H. Klank, and J. P. Kutter, "Microstructure fabrication with a CO 2 laser system," *J. Micromechanics Microengineering*, vol. 14, no. 2, pp. 182–189, Feb. 2004.

[171] T.-F. Hong, W.-J. Ju, M.-C. Wu, C.-H. Tai, C.-H. Tsai, and L.-M. Fu, "Rapid prototyping of PMMA microfluidic chips utilizing a CO2 laser," *Microfluid. Nanofluidics*, vol. 9, no. 6, pp. 1125–1133, May 2010.

[172] Z. K. Wang and H. Y. Zheng, "Investigation on CO2 laser irradiation inducing glass strip peeling for microchannel formation.," *Biomicrofluidics*, vol. 6, no. 1, pp. 12820–12831, Mar. 2012.

[173] H. Jordan, M. Wegner, and H. Tiziani, "Highly accurate non-contact characterization of engineering surfaces using confocal microscopy," *Meas. Sci. Technol.*, vol. 9, pp. 1142–1153, 1998.

[174] E. C. Teague, F. E. Scire, S. M. Baker, and S. W. Jensen, "Three-dimensional stylus profilometry," *Wear*, vol. 83, pp. 1–12, 1982.

[175] L. Deck and P. de Groot, "High-speed noncontact profiler based on scanning white-light interferometry.," *Appl. Opt.*, vol. 33, no. 31, pp. 7334–7338, 1994.

[176] K. W. Oh and C. H. Ahn, "A review of microvalves," *J. Micromechanics Microengineering*, vol. 16, no. 5, pp. R13–R39, May 2006.

[177] T. Laurell and J. Nilsson, "Cell and Particle Separation and Manipulation Using Acoustic Standing Waves in Microfluidic Systems," in *Handbook of Capillary and Microchip Electrophoresis and Associated Microtechniques*, 3rd ed., J. P. Landers, Ed. Boca Raton, FL, USA: CRC Press, Inc., 2008, p. 1229.

Chapter 2. The μSCAPE System: 3-Dimensional Profiling of Microfluidic Architectural Features Using A Flatbed Scanner

2.1 Overview and Introduction

The concepts, methods, capabilities and technologies associated with a 'lab-on-a-chip' have evolved dramatically since 2001 when a journal under the very name was launched[1]. From a single channel, single-function microchip to highly integrated systems[2], and silicon- or glass-based microstructures to disposable polymer or paper based microchip[3], 'lab-on-a-chip' systems have begun to tackle real-world analytical problems in a diverse spectrum of fields ranging from pathogen detection[4] to clinical diagnosis[5], [6], and even into forensic genotyping[7], [8]. As the technologies of the lab-on-a-chip embrace the outside world with more and more devices productized and commercialized[9][10], the quality control of the microdevice's feature becomes a significant issue that is critical to the success of the product.

In order to examine the geometric quality of the microdevices the 3D profile of the target structures needs to be obtained. The most commonly used contact profiling techniques such as stylus profilometry [11] and atomic force microscopy (AFM) [12] can provide remarkably high resolution for the examination of the microstructure's geometric properties, however the contact-based profiling procedure makes it impossible to detect the concealed inner part of the microstructures such as an enclosed channel. The relatively low scanning rate and small detection area make these techniques less desired for the inspection

of the microdevices with relatively large areas consisting of multiple functioning domains, not to mention the numerous quality control tasks in mass production.

Alternatively, being non-contact and non-invasive, various types of optical 3D profiling methods have been reported. The major types of optical profiling methods include (1) confocal scanning microscopy (CSM) [13]and (2) scanning white light interferometry (SWLI) [14]. Confocal scanning microscopy uses a photomultiplier tube(PMT) through a pin hole to solely accept the light signal from the focus point and can achieve sub-micron resolution, but the acquisition of the whole 3D profiles of the target object requires the point-by-point scanning in all x, y and z directions which is not suitable for high through-put inspections. SWLI, on the other hand, exploits the interference between the reflected light waves from the target substrate and the reference light waves, and is able to achieve vertical resolution down to nanometer scale. The SWLI uses widefield microscopic imaging onto a charge-coupled device (CCD) to simultaneously cover the region of interest and needs no z direction scanning, thus has much faster data acquisition rate than CSM. However when dealing with surfaces with high gradient and steep angles errors may be generated on the edge[15]. Although CSM and SWLI fundamentally differs in principles, they both use typical objective-PMT/CCD coupled microscopic optical system and the lateral range of inspection is limited to several millimeters. Besides, the investment of the whole set of equipment is nontrivial

All of these techniques have their individual pros and cons in terms of data acquisition rate, vertical/lateral resolution, and suitability for different applications[16]. However, due to the sophistication of microscale profilometry, these methods require delicate, sophisticated, high-cost instrumentation and well-trained personnel, even though

manufacturing costs may have been reduced through mass production. The capitalization of labor and instrumentation for quality control may come with a significant financial burden, one beyond the resource capabilities of start-up companies and like innovators. Furthermore, the limited field of view (FOV) that can be probed by these methods (normally on the order of tens of mm^2) makes them less desirable for the inspection of the microdevices with relative large areas and/or consisting of multiple domains. This is exacerbated when quality control inspection is required during mass production.

In this report, we describe our findings on the use of an office flatbed scanner to detect the 3D profiles of microfluidic structures. In 2010, we reported that, by measuring the absorbance of dye solution after it passed through the microchannels, the quality of the channels could be easily determined spectroscopically[17]. Here, we exploit absorbance of dye-filled channels again, but in a very different way. The fundamental principle here is the measurement of the absorbance of a dye solution while it is still in the microfluidic architecture. This process can be summarized in three steps: (1) filling of the microstructures with the colorimetric dye solution that has characteristic absorbing wavelength. In this work, we exploited allura red solution; (2) scanning for the acquisition of the image of the microfeatures; and (3) for each pixel of the microstructure image, the depth of the structure is calculated based on Lambert-Beer's law using the absorbance of that pixel and the pre-determined extinction coefficient of the dye solution. The concept of profile detection by Lambert-Beer's law has been validated in Broadwell et al.'s work[18] in which they used the absorbance of a dye to optically-represent the dimensions of a microfluidic structure. However, their approach required reasonably complex equipment (a bright-field microscope and a monochromatic CCD) and suffered limitations

in terms of the relatively small FOV that could be interrogated. A flatbed scanner, when used as described here, costs a fraction of that for a basic microscope, and has a built-in CCD. However, in addition to that, the scanner-acquired images present two other major advantages.

The first advantage is the built-in digital filter function in scanned image. Because each pixel of the CCD has a so called Bayer filter structure[19] that divides one pixel into four smaller grids assigned to the three sensing abilities of red (1 grid), green(2 grids) and blue(1 grid). During the scanning process, the light detected in each pixel is actually detected by these three types of sensing grids and consequently each type of sensing grid generates a value as the digital representation of the intensity of the light within that color range. Thus for each pixel there are three values generated and stored in red, green and blue (RGB) spaces to represent a specific color. This is the basic principle of color detection and representation in digital imaging. Exploiting the combination of the three values in RGB space has enabled scanner-based detection with various types of colorimetric assays including inorganic ions[20], [21], organic compounds[22] and bacterial identification[23]. Additionally, the generation of the RGB values described above can be regarded as a digital filtering process in which the incident light is filtered into three monochromic wavelength ranges corresponding to the red, green and blue light. The digital filtering mechanism enables the monochromatic absorbance measurements to be acquired without additional physical filtering. Measurement of absorbance or optical density (OD) in a single RGB channel enables quantitative analysis in a number of different formats, and has been applied to bacterial susceptibility testing[24], diffusion-based dynamics of dye solution[25] and scanner-based quantitative detection of polyphenol[26].

The second advantage of a flatbed scanner as a detection tool is its relatively large FOV. By moving the line CCD across the entire scanning field, a very large, high-resolution detection window can be interrogated (at the tens of gigapixels level); this is technically (and economically) unrealistic to achieve using a single CCD chip. The area of the FOV presented by a scanner is on the order of hundreds of cm^2, with a resolution down at the 2 μm level [27]. This allows the scanner to interrogate, simultaneously and in parallel, a large number of bioassay well-plates [27].

In this paper, we demonstrate the power of a conventional office scanner to examine the qualities of microfluidic structures including: (1) laser-ablated PDMS channels, (2) polyester-toner (PeT) film-derived chambers and, (3) micro-well arrays fabricated either in glass by HF etching or in PDMS by laser-ablation. The capabilities (and limitations) of a flatbed scanner for evaluating the geometric parameters of microscale features and quantitatively defining their uniformity are demonstrated.

2.2 Materials and methods

All reagents, unless specifically indicated, are all purchased from Sigma-Aldrich (Oakville, ON).

2.2.1 Scanning mode selection

"Reflective" is the most commonly used scanning mode for the scanning of documents, photos and majority of the previously reported analytical applications, in which the light source and the detector are on the same side of the object. However in this mode,

the detected incident light in the absorbance calculation is the reflected light from the white pad above the object, which may not have a uniform reflection rate due to the imperfectness of the pad surface. In addition because the detector and the light source are on the same side there is a position shift between them, so if the object has significant thickness there is a problem of shadow. While in "film scan" mode, the detector and the light source are on the different sides of the object, which ensures that the incident light is directly from the uniform light source, and no shadow will be detected since the beam is right below the detector (**Figure 2-1**).

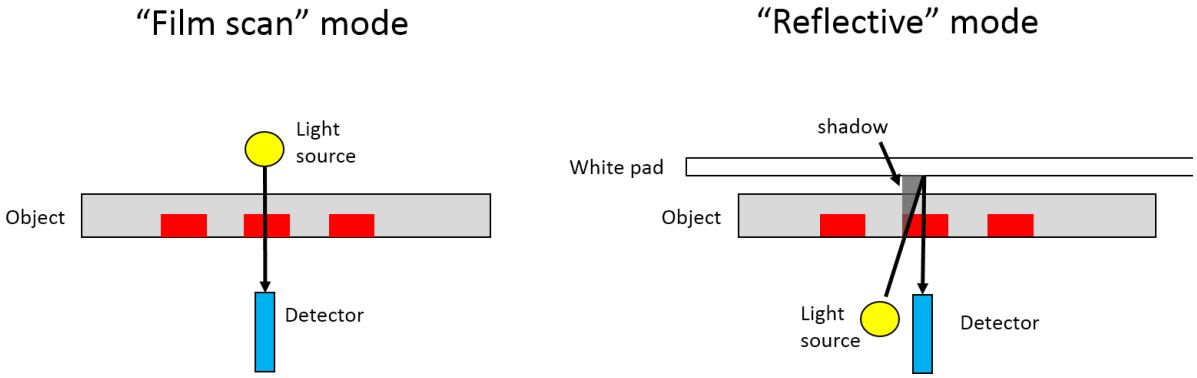

Figure 2-1. The light-detector setting of different scanning modes

2.2.2 Preparation of the dye solution

10X TE (pH 7.5)-glycerol mixture was used as the solvent for the dye solution to minimize evaporation and the difference in refractive indices (RI) between the dye solution and glass/PDMS.

Allura red solution was prepared by dissolving in 10X TE buffer-glycerol mixed solvent at desired concentrations (specified in following sections) as stock solutions for future use.

2.2.3 Fabrication of the microstructures

Standard channels for the determination of the extinction coefficient of the dye solution were fabricated by conventional photolithography and HF etching in glass. The mask was designed using AutoCAD and then printed in photographic film in high resolution (Thin metal parts, CO). Photoresist-chrome layers coated borofloat glass plate (Telic, Valencia, CA) was etched by HF solution (HF/HNO_3:200/30 (v/v)) after standard procedures of photolithography. The remaining photoresist and chromium on the plate were removed completely after the etching. The glass channels were dried by nitrogen purging and the depths were determined by stylus profilometry (KLA-Tencor, Milpitas,CA)

PDMS channels are fabricated by laser ablation into cured PDMS plate. Briefly, PDMS plates were prepared by mixing of monomer and curing reagent at mass ratio of 10:1 followed by oven heating at 70 ℃ for two hours. Channel are designed in CorelDRAW 10.0 (Corel Corporation, Ottawa, Canada), and then ablated by VersaLaser VLS 3.50 with 50W CO_2 laser source (Universal Laser System Inc.) into PDMS plate. Under the vector mode, at speed level of 20% and 1000 point per inch (PPI), power settings of 30%, 60% and 90% were used to make channels with different depths. Defocused laser beam was used to increase the smoothness of the wall of the PDMS channels[28]. PDMS was ablated by one pass of the laser beam at defocus height of 3.5mm. The fabricated

PDMS channels were cleaned by methanol wash and dried by nitrogen purge. Access holes are punched at both end to be the inlet and outlet of the channel.

Round PeT chambers are fabricated following the previously described procedures [29] with designed volume of 2.5, 5, 10, 20, 30, 40 and 50 μL. Briefly, polyester films (CG5000, 3M) were printed with black toner (HP C-4127X) and then cut by laser cutter to form the body of the chamber, followed by lamination at 130 ℃ with polyester film to form an enclosed chamber.

Micro well arrays are fabricated in two different ways:

(1) HF etching in glass using the methods described above. Designed diameter of the well was 80 μm and the etched three different depths were achieved at about 7, 10 and 14 μm, measured by stylus profilometry. Another array containing micro wells of different designed diameters (70, 80 and 90 μm) was also fabricated with identical etching depth about 10 μm

(2) Laser single-pulse ablation in PDMS. Briefly, the power density of the laser cutter was set to 200 PPI and parallel lines with spacing of 150 μm were ablated into the cured PDMS plate at speed 100%, and three power settings were used at 0.5%, 1% and 1.5% for increasing depth of the micro wells

2.2.4 Scanning settings and image analysis

Images were scanned by EpsonV600 in sRGB space and the scan mode was selected to "film scan" instead of commonly used "reflective" mode to avoid shadow and reflection problem discussed in 2.2.1.

The scanned images were saved in TIFF format with 48 bit RGB color space. The saved images were imported into ImageJ and split into three color spaces (Red, Greed and Blue, each space is in 16 bit format) for the subsequent calculation of absorbance.

The absorbance of the dye-filled microstructures are determined using $A=\log(I_0/I_t)$, in which I_0 and I_t are both in the unit of 16 bit grayscale(between 0 to 65535) and correspond to the intensity of the incident light and the transmitted light, respectively. The calculation of each point's absorbance and profile plotting was conducted in Matlab R2013b (MathsWorks, Natick, MA).

2.2.5 Determination of extinction coefficient

The extinction coefficient of the dye solution was determined by measuring the absorbance of (1) different thickness of dye solutions at fixed concentration, or (2) different concentration of dye solutions at fixed thickness.

To obtain absorbance-depth standard curve, glass standard chambers with different depths (8, 16, 27, 49, 89 and 161 μm) were filled with 6mM allura red solution, followed by scanning and image analysis in blue space.

To obtain absorbance-concentration standard curve, 27 μm glass standard chambers were filled with different concentrations of allura red solution (1.5, 3, 6, 12, 24 and 48 mM), followed by scanning and image analysis in blue space.

Blank solvent was used to fill the channel as the reference for the calculation of absorbance.

2.2.6 Examination of the cross section of laser-ablated PDMS channels

The laser ablated PDMS channels were reversibly bonded onto a 1.1mm glass plate (Corning, NY) and then filled with 6mM alura red solution. The filled channels were scanned at 12800 dpi and the depth of channel at each pixel was calculated using the absorbance of that pixel and the extinction coefficient determined in section 2.2.5. The cross-sectional profile of the channel was reconstructed, then compared with the actual profile of the channel examined by cut-and-check under microscope.

2.2.7 Examination of the volume of the PeT chambers

The PeT chambers were filled with 1.5mM allura red solution. Multiple filled chambers in a single device were scanned together at one time followed by image analysis, using blank solvent as the reference. The resolution of the scanning was 1200 dpi. The volume of each chamber was calculated by adding up all the depths of the pixels of the chamber image and then multiplied by the area of a single pixel.

2.2.8 Examination of the volume of the micro well array

The micro well array in glass was filled with 48mM (for depth of 7 μm and 10 μm)or 24mM (for depth of 14 μm) allura red solution and pressed against a PDMS plate to be sealed, and the excessive dye solution was absorbed away by Kimwipe tissue. The micro well array in PDMS was filled with 48mM (for power level of 0.5% and 1%) or 24mM (for power level of 1.5%) and pressed against a glass plate to be sealed, and the excessive dye solution was absorbed away by Kimwipe tissue.

The filled micro wells were scanned at 12800 dpi (2 μm per pixel) and analyzed using blank solvent as the reference. The volumes of all the micro wells in the array were calculated and the distribution of the volume of the examined array was obtained

2.3 Results and Discussion

2.3.1 Solvent selection

In the selection of the solvent for the dye solution, both water and glycerol-water mixture are tested. The calibration curve obtained in both solvent shows good linearity and the allura red in 10X TE has slightly larger coefficient of extinction (**Figure 2-2,** A&B). However, the profile of the channels filled with solvent of non-matching RI (water) or matching RI (glycerol-water mixture) show significant differences (**Figure 2-2,** C). The bottom part of the channels are quite similar between these two solvents, but at the channel's wall the profile of the aqueous solvent-filled channel presents abnormal bright and dark strips, while the glycerol-water mixed solvent gives a normal cross-sectional

profile (**Figure 2-2,** D & E). The reason for the distorted profile using water solvent might be the reflection of the light at the non-perpendicular interface between the aqueous solvent and the glass due to the unmatched RI. In addition, the glycerol-water solvent provides another advantage that it has a much slower evaporation rate, which is more desired in keeping a consistent concentration of the dye solution during scanning. So we used glycerol-water mixed solvent for all the following profiling tests.

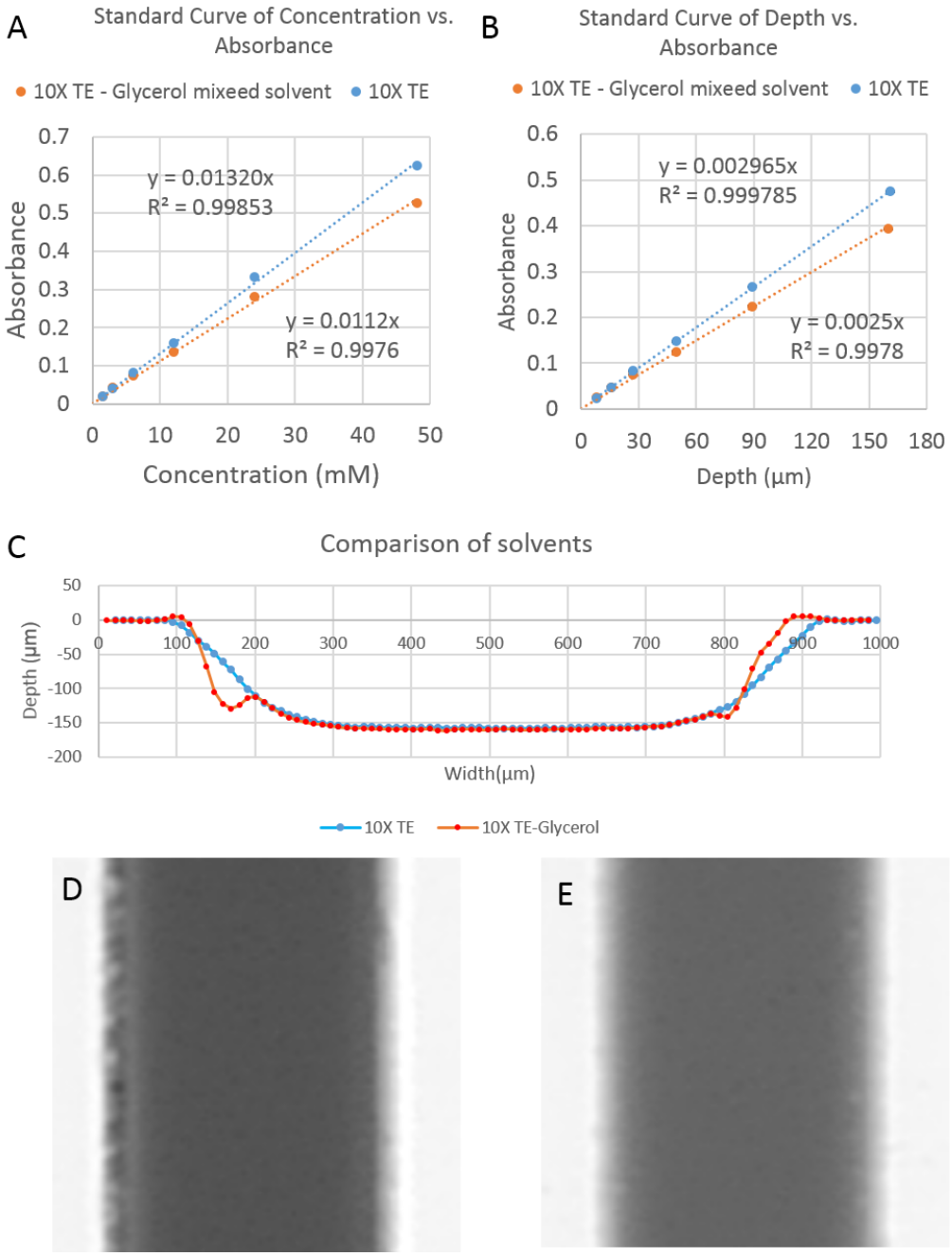

Figure 2-2. The effect of solvent on the scanned image. (A) The calibration curve of absorbance vs. concentration in either 10X TE and mixed solvent. (B) The calibration curve of absorbance vs. depth in either 10X TE and mixed solvent. (C) The comparison of the profile of the HF-etched glass channel's cross-section in either 10X TE and mixed solvent. (D-E) The scanned image of glass channel filled with either 10X TE (D) or mixed solvent (E).

2.3.2 Determining the extinction coefficient

The scanned images of the channels filled with allura red dye solution shows different values in each of the RGB spaces (**Figure 2-3**). The red space is almost identical to the white background, indicating that this dye absorbs little or no light in the wavelength range of red light. However, in the blue and green space, the fluidic channel shows an increasing grayscale as the depth increases. Blue space was selected for the absorbance test because of the better linearity.

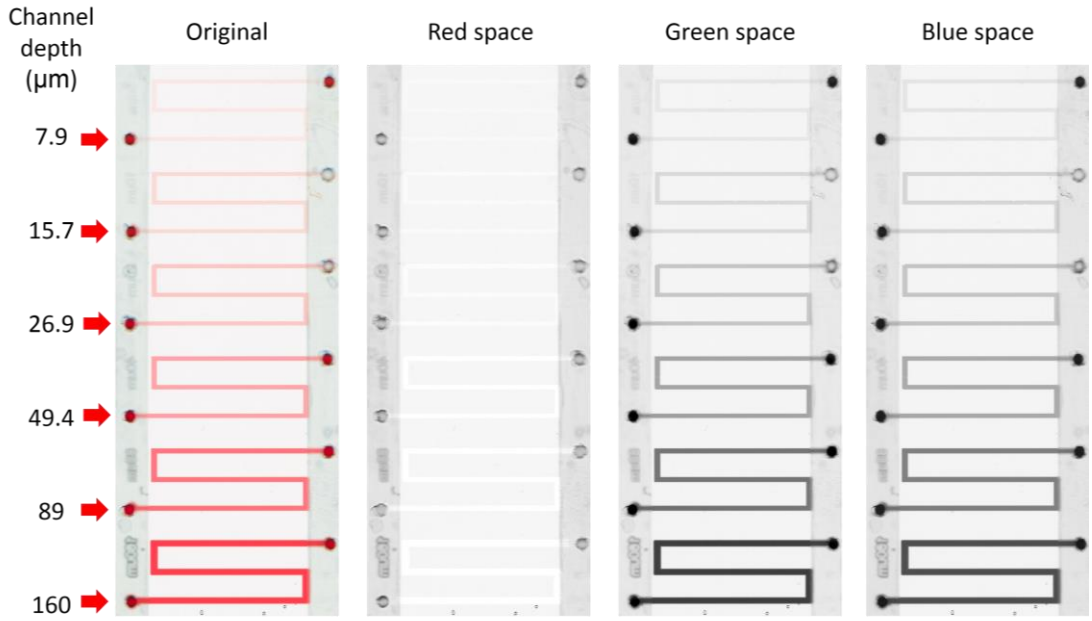

Figure 2-3. The scanned image of the standard glass channels filled with allura red solution (6mM in 10XTE-glycerol mixed solvent). From left to right: the original image, the split images in red, green and blue space.

In order to create calibration curves, absorbance of either a fixed concentration of dye in standard channels (with known depths), or a series of standard solutions (at known

concentrations) in a channel with fixed depth, are measured. When the data are plotted in blue space, they show a linear relationship between channel depth and the allura red dye absorbance up to a value of roughly 0.6 (**Figure 2-4**). This proportionality of the absorbance to both the dye concentration and the optical length verified the applicability of Lambert-Beer's law in the scanner-based absorbance measurement, and the subsequent extinction coefficient for allura red was calculated to be 0.00052 $mM^{-1}\mu m^{-1}$. As a result, the allura red dye concentration could be selected based on the estimated structure depth and the already determined extinction coefficient in **Figure 2-4** to assure the proper absorbance is below 0.6

After establishing the appropriate calibration curve, the feature depth at any particular micro-locale in a given architecture can be back-calculated based on the absorbance value at that point using the concentration of the dye used and the associated extinction coefficient. The **M**icrofluidic **SCA**nner-based **P**rofile **E**xamination (μSCAPE) method has been established.

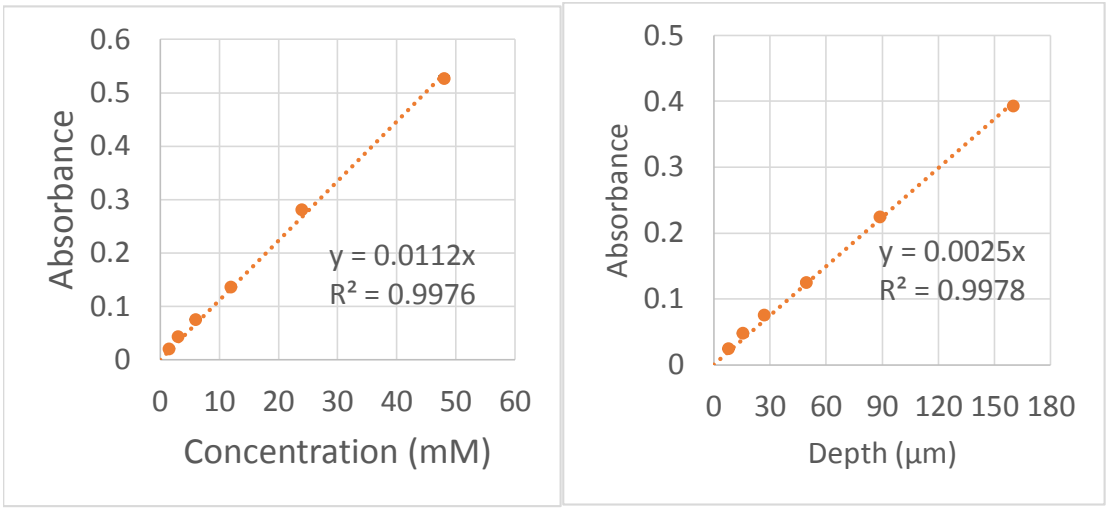

Figure 2-4. The calibration curve of absorbance vs. concentration (left) and depth (right) of alura red solution in the blue space (n=3).

2.3.3 Cross-sectional examination of PDMS channels

To test the capability of the µSCAPE system for defining 3D architecture, we evaluated microchannels that had been laser-ablated in PDMS. PDMS is the most commonly used polymer in the microfluidic community, and microstructures can be fabricated into this PDMS typically through 'pour and cure' molding, but also via laser ablation. Molded PDMS microstructures present fine and uniform features but require multiple steps for masking and lithography, and require generation of a new master when changing the design. Laser ablation, on the other hand, is a simple, faster process, requires no masking, but creates more irregular features in comparison with molding[30]. Examination of the laser-ablated PDMS structures is difficult to achieve with stylus profilometry (due to the elasticity of the polymer), and the large slope from the channel edge to the center of the cone-shaped channel can lead to ambiguities when using scanning white light interferometry [15]. Moreover, the commonly used 'cut-and-check' method[30]

is limited as it can only interrogate the cross-section at the cutting plane, leaving the analysis devoid of a thorough, 3D view of the structure(s). Finally, the 'cut-and-check' method causes irreversible damages to the PDMS microstructures and voids the possibility of future use, which is unnecessarily wasteful in an era where green chemistry is gaining increased attention.

Channels created by laser ablation at different power settings were evaluated with the μSCAPE system and compared with the actual profile examined under bright-field microscopy (**Figure 2-5**A). It is obvious that the cross-sectional profiles obtained with μSCAPE (red line) are in good agreement with the bright field micrographs. This agreement validated the feasibility and accuracy of the μSCAPE profiling in two dimensions. However, as a result of the large detection area of the scanner, we were also able to check the variation of the cross-sectional profile over a longitudinal distance of the channel (2.5 cm). Scanning three different 2.5cm long PDMS channels, each ablated at different laser power settings, we were able to assemble a 3D profile for each from a series of 12,500 cross-sectional slices. **Figure 2-5**B shows a set of 16 of those slices evenly-spaced over the length of that channel to compose a longitudinal 3D profile. Despite that fact that this is a low resolution image (16 of 12,500 slices), differences in the profiles are clear, specifically: (1) deeper channels have more dimensional variation than shallower channel, which is due to the differences in the applied laser power, and (2) there is more variation in the side wall of the channel than there is in the floor. This may be explained by the mode of ablation (a single stroke of the laser beam), where the higher side wall variation may be attributed to the power fluctuation in the dispersion region of the

Gaussian-shaped focal spot of the laser. It is clear that the larger the number of slices used to re-construct the channel dimensions, the higher in resolution the image will be.

In comparison with direct microscopic interrogation, the scanner-based profiling is more favorable in two ways: (1) the method is completely non-invasive and the microdevice remains functional for use after examination, and (2) one can quickly check the cross-sections of the microstructure at any point in any orientations after the image is acquired. It is noteworthy that the μSCAPE approach can interrogate relatively long channel distances, as this this limit is set by the scanner 'scanning window' which, in our case, is 250mm by 8mm. For proof of principle here, we chose three 25mm long channels scanned simultaneously, as this is more relevant to the feature scale of common microfluidic devices.

A

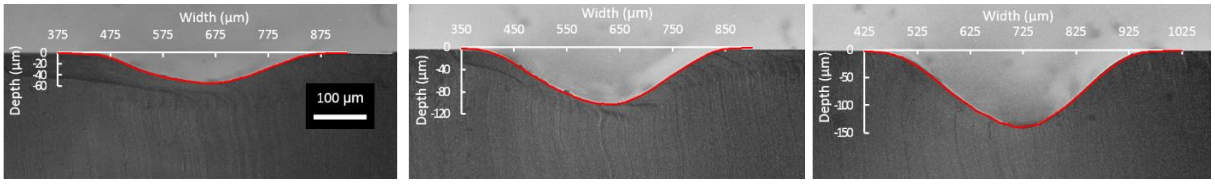

B

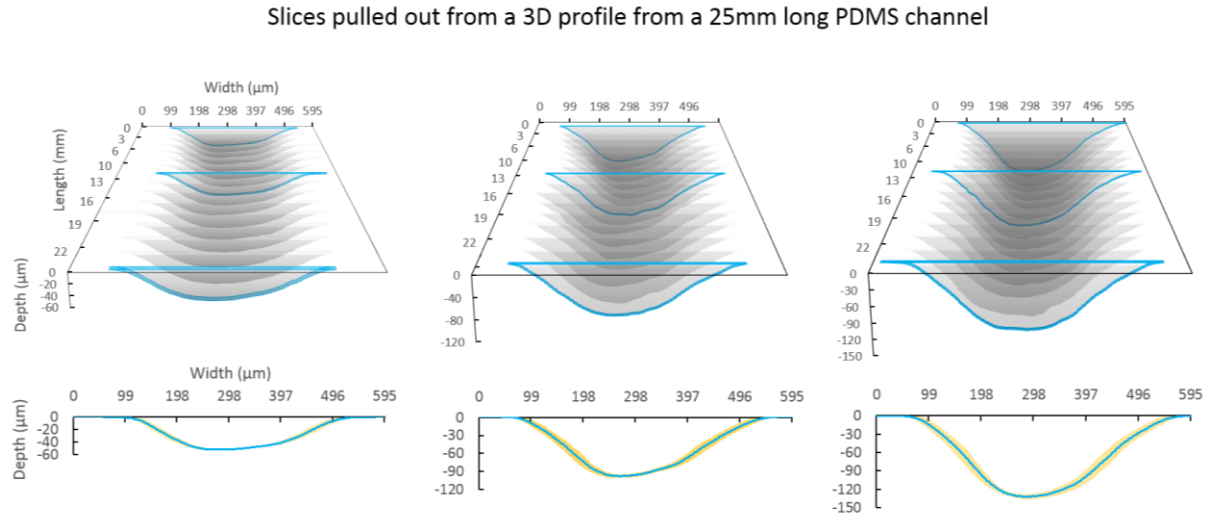

Figure 2-5. The examination of the cross-section of laser-ablated PDMS channels. (A) The comparison of the scanner-acquired profile (red) and the actual profile revealed by microscopy. (B) The inspection of the longitudinal cross-section variation of 25mm PDMS channels ablated at different power setting. The interval of ±1 standard deviation of the 16 slices of cross-sectional profiles are shown in yellow shade.

2.3.4 Examination of the volume of the PeT chamber

We have recently reported on a new fabrication method for multilayer microdevices using laser printed, cut and laminated (PCL) polyethylene terephthalate with toner-based bonding[31]. These polyethylene-toner (PeT) devices represent an emerging low-cost substrate for fast and convenient fabrication using fairly common office or lab equipment; a number of applications have been addressed with PeT microdevices, including microchip

electrophoresis[32][33], DNA extraction[34] and centrifugal microfluidics[29]. However, the volume of the PeT chamber may be subject to variation due to the expansion of the polyester film during the heat lamination step; this is of particular concern with larger chambers (>5 mm diameter) that have the potential to deform due to a 'sagging' effect in the capping layer, which ultimately affects accuracy in achieving a desired volume. While the theoretical chamber volume can be defined by stylus profilometry or SWLI prior to lamination of the capping layer, there are two obvious limits to this approach. First, these methods cannot be used to probe a closed chamber. Thus, they provide no information about the chamber after it has been capped and laminated, and no empirical volume measurement can be easily made to assure that no feature deformation has occurred. Second, larger microdevices (e.g., CD-sized centrifugal microfluidic devices) are more challenging for stylus profilometry or SWLI, as the area that can be probed by these methods is limited. It is in this respect that the μSCAPE approach addresses a significant need.

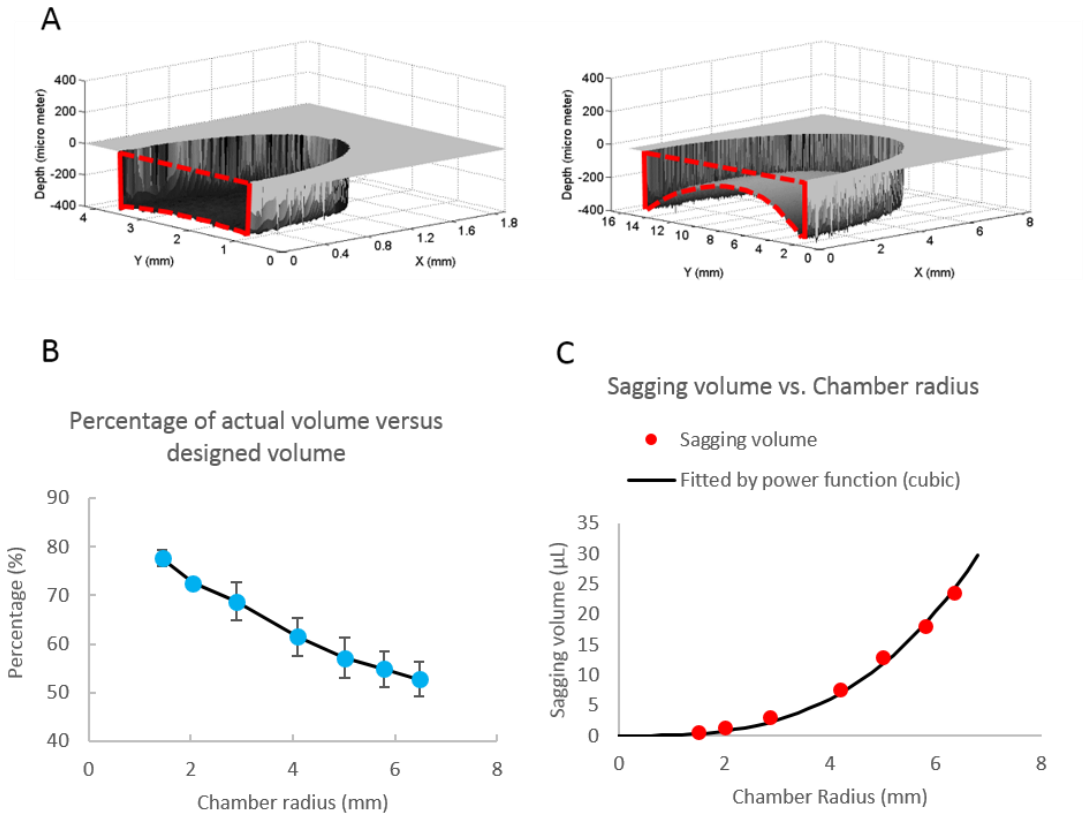

Figure 2-6 The volume determination of PeT chambers. (A) the cap deformation of a d=2.5mm PeT chamber (left) and a d=13mm PeT chamber. The curve part of the red dash line in the cross-sectional cut shows the sum of the deformation of both the floor and the ceiling of the chamber. (B) The actual volume as the percentage of the designed volume (n=3). (C) The decreased volume of the chamber versus the radius of the chamber. (n=3)

The 3D profile in **Figure 2-6**A shows the visualization of a deformed chamber surface using the μSCAPE approach. Inherent in the optical length (absorbance) reconstruction is the assumption that the opposing surface is flat. This is certainly the case when profiling the glass or PDMS channels described in the previous section, where at the opposite surface of the channel (a glass plate for the PDMS channel or a PDMS plate for the glass channel) can be assumed to be, indeed, flat. However, in the case of a post-

laminated PeT chamber, there is possibility for both the capping (ceiling) and base (floor) layers to be deformed. The reconstructed model shown in **Figure 2-6**A is actually the sum of the deformation for both the upper and lower surfaces. While this may not accurately reflect the 'true' inner surface profile of the chamber, the volume determined remains not affected since it is based on the sum of the total optical length at each pixel within the microstructure, thus can still be accurately calculated.

The μSCAPE-calculated volumes are given as the percentage of the theoretical volume expected based on the feature design. **Figure 2-6**B clearly shows that, not surprisingly, as the radius of the chamber increases, the deformation (sagging) of the chamber cap becomes more severe; for the largest chamber in this series, the actual volume is only ~50% of the volume predicted by design. This trend with volume deviation vs. chamber size is anticipated since the designed volume is proportional to the square of radius (r^2) but the decreased volume (what we term the sagging volume) is proportional to the cubic of radius (r^3) (**Figure 2-6**C and Section 2.3.5).

2.3.5 Theoretical relation between sagging volume and chamber radius

Assuming the one-dimensional expansion of the polyester film under heating is anisotropic with a constant ratio α, supposing two chambers with radius r_1 and r_2, then the ratio of the these two chamber's new cap areas after the expansion, A_1/A_2 is:

$$\frac{A_1}{A_2} = \frac{2\pi(r_1)^2(1+\alpha)^2}{2\pi(r_2)^2(1+\alpha)^2} = \frac{(r_1)^2}{(r_2)^2} \qquad (1)$$

Assuming the shape of the sagged surface is a spherical cap, then the surface ratio could also be expressed as:

$$\frac{A_1}{A_2} = \frac{2\pi h_1 r_1}{2\pi h_2 r_2} = \frac{h_1 r_1}{h_2 r_2} \qquad (2)$$

Where h_1 and h_2 are the height of the spherical-cap shaped sagged volume of chambers. Combining (1) and (2),

$$\frac{r_1}{r_2} = \frac{h_1}{h_2} \qquad (3)$$

The ratio of the sagging volumes (i.e. the volumes of the concave spherical caps) of these two chambers is:

$$\frac{V_1}{V_2} = \frac{\frac{\pi}{6} h_1 (3{r_1}^2 + {h_1}^2)}{\frac{\pi}{6} h_2 (3{r_2}^2 + {h_2}^2)} \qquad (4)$$

After proper transformation giving eq.(3), eq. (4) becomes:

$$\frac{V_1}{V_2} = \frac{{r_1}^3}{{r_2}^3} \qquad (5)$$

Which shows that the decreased volume is proportional to r^3. However for a non-sagging cylinder chamber with fixed height the designed volume is only proportional to r^2. This explains the trend that the deviation of the volume from the designed volume becomes larger and larger as the radius of the chamber increases, and the reduced volume is proportional to the cubic of chamber radius shown in **Figure 2-6**C.

2.3.6 The 3D profiling of array of micro-wells

One of the most appealing features of analytical microfluidic systems is the potential to exploit small features for higher throughput bioassays, and subsequently generate large amounts of data. The integration of thousands or even millions of assays on a single microdevice has been realized by micro well arrays, and a number of diverse applications have been reported including DNA quantitation[5], [35]–[37], drug screening[38] and single cell genotyping[39], [40].

To obtain accurate and reproducible results from micro-well arrays, it is essential to assure that certain critical geometric parameters, like micro-well volumes, are constant; e.g., in the determination of the DNA concentration by digital PCR[35][5][41]. In large arrays, it is important to define the well-to-well variation in volume, as well as identifying 'bad' wells whose volume exceeds some specifications (i.e., standard deviation) that have been determined to be acceptable *a priori*. However, if only inspected by random low-number sampling of select micro-wells in the large micro-well array, the probability of identifying the 'bad' wells or small-fraction sub-groups is low. This can be solved by a comprehensive, population level inspection of the entire array. We demonstrate that the μSCAPE approach allows this to be carried out on micro wells fabricated by two different methods; conventional HF etching in glass and laser ablation in PDMS. Moreover, the scanner-based profiling effectively identifies wells in an array that fall outside the accepted volume standard deviation.

2.3.7 Comparison of different fabrication methods

The 3D scanner-based profiling of micro-wells involves features that are significantly smaller than those described in the previous sections. As a result, the resolution needs to be much higher than 1200 dpi used earlier in the scanning of the PeT chambers and, specifically in this case, 12800 dpi. Associated with the higher resolution is an increased noise level, which may mask certain features. In order to improve the S/N ratio to more effectively reveal the profiles of the micro-wells, multiple scans were carried out followed by an averaging of the profile. **Figure 2-7**A&B show the 3D profiles of micro-wells in HF-etched glass and laser-ablated PDMS, with averaged images resulting from 1, 4 and 9 scans. It is noteworthy that the surface noise (roughness) of the well profile in a single scan is too large to correctly reveal the details of the structure, and that multiple 3D scans of each micro-well array were needed to average out the noise. Theoretically, the average of N scans will give a reduce the noise by a factor of $\sqrt{N}$. It is obvious that the 4-scan-average is much smoother than the single-scan profile, and the 9-scan-average enhances it further, but without significant improvement relative to 4-scan average. Therefore, to adequately balance the 'scanning time' with the resultant 'profile quality', 4 scans is used for analysis. Due to the differences in these fabrication modes, the shape of the HF-etched glass micro-wells appears to be a basin-shaped structure with a flat bottom, while laser-ablated PDMS micro-wells shows a cone-shaped pit.

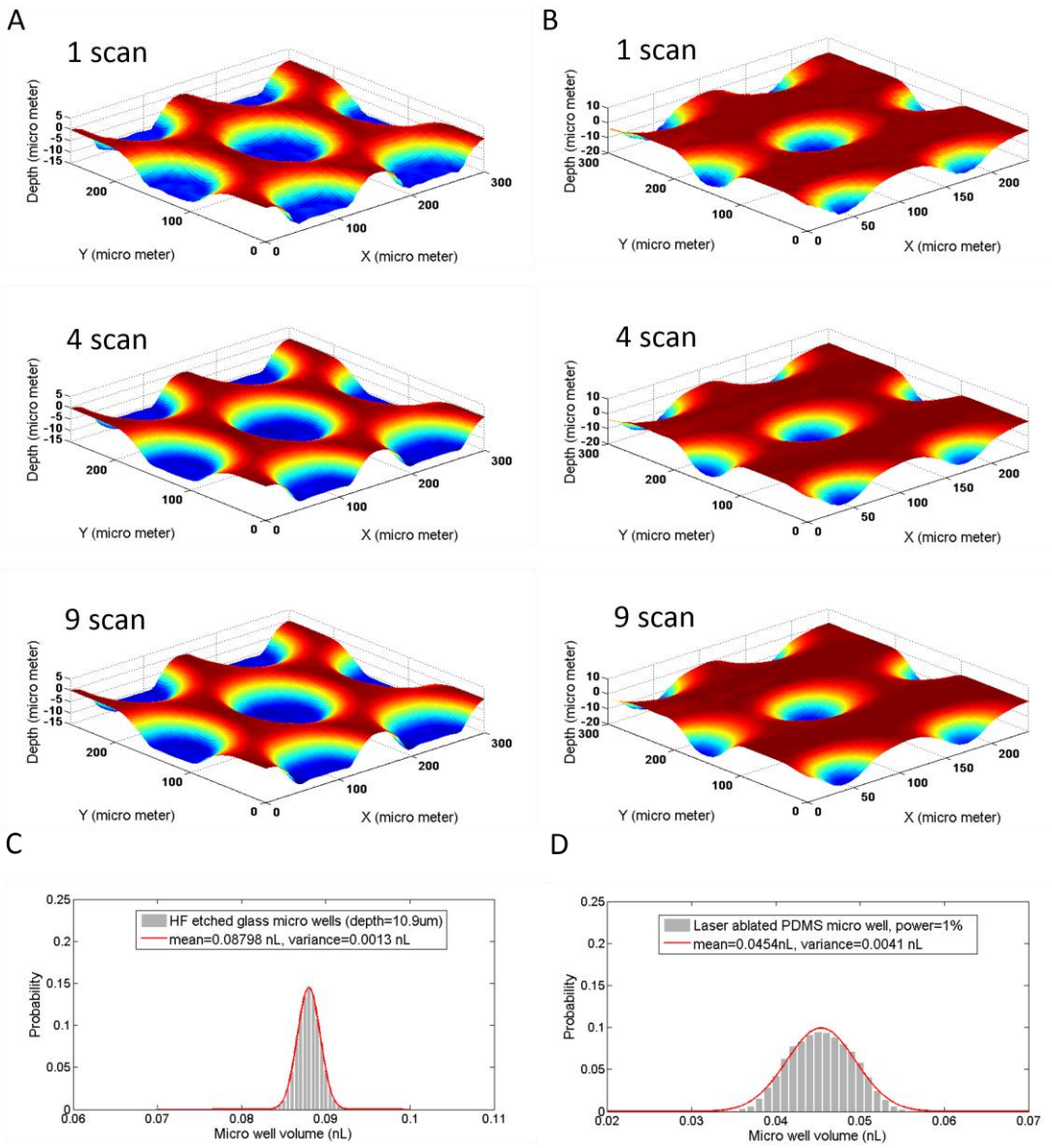

Figure 2-7. The volume distribution of micro wells in HF-etched glass and laser-ablated PDMS. Samples of 3D profiles of micro wells in glass (A) and PDMS (B) obtained in single scan, 4 scans and 9 scans, from top to the bottom. The volume distribution of the glass and PDMS micro wells is shown in (C) and (D), respectively.

The volumes of 10,000 wells were calculated from the average of four 3D-scan profiles of the glass and PDMS micro-well arrays (**Figure 2-7**C&D). For glass micro-wells, the calculated volumes show a Gaussian distribution with a mean of μ=0.0880 nL

and variance of σ=0.0013 nL, while the laser-ablated PDMS micro-wells have a mean of μ=0.0454 nL and a variance of σ=0.0041nL. The apparent reduction in quality of the laser-ablated PDMS micro-wells might be attributed to the variation of focal distance across the substrate, and the variation of the output power of the laser pulse.

To further investigate the quality of these two methods, we fabricated micro-wells under different conditions. For HF-etched glass, we created micro-wells with three different depths, achieved by simply increasing the etching time (with same designed diameter of 80 μm), and for laser-ablated PDMS, micro-wells with three different depths were created by increasing the power output of the laser pulse. Both methods show increased variance of the volume as the well depth increases, but the coefficient of variance (percentage of variance/mean) decreases (**Table 2-1&Table 2-2**, and **Figure 2-8).**

Overall, the information revealed represents the first comprehensive whole-population-scale quality assessment of the volume distribution of the micro wells arrays, which also provides a useful guidance for the selection of fabrication conditions in order to control the quality of manufacturing.

Table 2-1. Volume distribution of glass micro wells with increasing HF etching depth

HF etched depth (μm)	6.8	10.9	14.4
Mean (nL)	0.0482	0.0880	0.1184
Variance (nL)	0.0011	0.0013	0.0014
Coefficient of variation	2.5%	1.5%	1.2%

Table 2-2. Volume distribution of PDMS micro wells with increasing laser power

Laser power (%)	0.5	1.0	1.5
Mean (nL)	0.0226	0.0454	0.0684
Variance (nL)	0.0023	0.0041	0.0048
Coefficient of variation	10%	9%	7%

The distributions of the different volumes of micro wells achieved by either HF etching or laser ablation is shown in **Figure 2-8.**

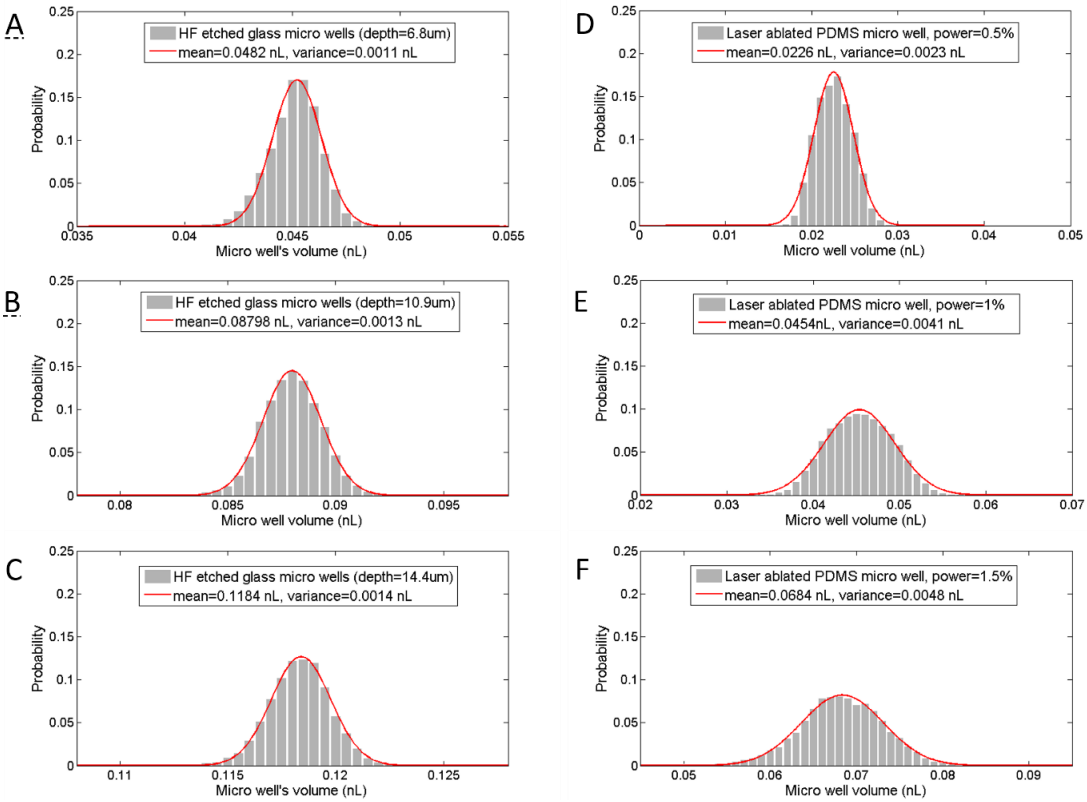

Figure 2-8. The distribution of different volumes controlled by fabrication processes. (A-C) glass micro wells with increasing HF etching time, giving depths of 6.8, 10.9 and 14.4µm, respectively. Depths are measured by stylus profilometry. (D-F) PDMS micro wells with increasing laser power at 0.5, 1 and 1.5% respectively.

2.3.8 Inspection of multiple well types

To demonstrate the detection of systematic volume differences within a well array we designed and fabricated a 10000-well array with 3 different types of wells: (1) 1000 wells with a design diameter d=70 µm; (2) 8000 wells with design diameter d=80 µm; and

(3) 1000 wells with design diameter d=90 μm. The volumes associated with the 10000 array wells appear as three well-resolved distributions at 0.065, 0.08 and 0.095 nL, respectively (**Figure 2-9**A). In addition, we plotted a volume versus half-depth-area scatterplot in which three distinct groups are obvious. In order to 'type' each well, we used a K-means clustering algorithm commonly used in data mining to assign each well to each group. The spots in the scatter plot were classified into three groups, each corresponding to one of the types of wells we designed (**Figure 2-9**B). The accuracy of the classification is shown in **Figure 2-9**C with only 22 misclassified wells out of a total of 10000 wells. This result demonstrated that the scanner-acquired full-size 3D profiles can be used to detect systematic differences of sub-groups in a micro-well array, and accurately categorized the well types.

A

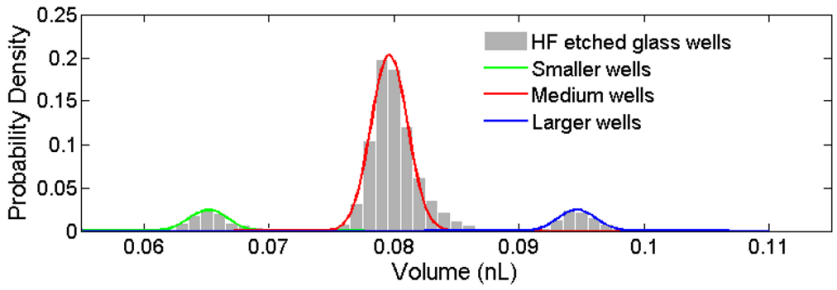

B

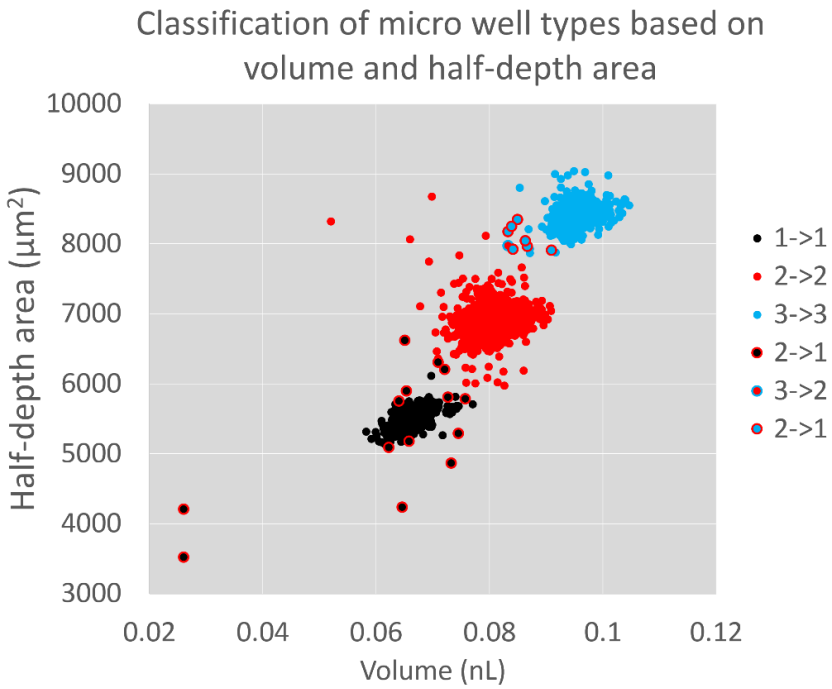

C

Classified type	True type		
	1	***2***	***3***
1	1000	14	0
2	0	7979	1
3	0	7	999

Figure 2-9. The detection of multiple well types in a single 10000 micro-well array. (A) The volume distribution of the three types of wells in the array. (B) The three clusters classified using the well's volume and half-depth area (legend: 1->1 means type-1 well is classified as type-1, and so forth). The summary of the result of the classification is shown in (C).

2.4 Summary

We have established a scanner-based profilometry method for the examination of micro-structures. The reported method is based only on a two-hundred dollar office scanner and features relatively large inspection area at level of 2000 mm^2 with ~2 μm resolution at maximum. Using this method, we demonstrated (1) the inspection of the longitudinal cross-sectional variation of laser-ablated PDMS channels; (2) the actual volumes in sagged PeT chambers after lamination for CD-sized centrifugal microfluidic devices; (3) the examination of micro well arrays' volume distribution fabricated by different methods as well as the multiple subgroups of micro wells in a single array. Some of these inspection tasks have revealed unprecedented quality assessment either in whole-population scale (micro well array) or in large inspection area (PeT chambers). The flatbed scanner based profilometry has been established as a low-cost, user-friendly and high-inspection-FOV method for the quality assessment of various types of transparent, enclosed microstructures.

2.5 Reference

[1] M. A. Schwarz and P. C. Hauser, “Recent developments in detection methods for microfabricated analytical devices.,” *Lab Chip*, vol. 1, no. 1, pp. 1–6, Sep. 2001.

[2] I. E. Araci and P. Brisk, “Recent developments in microfluidic large scale integration.,” *Curr. Opin. Biotechnol.*, vol. 25, pp. 60–8, Feb. 2014.

[3] K. Ren, J. Zhou, and H. Wu, “Materials for microfluidic chip fabrication,” *Acc. Chem. Res.*, vol. 46, no. 11, 2013.

[4] W. Su, X. Gao, L. Jiang, and J. Qin, “Microfluidic platform towards point-of-care diagnostics in infectious diseases.,” *J. Chromatogr. A*, vol. 1377, pp. 13–26, Jan. 2015.

[5] H. C. Fan, Y. J. Blumenfeld, Y. Y. El-Sayed, J. Chueh, and S. R. Quake, “Microfluidic digital PCR enables rapid prenatal diagnosis of fetal aneuploidy.,” *Am. J. Obstet. Gynecol.*, vol. 200, no. 5, pp. 543.e1–7, May 2009.

[6] H. C. Fan and S. R. Quake, “Detection of aneuploidy with digital polymerase chain reaction.,” *Anal. Chem.*, vol. 79, no. 19, pp. 7576–9, Oct. 2007.

[7] D. Le Roux, B. E. Root, C. R. Reedy, J. A. Hickey, O. N. Scott, J. M. Bienvenue, J. P. Landers, L. Chassagne, and P. de Mazancourt, “DNA Analysis Using an Integrated Microchip for Multiplex PCR Amplification and Electrophoresis for Reference Samples,” *Anal. Chem.*, vol. 86, no. 16, pp. 8192–8199, 2014.

[8] D. Le Roux, B. E. Root, J. A. Hickey, O. N. Scott, A. Tsuei, J. Li, D. J. Saul, L. Chassagne, J. P. Landers, and P. de Mazancourt, “An integrated sample-in-answer-out microfluidic chip for rapid human identification by STR analysis,” *Lab Chip*, vol. 14, no. 22, pp. 4415–4425, 2014.

[9] C. D. Chin, V. Linder, and S. K. Sia, “Commercialization of microfluidic point-of-care diagnostic devices.,” *Lab Chip*, vol. 12, no. 12, pp. 2118–34, Jun. 2012.

[10] D. Mark, F. von Stetten, and R. Zengerle, “Microfluidic Apps for off-the-shelf instruments.,” *Lab Chip*, vol. 12, no. 14, pp. 2464–8, Jul. 2012.

[11] E. C. Teague, F. E. Scire, S. M. Baker, and S. W. Jensen, “Three-dimensional stylus profilometry,” *Wear*, vol. 83, pp. 1–12, 1982.

[12] T. R. Albrecht and C. F. Quate, “Atomic resolution imaging of a nonconductor by atomic force microscopy,” *J. Appl. Phys.*, vol. 62, no. 7, p. 2599, 1987.

[13] H. Jordan, M. Wegner, and H. Tiziani, “Highly accurate non-contact characterization of engineering surfaces using confocal microscopy,” *Meas. Sci. Technol.*, vol. 9, pp. 1142–1153, 1998.

[14] L. Deck and P. de Groot, “High-speed noncontact profiler based on scanning white-light interferometry,” *Appl. Opt.*, vol. 33, no. 31, pp. 7334–7338, 1994.

[15] F. Gao, R. K. Leach, J. Petzing, and J. M. Coupland, “Surface measurement errors using commercial scanning white light interferometers,” *Meas. Sci. Technol.*, vol. 19, no. 1, p. 015303, Jan. 2008.

[16] M. Conroy and J. Armstrong, “A comparison of surface metrology techniques,” *J. Phys. Conf. Ser.*, vol. 13, pp. 458–465, Jan. 2005.

[17] D. C. Leslie, B. A. Melnikoff, D. J. Marchiarullo, D. R. Cash, J. P. Ferrance, and J. P. Landers, “A simple method for the evaluation of microfluidic architecture using flow quantitation via a multiplexed fluidic resistance measurement,” *Lab Chip*, vol. 10, no. 15, p. 1960, 2010.

[18] I. Broadwell, P. D. Fletcher, S. J. Haswell, T. McCreedy, and X. Zhang, “Quantitative 3-dimensional profiling of channel networks within transparent lab-on-a-chip microreactors using a digital imaging method.,” *Lab Chip*, vol. 1, no. 1, pp. 66–71, Sep. 2001.

[19] B. E. Bayer, “Color imaging array,” US 3971065 A,1976.

[20] A. Lapresta-Fernández and L. F. Capitán-Vallvey, “Scanometric potassium determination with ionophore-based disposable sensors,” *Sensors Actuators B Chem.*, vol. 134, no. 2, pp. 694–701, Sep. 2008.

[21] J. Lee and C. Mirkin, “Chip-based scanometric detection of mercuric ion using DNA-functionalized gold nanoparticles,” *Anal. Chem.*, vol. 80, no. 17, pp. 6805–6808, 2008.

[22] C. Zhang and K. Suslick, “A colorimetric sensor array for organics in water,” *J. Am. Chem. Soc.*, vol. 127, pp. 11548–11549, 2005.

[23] J. Carey and K. Suslick, “Rapid identification of bacteria with a disposable colorimetric sensing array,” *J. Am. Chem. Soc.*, vol. 133, pp. 7571–7576, 2011.

[24] M. Rahman and I. Kühn, “Evaluation of a scanner-assisted colorimetric MIC method for susceptibility testing of gram-negative fermentative bacteria,” *Appl. Environ. Microbiol.*, vol. 70, no. 4, pp. 2398–2403, 2004.

[25] M. H. V Werts, V. Raimbault, R. Texier-Picard, R. Poizat, O. Français, L. Griscom, and J. R. G. Navarro, “Quantitative full-colour transmitted light

microscopy and dyes for concentration mapping and measurement of diffusion coefficients in microfluidic architectures.," *Lab Chip*, vol. 12, no. 4, pp. 808–20, Feb. 2012.

[26] N. Fujita, Y. Saito, Y. Nitto, T. Ito, H. Mizuguchi, M. Endo, and T. Ogata, "Folin-Chiocalteu colorimetric analysis using a scanner for rapid determination of total polyphenol content in many test samples," *Stud. Sci. Technol.*, vol. 1, no. 2, pp. 139–144, 2012.

[27] Z. Göröcs and A. Ozcan, "Biomedical imaging and sensing using flatbed scanners.," *Lab Chip*, vol. 14, no. 17, pp. 3248–57, Sep. 2014.

[28] L.-M. Fu, W.-J. Ju, R.-J. Yang, and Y.-N. Wang, "Rapid prototyping of glass-based microfluidic chips utilizing two-pass defocused CO2 laser beam method," *Microfluid. Nanofluidics*, vol. 14, no. 3–4, pp. 479–487, Oct. 2012.

[29] Y. Ouyang, S. Wang, J. Li, P. S. Riehl, M. Begley, and J. P. Landers, "Rapid patterning of 'tunable' hydrophobic valves on disposable microchips by laser printer lithography.," *Lab Chip*, vol. 13, no. 9, pp. 1762–71, May 2013.

[30] H.-B. Liu and H.-Q. Gong, "Templateless prototyping of polydimethylsiloxane microfluidic structures using a pulsed CO2 laser," *J. Micromechanics Microengineering*, vol. 19, no. 3, pp. 37002–37010, Mar. 2009.

[31] B. L. Thompson, Y. Ouyang, G. R. M. Duarte, E. Carrilho, S. T. Krauss, and J. P. Landers, "Inexpensive, rapid prototyping of microfluidic devices using overhead transparencies and a laser print, cut and laminate fabrication method.," *Nat. Protoc.*, vol. 10, no. 6, pp. 875–86, Jun. 2015.

[32] C. L. do Lago, "A dry process for production of microfluidic devices based on the lamination of laser-printed polyester films," *Anal. Chem.*, vol. 75, no. 15, pp. 3853–3858, 2003.

[33] W. K. Tomazelli Coltro, J. A. Fracassi da Silva, H. D. Torres da Silva, E. M. Richter, R. Furlan, L. Angnes, C. L. do Lago, L. H. Mazo, and E. Carrilho, "Electrophoresis microchip fabricated by a direct-printing process with end-channel amperometric detection.," *Electrophoresis*, vol. 25, no. 21–22, pp. 3832–9, Nov. 2004.

[34] G. R. M. Duarte, C. W. Price, B. H. Augustine, E. Carrilho, and J. P. Landers, "Dynamic solid phase DNA extraction and PCR amplification in polyester-toner based microchip.," *Anal. Chem.*, vol. 83, no. 13, pp. 5182–9, Jul. 2011.

[35] E. A. Ottesen, J. W. Hong, S. R. Quake, and J. R. Leadbetter, "Microfluidic digital PCR enables multigene analysis of individual environmental bacteria.," *Science*, vol. 314, no. 5804, pp. 1464–7, Dec. 2006.

[36] Y. Men, Y. Fu, Z. Chen, P. A. Sims, W. J. Greenleaf, and Y. Huang, "Digital polymerase chain reaction in an array of femtoliter PDMS microreactors," *Anal. Chem.*, vol. 8, pp. 4262–4266, 2010.

[37] A. C. Hatch, J. S. Fisher, A. R. Tovar, A. T. Hsieh, R. Lin, S. L. Pentoney, D. L. Yang, and A. P. Lee, "1-Million droplet array with wide-field fluorescence imaging for digital PCR.," *Lab Chip*, vol. 11, no. 22, pp. 3838–45, Nov. 2011.

[38] R. Iino, Y. Matsumoto, K. Nishino, A. Yamaguchi, and H. Noji, "Design of a large-scale femtoliter droplet array for single-cell analysis of drug-tolerant and drug-resistant bacteria.," *Front. Microbiol.*, vol. 4, no. October, p. 300, Jan. 2013.

[39] X. Shi, L.-I. Lin, S. Chen, S.-H. Chao, W. Zhang, and D. R. Meldrum, "Real-time PCR of single bacterial cells on an array of adhering droplets.," *Lab Chip*, vol. 11, no. 13, pp. 2276–81, Jul. 2011.

[40] J. Wang, H. C. Fan, B. Behr, and S. R. Quake, "Genome-wide single-cell analysis of recombination activity and de novo mutation rates in human sperm.," *Cell*, vol. 150, no. 2, pp. 402–12, Jul. 2012.

[41] F. Shen, W. Du, J. E. Kreutz, A. Fok, and R. F. Ismagilov, "Digital PCR on a SlipChip.," *Lab Chip*, vol. 10, no. 20, pp. 2666–72, Oct. 2010.

Chapter 3. Laser-ablated microdevice for passive flow control and finger-driven dispensing of multiple reagents

3.1 Overview and Introduction

The accurate manipulation of low (nanoliter to microliter) volume of fluid is an evolving art in microfluidics. To control the direction of fluid and the flow rate, active microscale valves are routinely employed. While a variety of mechanical valves exist, the use of 'normally-open'[1] or 'normally-closed'[2] PDMS check valves is common, and these have led to large scale integrated microfluidic devices[3] and integrated 'all-in-one' microdevices[4,5]. However, the control of pneumatic check valves require external pressure sources and often sophisticated electronic systems, which can have a relatively large footprint, limiting the use of microfluidic devices to the laboratory. To broaden the impact of microfluidic analytical devices, more portable and less expensive on-chip flow control strategies are needed; such advances will make the devices more accessible to a broader range of users, notably those focusing on the development and implementation of point-of-care diagnostics.

In contrast to actively-controlled valving, passive flow control is markedly less complicated and reduces the need for external hardware, as there is no need for the external pressure control of the deformable flap membranes. Passive valving techniques such as abrupt capillary valves[6]–[9] and hydrophobic patch valves[10]–[12] have been shown to

open when the inlet pressure exceeds a 'burst threshold' defined by the geometry and surface properties, and remain closed when the inlet pressure is beneath the threshold. However, many applications require valves that enable a broader range of activation pressures and/or extremely different activation pressures for each flow's direction. Flap or membrane-based fluidic diode are promising examples of such valves, and have been fabricated from silicon, metals, parylene or SU-8 for various applications, especially in combination with micropumps[11,12]. As a result of its elasticity and simplicity of mold-based fabrication processes, silicone has emerged as the leading material for fluidic diodes: for example, Santra et al. developed a fluidic diode-based micropump using silicone[15], while Adams et al. reported an all-PDMS fluidic diode with a vertically hanging flap to prevent backflow[16]. Using the same diode structure, Iwai et al. developed a finger-powered cell encapsulation system[17]. Leslie et al. used PDMS membrane-capped fluidic diodes to rectify the flow in the frequency-specific flow switching[18], while Mosadegh et al. reported automated oscillatory flow switching using three-layer PDMS flap fluidic diodes[19].

A fundamental operation critical to the function of microfluidic devices is the precise metering and dispensing of solution, or combinations of solutions in a desired ratio. This has been achieved by active manipulation of a series of check valves that require multiple, independently-controlled pressure sources, and/or complicated logic operation[20]–[24]. In contrast, by taking advantages of modified Mosadegh's three-layer fluidic diodes, Li et al. constructed a fluidic circuit that could be driven by finger pressure to achieve the metering and delivery (*MaD*) of liquid solutions[25]. However, in the reagent metering stage, the design described requires finger actuation at independent

pumps for each reagent, and the arrangement of the fluidic paths, as well as the work flow, were still relatively complicated; this limits the extrapolation of this fluidic circuit to other multi-reagent applications.

Although PDMS-based fluidic diodes have demonstrated value in enhancing the functionality of microfluidic systems, fabrication and assembly of a fluidic diode remains relatively complicated and time-consuming. This is primarily due to the thin layer PDMS flap that requires spin-coating, photolithography, molding and polymer curing[16]–[19], [25]. In comparison with conventional soft-lithography based fabrication techniques, laser ablation-based micro-machining is gathering increasing attention because of its markedly faster prototyping speed, lower labor cost and higher level of automation[26]–[29]. The conditions for laser ablation of PDMS have been previously discussed by Liu et al.[29] and Forgarty et al.[30], and various laser-ablated PDMS structures have been reported by several other research groups[31]–[35].

With the present work, we report a fluidic diode structure partially fabricated in PDMS by laser-ablation. The basic structure of the fluidic diode is similar to that reported previously[19]; however, the flap membrane and controlling chamber are created by single-step laser ablation of a monolithic commercially-available PDMS film, followed by bonding with glass. We incorporate the laser-ablated fluidic diode into a 'finger-driven microdevice' that carries out precise metering and delivery of reagents. In comparison with the previously reported microdevice[25], this finger-driven system is more accurate in fluid delivery, and the fluidic circuit architecture can be modularized to allow for structural expansion to create a multi-reagent *meter-and-deliver* (*MaD*) system. This is demonstrated by the dispensing of: (1) two reagents for colorimetric quantitation of protein

solution, and (2) four reagents needed to create a mixture for the enzyme-mediated DNA amplification (PCR) in a manner comparable to conventional pipette-based reagent dispensing.

Furthermore, as an extension of the MaD fluidic circuit, a proof-of-concept finger driven serial diluter fluidic circuit is designed and tested with some preliminary results shown in the last part of this chapter.

3.2 Materials and Methods

Unless otherwise specified, all reagents are from Sigma Aldrich.

3.2.1 Fabrication of glass-PDMS-glass (GPG) microfluidic device

Features in PDMS layer was designed using CorelDraw 10.0 and then engraved by VersaLaser VLS 3.50 with 50W CO_2 laser source (Universal Laser System Inc.), into either a 290 μm (for diode and metering chamber) or 1.5mm (for finger pump) thick commercial PDMS film (Rogers Corp.). The diode flap was formed by partially ablating the PDMS film, and the metering chambers were created by complete cutting-through in the same film. After brief sonication in ethanol to remove ash and residue, the PDMS layer was dried and the geometry of the feature was characterized by examination of their cross-sections under microscope.

The glass bottom layer of the microdevice was fabricated using conventional photolithography and HF etching. The mask was designed using AutoCAD and then manufactured in photographic film in high resolution (Fineline Imaging, CO). Borofloat glass plate (Telic, Valencia, CA) pre-coated with photoresist and chrome layers was etched

by HF solution (HF/HNO_3:200/30 (v/v)) after UV exposure, development and removal of the exposed chromium layer. The photoresist and chromium remaining on the plate were removed completely after the etching. The diode valve seats were protected using dilute photoresist, and then bonded with the PDMS layer using a conventional plasma bonding technique. Protected photoresist was removed by ethanol flushing after PDMS recovery. (**Figure 3-1**)

3.2.2 Determination of the open pressure

An empty 100 μL syringe (Hamilton) was connected with a flow chamber that has a diode in the inlet channel (**Figure 3-2**). Initially the system (syringe, fittings, tubings, channels and flow chambers) were filled with air at room temperature. We used a camera to record the infusion of the liquid into the flow chamber. We used a syringe pump (neMESYS Syringe Pump, Cetoni) to start pulling the syringe at a fixed flow rate, so that the volume of air in the system as well as the inner pressure of the system can be calculated at a given time point (detailed discussion in 3.3.3). The opening pressure (defined in 3.3.2) was experimentally determined at the time point when solution started to infuse.

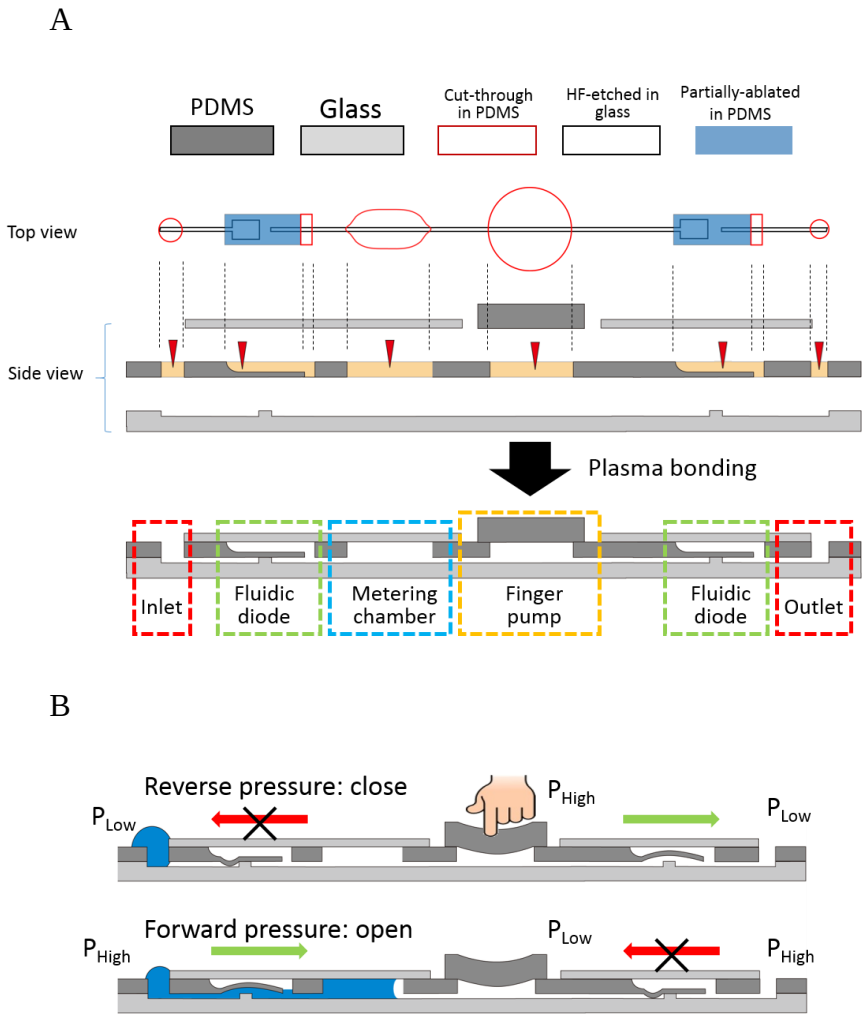

Figure 3-1. (A) Fabrication of a laser-ablated fluidic diode, together with other essential components (inlet, metering chamber and finger pump) fabricated in the same finger-driven microdevice (these structures are not in scale). The movable flap of the fluidic diode is laser-ablated in a single PDMS film and sandwiched by a valve seat layer (glass) and a top plate (glass). (B) Fluidic diode-enabled one-way liquid flow in a finger-driven fluidic circuit. Liquid flow is only permitted from the inlet through the diode under forward pressure.

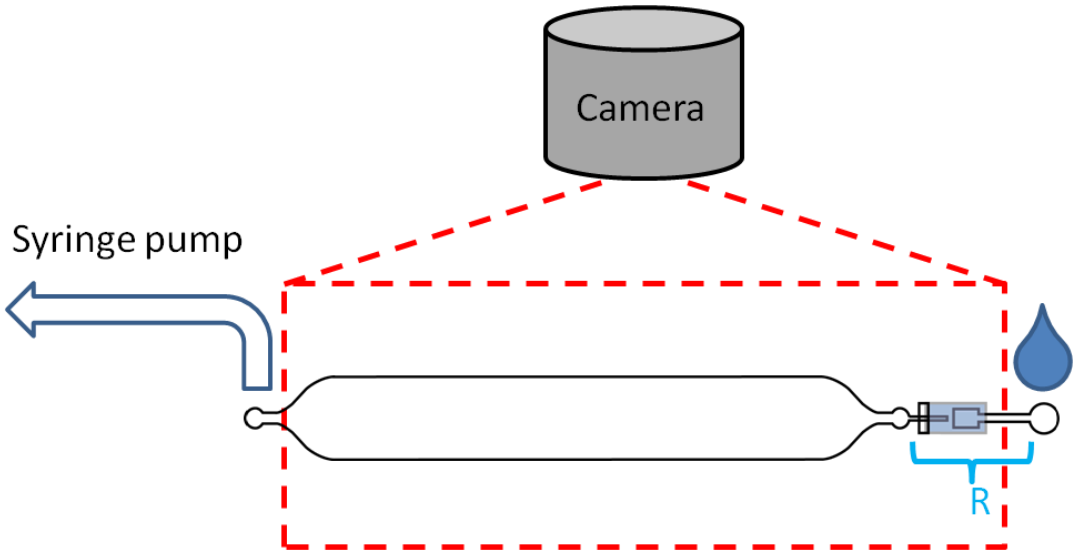

Figure 3-2. Settings for open pressure and flow profile determination

3.2.3 Design of the MaD micodevice and assembly

The basic structure and stepwise function of a finger-driven *MaD* circuit is shown in **Figure 3-3**. In the first stage, air in the finger pump is expelled from the device by finger pressing that deforms the PDMS plate of the pump. In the second stage, after releasing one's finger, the deformed PDMS will relax to its initial state and draw solution into the metering chamber. After the complete filling of the metering chamber the excess liquid enters the pump but does not completely fill it, because the replaced air from the metering chamber is drawn into the pump and stored together with the remaining air from the preceding stage. In the third stage, the finger pump is depressed again, and the remaining air stored in the pump will replace the solution in the metering chamber until all metered solution is completely discharged into the outlet, with the excess liquid still in the finger pump. Release the finger when the discharge completes and the metering stage will start again, so this cycle of operation can function repetitively.

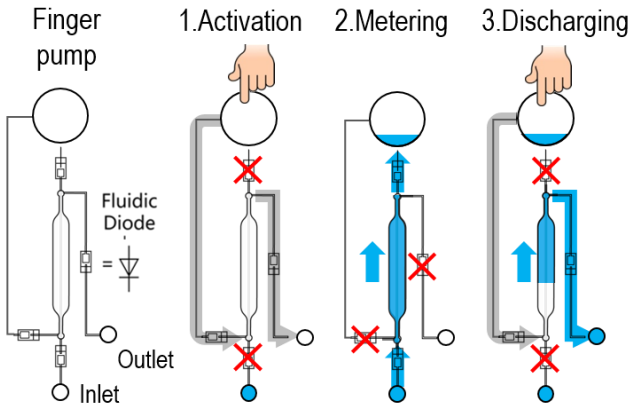

Figure 3-3. The operation and procedural details of the finger-driven MaD. The MaD operation is accomplished using two sequential finger compressions in three steps.

3.2.4 Determination of volume metered and delivered

All pipettes used were calibrated before the experiments of 3.2.4-3.2.7. Blue dye solution was prepared using erioglaucine at concentration of 6 mM in 1X Tris-EDTA buffer (pH 7.5), Approximately 20 µL of blue dye solution was pipetted into the inlet reservoir and metered in a series of metering chambers varying in volumes from 0.15 µL to 9 µL. The solution reaching the outlet reservoir was pipetted out and be diluted to 500 µL using 1X Tris-EDTA buffer (pH 7.5). Diluted solutions were then analyzed by UV-Vis spectrometer (Shimadzu) at 427 nm to determine the delivered volumes. Standard series was prepared by pipetting the 6 mM erioglaucine solution at the designed volumes of the metering chambers each into 500 µL 1X Tris-EDTA buffer (pH 7.5)

3.2.5 Determination of the mixing ratio of the dmultiple solutions delivery

Erioglaucine, tartrazine and allura red solutions were prepared at concentrations of 6mM, 15mM and 30mM, respectively, in 1X Tris-EDTA buffer (pH7.5). Dye solutions as well as 1X TE buffer (pH7.5) were metered in specific volumes and delivered to mix. 5 μL of the delivered mixture of the four solutions was pipetted out and diluted to 500 μL by 1X TE buffer (pH7.5). Diluted solutions were then analyzed by UV-Vis spectroscopy (Shimadzu) from 300nm to 700 nm to determine the overall absorbance spectrum, and then the fraction of each solution was calculated by their extinction coefficient matrix using the procedure previously described by Leslie et al.[36] (detail is discussed in 3.3.7)

3.2.6 Colorimetric test of protein solution

A commercial protein quantitation kit, Coomassie Brilliant Blue G(CBBG) solution, was used to demonstrate the delivery of two reagents for a rapid quantitation of total protein concentration. Equal amount of CBBG and Bovine serum albumin (BSA) solution (12.5, 25, 50, 100, 200 μg/mL) were metered, delivered and mixed either using a pipette or the finger driven microdevice. Mixed solutions were placed in room temperature for 1min for complete chromogenesis and then pipetted into a 290 μm high GPG chamber and get scanned (Epson Perfection V100 PHOTO, Epson). Scanned images were analyzed using ImageJ and the saturation values were used to quantitate the concentrations of the protein (section 3.3.8). To avoid adsorption of the CBBG on the surface of the glass, before each *MaD* procedure, all metering chambers were pre-loaded with CBBG then aspirated to get air dried.

3.2.7 Preparation of the polymerase chain reaction (PCR)

A commercial PCR kit (AmpFLSTR® Identifiler® PCR Amplification Kit, Life Technology) for amplification of short tandem repeats (STR, tetra- and penta-nucleotide-long repeating sequences) at 16 different loci in the human genome was used to assess the biochemical compatibility and performance of the finger-driven microdevice. Briefly, 2 μL of *Taq* Gold polymerase, 15 μL of standard DNA, 15 μL reaction mix and 15 μL of DNAse-free distilled H_2O were added to their corresponding inlet reservoirs prior to the operation. A total volume of 25 μL of the mixture was dispensed after three cycles with the finger-driven *MaD* of each solution in their specific needed volumes (**Table 3-1**). Prepared PCR mix was run in a thermal cycler (Bio-Rad) and the amplicons were analyzed by capillary electrophoresis (ABI 300, Applied Biosystems).

3.3 Results and Discussion

3.3.1 CO_2 laser ablation of PDMS

In order to control the depth of laser ablation in PDMS, both the scan speed and power of the CO_2 laser were adjusted[32]. We maintained a constant laser scan speed and varied the power in order to achieve an ablation depth that fully covers the thickness of PDMS film (**Figure 3-4**). The floor and wall of the ablated channels were rough compared with that of cured PDMS using an SU-8 mold. This is, however, of no consequence to the bonding and performance of the diode, because only the non-ablated PDMS surfaces are in contact with the glass valve seats and cover plate. The trapezoid-shaped cross-section of the channels with a width gradient was consistent with the cone-shaped cross-section of

CO_2 laser cutting line[29]. This indicates that the Gaussian-shape of the focused laser beam and the width expansion of ~75 µm on each side at the top of the cone defines the spatial resolution of laser ablation. At a fixed scan speed, the ablation depth in the PDMS film is linear with respect to the laser power. The linear relationship between depth and power is consistent with previously reported work[29][30][32] and implies that the depth of ablation can easily be controlled by simply adjusting the power input of laser ablation. A minimum power threshold of ~2W was required to initiate the ablation. For consistent flap thickness that has less than 10% variation, a 60 µm thick PDMS flap was fabricated by engraving down 230 µm in the commercialized film.

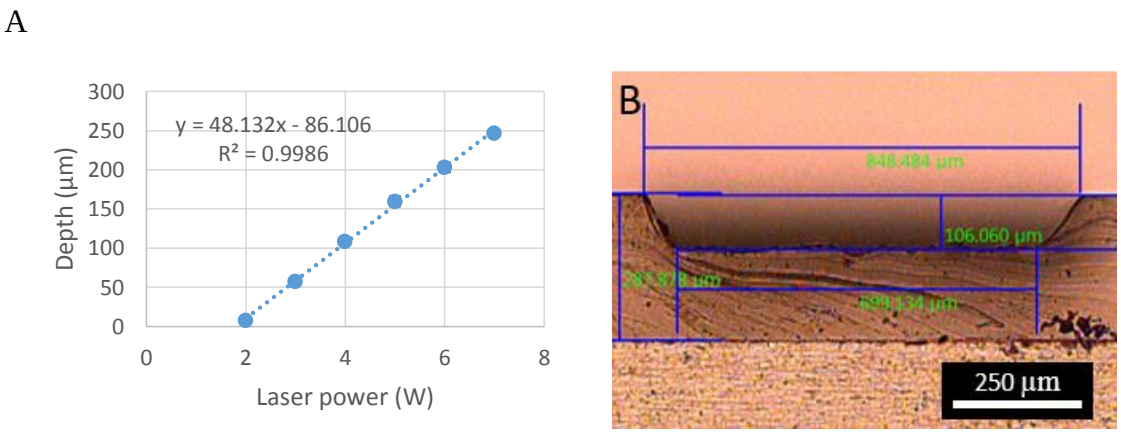

Figure 3-4. Laser ablation in PDMS film. (A) engraving depth of laser ablation in PDMS versus laser power (n=6). (B) cross-sectional views of laser-engraved PDMS channel at laser power = 4W.

3.3.2 Opening pressure of the fluidic diode

A functioning fluidic diode should be able to open under forward pressure. We define the pressure required to open a fluidic diode as the 'opening pressure' (OP). Investigation of the OP is critical in understanding whether a human finger can provide

adequate pressure to open a fluidic diode and drive flow. We experimentally determined the OP for different thickness of the flap of a fluidic diode and the trend shows that the OP increases as flap gets thicker (**Figure 3-5**A). The increased opening pressure reflects the increased energy required to deform the flap and delaminate the PDMS from the glass valve seat.

For the flap thickness used in the finger-driven *MaD* circuit, 60 μm in this case, the threshold OP is ~9 kPa. The finger pressing, and the relaxation of the PDMS upon release, provide the driving pressures for the discharging and metering flow, respectively. In order to open the diodes to initiate flow, those two pressures should be higher than the OP. The force that can be applied by a human finger is gender-dependent and ranges from 35-60 Newtons (N) for a male and 21-36 N for a female[37]. Therefore, the force applied by the weakest human finger on our finger pump (area = 50 mm^2) generates a pressure of ~420kPa, which is two orders of magnitude higher than the fluidic diode's OP.

3.3.3 Resistance of the Fluidic Diode in the Open State

The resistance of the fluidic diode is studied though both simulation and experiments. A 3D simulation of the fluidic diode in the open state was done using COMSOL Multiphysics®. The fluidic diode in simulation is under forward pressure wherein flow is permitted through (**Figure 3-6**A). The simulation shows the deformation of the flap as well as the flow of the liquid, and the deflection of the flap increases as the pressure difference (ΔP) increases (**Figure 3-6**B), which reduces the resistance of the fluidic diode due to the creation of an enlarged flow passage.

Experimentally, the resistance of the fluidic diode is extracted from the flow profile after it is opened. The flow chamber and connection set-up are shown in **Figure 3-2**. A fluidic diode is located in between the inlet reservoir and the flow chamber. Initially a drop of erioglaucine solution is placed in the inlet reservoir and then we start drawing by a syringe pump at a fixed flow rate. The inner pressure p changes as the syringe progresses with following relation:

$$p(t) = p_0 \frac{V_0}{V_0 + V(t)} = p_0 \frac{V_0}{V_0 + qt} \quad (1)$$

wherein V_0 is the initial total volume of the system and V is the volume that has been drawn into the syringe on time point t at fixed flow rate q. p0 is the initial inner pressure (1 atm).

At closed state, the pressure difference across the fluidic diode is:

$$\Delta p = p_0 - p(t) \quad (2)$$

When Δp is over the open pressure threshold p_{open}, solution begins to flow in and we stop the syringe pump immediately. After that point, the inner pressure changes as:

$$P(t) = p_0 \frac{V_0}{V_0 + V1 - V'(t)} \quad (3)$$

wherein V_1 is the volume that has been drawn into the syringe when it stops, and V'(t) is the volume of liquid that has flown into the chamber and can be determined from the video at each time point.

The overall resistance of the liquid flowing is then calculated as:

$$R = \frac{\frac{dV'(t)}{dt}}{p(t)} \quad (4)$$

where $\frac{dV'(t)}{dt}$ is determined from the plot of V'(t) versus t. Because the resistance of flow chamber and the air-filled downstream channel are much smaller than that of the liquid filled connecting channel and diode, the measured resistance is dominated by the incoming channel and diode. We minimized the incoming channel's resistance so that the resistance change of the fluidic diode versus pressure can be shown in the overall resistance profile.

The relationship between fluidic resistance and pressure difference shows a trend of decreasing resistance with increasing ΔP (**Figure 3-5**B). The resistance reaches a stable level that represents the baseline resistance of the upstream and downstream connecting channels and a fully-opened diode. As the pressure decreases, an opened diode will approach the closed state, and the fluidic diode enters a bi-state transition stage wherein it is sensitive enough to be switched between the open and closed states by small perturbation, generating unpredictable discrete flow. This is reflected in the markedly increased resistance and associated variation when the ΔP is lower than 4 kPa, the point that we define as the threshold pressure for an already opened fluidic diode to remain open.

A B

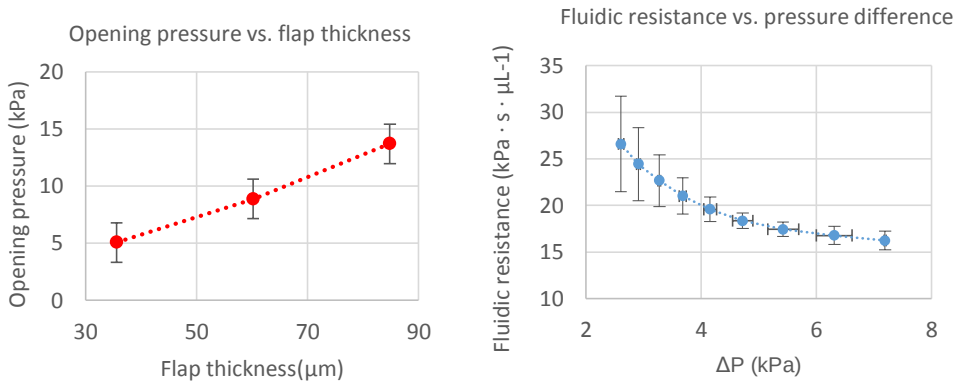

Figure 3-5. Fluidic characteristics of the fluidic diode. (A) Open pressure of fluidic diode at forward direction versus flap thickness. (n=3) (B) Relationship between fluidic resistance and pressure difference across the fluidic diode. (n=4)

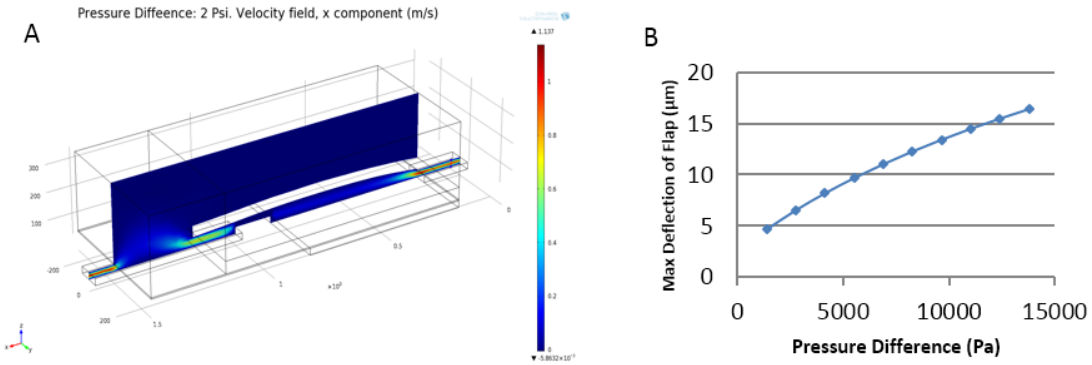

Figure 3-6. 3D Simulation of an open fluidic diode. (A). 3D simulation of fluidic diode in open state showing the flow rate distribution; (B): the maximum deflection of diode flap versus pressure difference

3.3.4 A fluidic diode-based finger-driven *MaD* process

The fluidic diodes are used in a finger-driven microfluidic circuit, and the expected *MaD* process was successfully demonstrated (**Figure 3-7**). In the metering stage, no introduction of air was observed through the closed diode and, in the delivery stage when finger pressure is applied to the pump, no air was pushed out back to the inlet. The entire process associated with a single *MaD* cycle was complete in 20 sec, and multiple cycles (n=3) could be done consecutively.

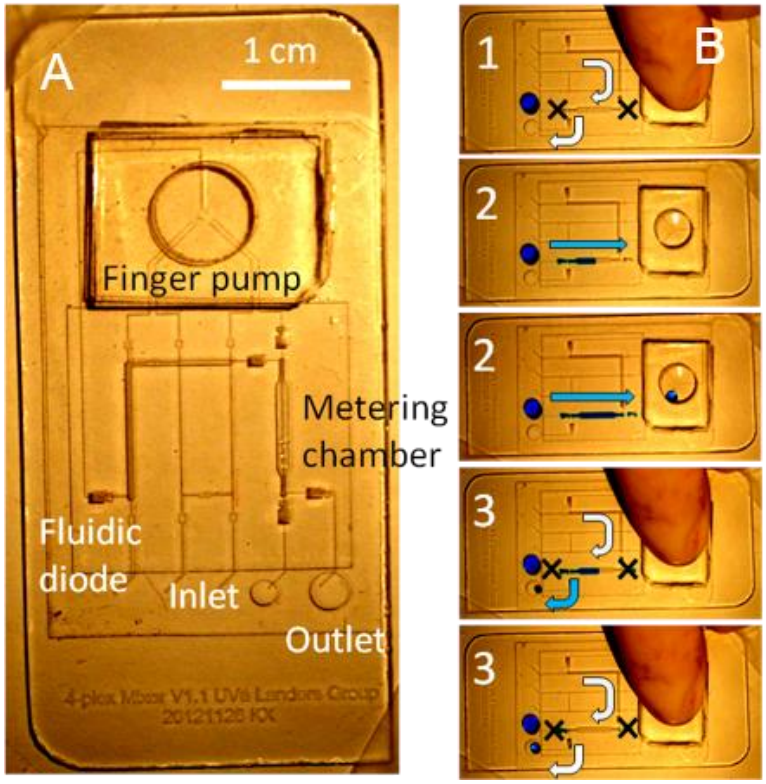

Figure 3-7. The MaD process in a finger-driven microfluidic chip. (A) The photo of the microfluidic chip with labels of the microfluidic components. (B) stepwise snap shots of the MaD process, from step 1 to step 2 corresponding to the steps in Figure 3-3

3.3.5 Precision and accuracy of the *MaD* process

During the metering process, the internal pressure of the system is lower than the ambient pressure and, thus, the floor and ceiling of the metering chamber may experience significant deformation if not rigid enough, which may inconsistency and error in the metered volume. To minimize such problem, we used a glass-PDMS-glass sandwiched structure to provide a much more rigid chamber floor and ceiling than those provided by an all-PDMS system. The consistency of the metered volumes (**Figure 3-8**, R^2=0.99995, 3% standard error) was markedly better than previously reported in an all-PDMS finger-driven microdevice[25].

The slope of the correlation in Figure 3-8 shows that the volume of the solution discharged into the outlet after *MaD* is ~3.9% less than the designed values. However, we did not observe any residual solution left in the metering chamber after the discharge. We attribute this deviation to the roughness of the PDMS side-wall of the metering chamber. It is possible that microscale 'hydrophobic pockets' may form at those concave sites during the infusion of aqueous solution, and a very small fraction of air is trapped, decreasing the amount of solution that is actually metered. Although this error is caused by the intrinsic hydrophobicity of the PDMS and it is difficult to be eliminated, the deviation is still comparable with the average error of a 20 μL micropipette.

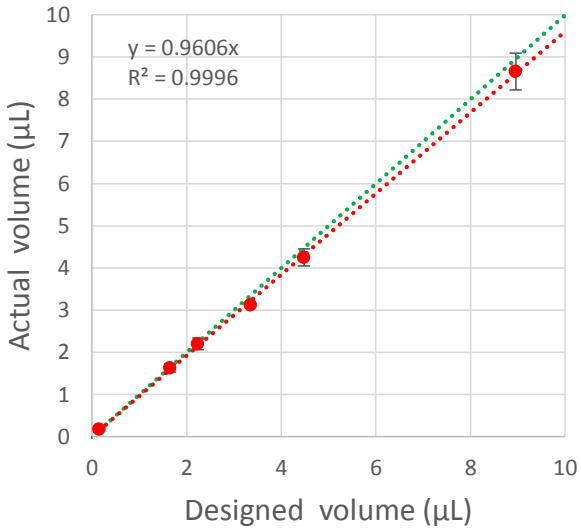

Figure 3-8. The correlation between the actual MaD-ed volumes and the designed volumes ranging from 160 nL to 9 µL (n=3).

3.3.6 *MaD* of multiple reagents

The single finger-driven *MaD* circuit can be extended to achieve the *MaD* of multiple solutions without increasing the number of finger-actuated pumps. To demonstrate this, we fabricated a fluidic circuit with four *MaD* units each having a corresponding inlet and metering chamber with a desired volume, and connecting to a single common outlet in series (**Figure 3-9**A). In a single *MaD* unit, only a type I diode (Mosadegh et al. [19]) is needed to prevent back-flow. In the dispensing of multiple reagents, however, type II diodes (Leslie et al. [18]) are required. The function of type II fluidic diode is to prevent cross-flow from either side between two adjacent *MaD* units during metering. Four solutions were used, three containing dyes [allura red (red), erioglaucine (blue), tartrazine (yellow)] and a fourth colorless buffer (1X TE, pH 7.5), to

test the ratio of components in the final delivered mixture. The red, blue, yellow and colorless solutions were drawn into circuits having volumes of 0.15, 1.65, 3.2 and 3.3 μL, respectively. The significance of these volumes will become apparent in a later section. The requisite initial concentration of each dye solution was calculated based on their volume ratio during the preparation so that they have minimum overlap in spectrum and all dye solution's absorbance peaks could be well resolved.

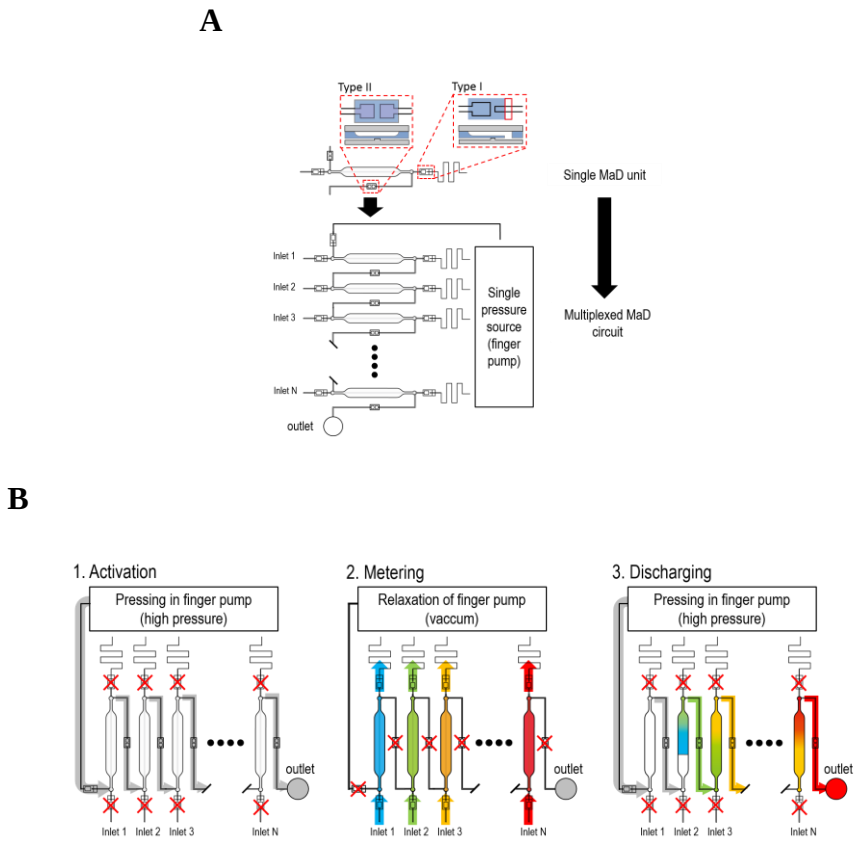

Figure 3-9. MaD of mutiple reagents on a finger driven microdevice. (A) The structure of a multiplexed MaD circuit by serial connection of multiple single MaD units. Two types of diodes are shown in both top view and cross-sectional view. (B) A step-wise schematic showing a fluidic circuit with N stackable MaD units for the MaD of N different reagents. Colored arrows represent different reagent flows during metering, and grey arrows represent the air flow during delivery.

3.3.7 Determination of the actual volume ratios of the dye solutions in the *MaD*-ed mixture

After all of the metered solutions were delivered to the outlet reservoir, a fraction (5 μL out of 8.3 μL) of the mixture was pipetted out for spectral quantitation and volumetric calculation. To determine the volume of each dye solution in the mixture, the matrix of the extinction coefficients of dye solutions is used[36],

$$\begin{bmatrix} \varepsilon_{t,\lambda t}b & \varepsilon_{a,\lambda t}b & \varepsilon_{e,\lambda t}b & \varepsilon_{T,\lambda t}b \\ \varepsilon_{t,\lambda a}b & \varepsilon_{a,\lambda a}b & \varepsilon_{e,\lambda a}b & \varepsilon_{T,\lambda a}b \\ \varepsilon_{t,\lambda e}b & \varepsilon_{a,\lambda e}b & \varepsilon_{e,\lambda e}b & \varepsilon_{T,\lambda e}b \\ \varepsilon_{t,\lambda T}b & \varepsilon_{a,\lambda 4T}b & \varepsilon_{e,\lambda T}b & \varepsilon_{T,\lambda T}b \end{bmatrix} \begin{bmatrix} c_t \\ c_a \\ c_e \\ c_T \end{bmatrix} = \begin{bmatrix} A_{\lambda t} \\ A_{\lambda a} \\ A_{\lambda e} \\ A_{\lambda T} \end{bmatrix} \quad (5)$$

or

$$\begin{bmatrix} \varepsilon_{t,\lambda t}b & \varepsilon_{a,\lambda t}b & \varepsilon_{e,\lambda t}b & \varepsilon_{T,\lambda t}b \\ \varepsilon_{t,\lambda a}b & \varepsilon_{a,\lambda a}b & \varepsilon_{e,\lambda a}b & \varepsilon_{T,\lambda a}b \\ \varepsilon_{t,\lambda e}b & \varepsilon_{a,\lambda e}b & \varepsilon_{e,\lambda e}b & \varepsilon_{T,\lambda e}b \\ \varepsilon_{t,\lambda T}b & \varepsilon_{a,\lambda T}b & \varepsilon_{e,\lambda T}b & \varepsilon_{T,\lambda T}b \end{bmatrix} \begin{bmatrix} c_{t0}V_{tx}/V \\ c_{a0}V_{ax}/V \\ c_{e0}V_{ex}/V \\ c_{T0}V_{Tx}/V \end{bmatrix} = \begin{bmatrix} A_{\lambda t} \\ A_{\lambda a} \\ A_{\lambda e} \\ A_{\lambda T} \end{bmatrix} \quad (6)$$

The subscripts ***t, a, e, T*** represent tartrazine, allura red, erioglaucine and TE, respectively. c_{m0} is the original concentration of the stock solution of dye ***m***; λ_m is the peak absorption wavelength of dye ***m***; $\varepsilon_{n,\lambda m}$ is the extinction coefficient of dye ***n*** at the dye ***m***'s peak absorption wavelength λ_m. For example, $\varepsilon_{a,\lambda e}$ is the extinction coefficient of tartrazine at the peak absorption wavelength of erioglaucine, 629nm, which is 0. ***V*** is the total volume of the mixture after delivery and V_{mx} is the dispensed volume of dye ***m*** which is the unknown parameter to be solved. ***V*** is the sum of all V_{mx}. $A_{\lambda m}$ is the overall absorbance of the mixture at λ_m. In this set

To minimize the overlapping of the spectra of different dye solutions we only used 3 types of dye and the fourth reagent is TE buffer. However, because TE buffer is transparent so the last column of the coefficient matrix is zero and this set of simultaneous equations doesn't have a definite solution. By draw and dilute a 5 μL aliquot of *MaD*-ed mixture rather than all of it, we introduce another linear independent equation into this equation set:

$$\begin{bmatrix} \varepsilon_{t,\lambda1,}b & \varepsilon_{a,\lambda1,}b & \varepsilon_{e,\lambda1,}b & \varepsilon_{T,\lambda1,}b \\ \varepsilon_{t,\lambda2,}b & \varepsilon_{a,\lambda2,}b & \varepsilon_{e,\lambda2,}b & \varepsilon_{T,\lambda2,}b \\ \varepsilon_{t,\lambda3,}b & \varepsilon_{a,\lambda3,}b & \varepsilon_{e,\lambda3,}b & \varepsilon_{T,\lambda3,}b \\ V/c_{t0} & V/c_{a0} & V/c_{e0} & V/c_{T0} \end{bmatrix} \begin{bmatrix} c_{t0}V_{tx}/V \\ c_{a0}V_{ax}/V \\ c_{e0}V_{ex}/V \\ c_{T0}V_{Tx}/V \end{bmatrix} = \begin{bmatrix} A_{\lambda1} \\ A_{\lambda2} \\ A_{\lambda3} \\ V_{aliquot} \end{bmatrix} \quad (7)$$

where $\boldsymbol{V_{aliquot}}$ is the volume of the mixture drawn out from the outlet reservoir by pipetting.

By doing so this set of equations has a definite solution and all $\boldsymbol{V_{mx}}$ can be calculated given a mixture's spectrum as well as all other known parameters.

Figure 3-10A&B show the overall spectrum of the standard reference and the mixture, respectively. The ratios of all four solutions are compared between the microdevice-prepared mixture and the pipette-prepared mixture (**Figure 3-10**) and the difference is determined to be less than 6%.

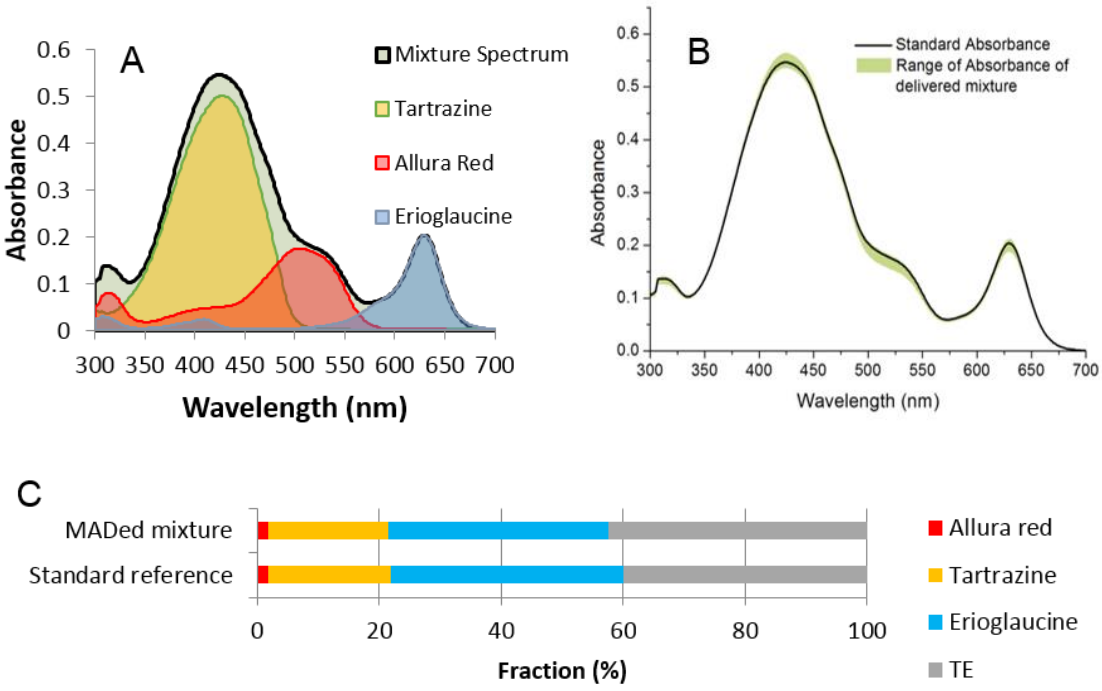

Figure 3-10. The accuracy of finger-driven multi-reagent MaD process. (A) The spectra of the reference mixture containing three different dye solutions at the desired ratio. (B) The comparison between the spectrum of reference mixture and the on-chip metered and delivered mixture with the range shown in green (n=3); (C) Comparison between the ratio of components in the MaD-ed mixture and standard reference

Unlike the previously reported finger-driven microdevice[25], the *MaD* circuit we designed highlights the key benefit of a simplified manual operation as well as the structure with the ability to meter multiple solutions from different reservoirs using only one single finger pump. The advantage comes from the feature that the metering of multiple solutions is accomplished in parallel by a single action of finger pressing/release and the delivery path is connected in series. This means that these *MaD* circuits are mutually independent

but, more importantly, structurally "stackable", giving the design the potential to be expanded for the *MaD* of larger number of reagents (**Figure 3-9**B).

3.3.8 Colorimetric quantitation of protein on finger-driven microdevice

A potential application of the finger driven microdevices is to provide platforms for point-of-care diagnostics where sensitive, simple and rapid tests are highly desired. Total protein concentration in body fluid is a significant indicator of health conditions, and convenient monitoring of protein level is of great significance in the prevention and early treatment of malignant diseases such as uremia. We transplanted a CBBG-based rapid colorimetric test of protein onto the finger driven microdevice and used a home scanner to detect the signal intensity.

CBBG-protein solution was incubated for 1 min and then the scanned raw image (**Figure 3-11** upper panel) was converted to into HSB space (Hue, Saturation and Brightness) (**Figure 3-11** lower panel). The saturation value in unit of grayscale is measured and correlated with protein concentration, using water as background.

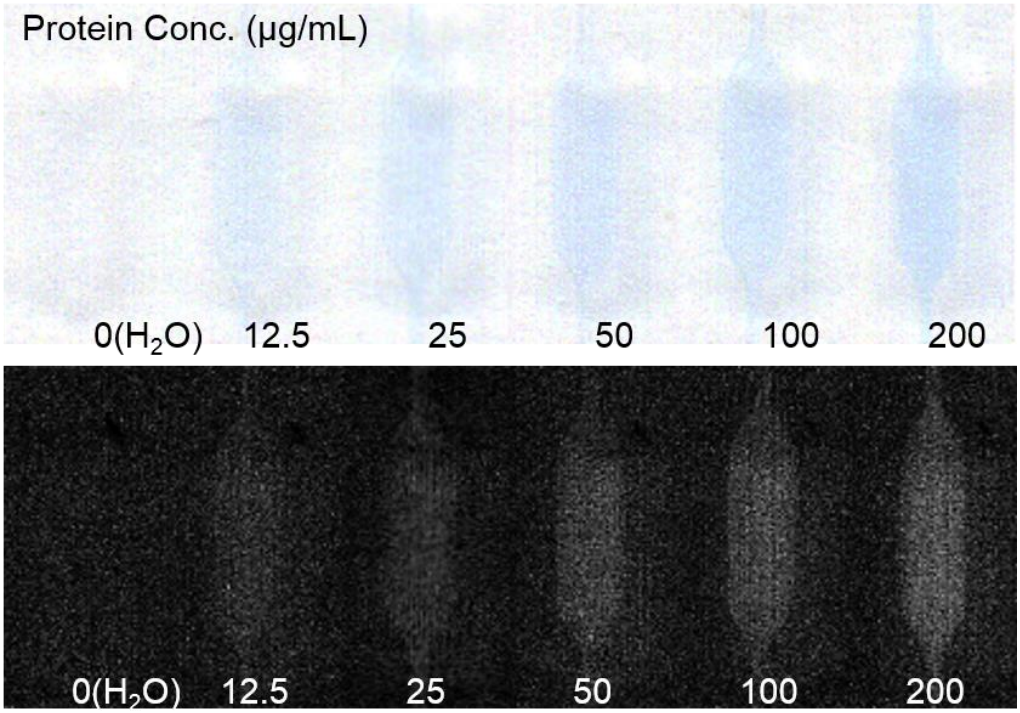

Figure 3-11. Image of the CBBG-protein solution shown as raw scanned file (upper) and in the saturation scope of HSB space (lower)

The saturation values of the scanned images of CBBG-protein solution in the detection chamber is linearly correlated with the logarithm of protein concentration in µg/mL (**Figure 3-12**A). A comparison between finger-driven microdevice and pipette in quantitation is shown to have less than 3% difference (**Figure 3-12**B). The range of detection covers the normal range of the concentration of total protein (20-150 µg/mL) in urine[38].

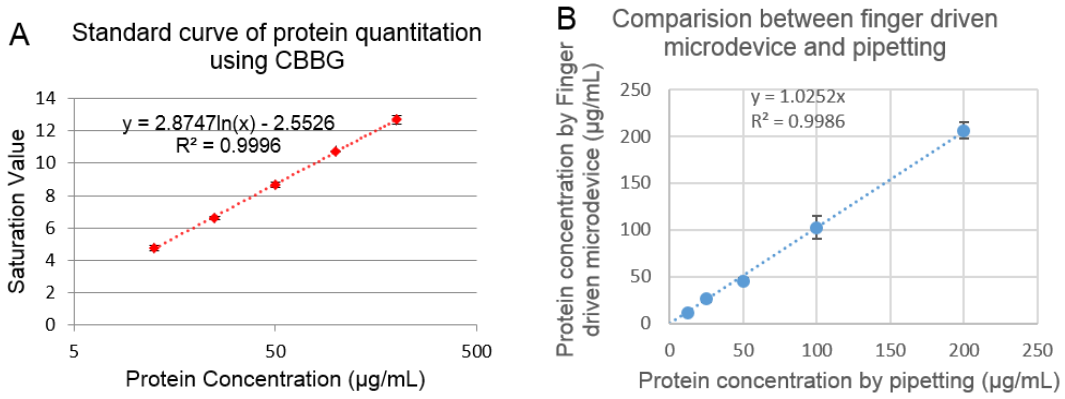

Figure 3-12. Colorimetric quantitation of protein using CBBG. (A) The calibration curve of BSA standard solutions from 12.5 to 200 µg/mL(n=3); (B) The comparison between the protein concentrations determined by pipetting and finger driven MaD(n=3).

3.3.9 Preparation of the PCR mixture on finger-driven microdevice

Having used dyes to demonstrate that metering of architecture-defined volumes was possible, we sought to demonstrate the accurate preparation of a biologically-relevant mixture. The polymerase chain reaction (PCR) is an enzyme-mediated amplification of select sequences of DNA in a reaction mixture that is cycled through temperatures which facilitate the denaturing of the template DNA (94 ℃), annealing of primers (~60 ℃) and enzymatic synthesis of copies of the sequences (72°C). The composition of this 'mixture' is important to the PCR chemistry and becomes increasingly so when multiple sequences are synthesized at the same time (multiplex PCR). The mixture that is thermally-cycled contains 4 different reagents - the polymerase (a), the primers (b) the PCR reaction mix (c) and the DNA template (sample) (d), with the a:b:c:d ratio varied slightly from PCR to PCR. Significant deviation from these relative ratios, especially on (c), can adversely affect the

efficiency of the PCR because the PCR reaction mix contains dNTP and Mg^{+2} and the efficiency of the PCR amplification is particularly sensitive to slight changes in $[Mg^{2+}]$.

The model PCR system we chose is a multiplex PCR that amplifies short tandem repeat (STR) sequences from 16 loci in the genome for use in human identification. With each loci having the potential to present one or two different STRs, for any given sample, anywhere from 16 to 32 DNA sequences are amplified. The STR amplification is a finicky one, being very sensitive to the mass (pg) of DNA template (d) supplied, and the volume of PCR reaction mix (c) added. The a:b:c:d ratio required for the STR amplification is 1:11:21:22 (**Table 3-1**). As such, this represents a reasonable system to test the effectiveness and the biocompatibility of the finger-driven microdevice.

	Taq Gold Polymerase	Primers	Reaction mix	Standard DNA (or sample DNA)
Volume needed per run in a tube	0.45	5	9.5	10
Dispensed volume per *MaD* cycle	0.15	1.65	3.2	3.3

Table 3-1 Essential reagents in AmpFLSTR® Identifiler® PCR Amplification Kit and their optimal volumes (unit: µL)

Using the chip design and chamber combination that was described and validated in previous section 3.3.6, reagents were added to the microdevice, metering and delivery carried out, and the results are shown in **Figure 3-13**

Three consecutive cycles of metering and delivery of combinations of reagents gave a total volume of 25 μL within 2 min. The correlation of peak area of all 16 loci between conventional pipetting-prepared PCR and microdevice-*MaD*-prepared PCR is close to 1, proving that the biochemical reagents, especially those bio-macromolecules such as DNA and polymerase were not affected after going through the microdevice, and the PCR results are similar to those by the conventional method.

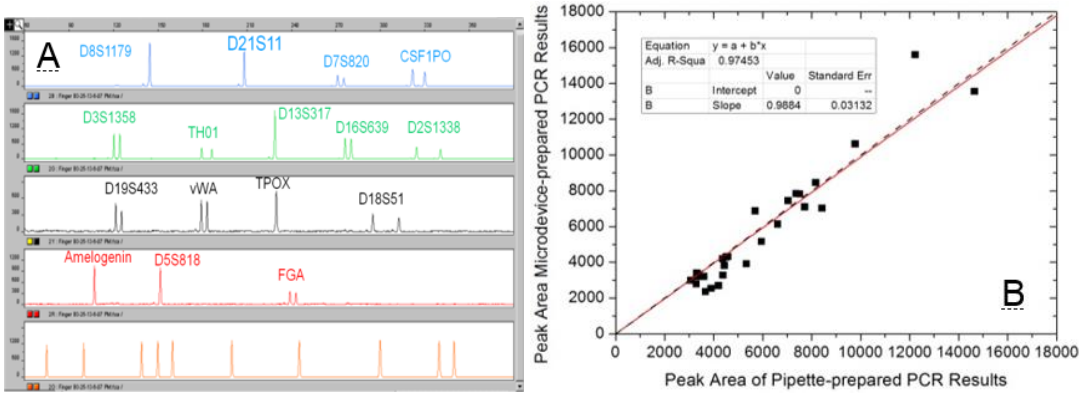

Figure 3-13. PCR results prepared by finger driven microdevice. (A) The electrophoretic STR profile of standard female DNA showing all 16 loci. The reaction mixture was prepared by the finger-driven microdevice; (B) Correlation of peak areas between pipetting-prepa

3.3.10 Finger-driven serial diluter: concept, design and test

Serial dilution is one of the most commonly used liquid handling techniques in biochemical assays which can dilute a solution from its original concentration to much

lower levels in only a few repeating steps. The general idea of serial dilution is quite simple, which only requires the cycling of common dilution operations.

The on-chip realization of the serial dilution process has been presented by several other groups and the reported microfluidic structures can be generally categorized into two types: (1) active dilution: valve-controlled dilution cycles containing steps of metering, mixing and fractionation[21]; (2) passive dilution: fluidic resistance-controlled, hierarchical steps of diffusive mixing and fractionation in a ladder-structured microfluidic circuits[39]–[41]. The limitation of the active serial diluter is that they require external pressure sources and controlling components to control the on-chip check valves which significantly reduce the portability of the microdevice, while for the passive serial diluters they require a continuous, stable flow to ensure a desired concentration gradient, which also requires external equipment such as syringe pumps.

In the work shown below, we present a proof-of-concept novel design of a finger-driven serial diluter and some preliminary test results of the microdevice. The finger driven serial diluter avoids the disadvantages of both types of serial diluters introduced above and performs serial dilution at arbitrary diluting ratios. It also exploits the power of the fluidic diodes to passively manipulate the direction of flow so that it doesn't require external components for valve control, and since the dilution is not based on diffusion in laminar flow, the condition of a continuous, consistent flow is not required. The concept of the work flow and the schematic design of the microdevice is shown in **Figure 3-14** and the operation of the microdevice is illustrated in **Figure 3-15.** The basic cycle of the serial dilution consists the metering and delivery of both solvent and the reagent solution. The metering of both solutions are conducted simultaneously , and by adjusting the fluidic

resistance of the metering pathways the velocity of the flow in the reagent pathway is designed to be slower than that in the solvent pathway's, so the metering chamber for the reagent solution is filled up later than the solvent metering chamber. Once the metering chamber for the reagent solution is filled up (at that point the solvent metering is already done), the delivery starts immediately by pressing the finger pump again. The metered solvent is delivered to the reagent inlet reservoir where it is mixed with the left-over aliquot of the reagent solution and dilute it, while the metered reagent solution is delivered to a collection tube through a tubing connection. When all solutions are fully discharged, release the finger pump to enter the next cycle which starts from the metering of the solvent and the diluted reagent solution from the inlet reservoirs.

The serial dilution process described above can achieve different diluting ratios using the same microdevice because the diluting ratio is determined by the volume ratio between the left-over aliquot and the metered volume of the solvent solution, and the volume of the left-over aliquot is determined by the subtraction of the metered volume of the reagent from the initial volume of original reagent solution added to the inlet reservoir. For example if the volumes of the metering chambers of reagent and solvent are both 10 μL, and 12 μL of the original reagent is added to the inlet reservoir, then 2 μL is the left-over volume after the metering of the reagent and will be further diluted by 10 μL of the metered and delivered solvent, resulting a 1/5 dilution as the new starting reagent solution with the volume of 12 μL again for the next cycle. Similarly by simple calculation if the starting volume of the reagent is 20 μL then the diluting ratio will be 1/2.

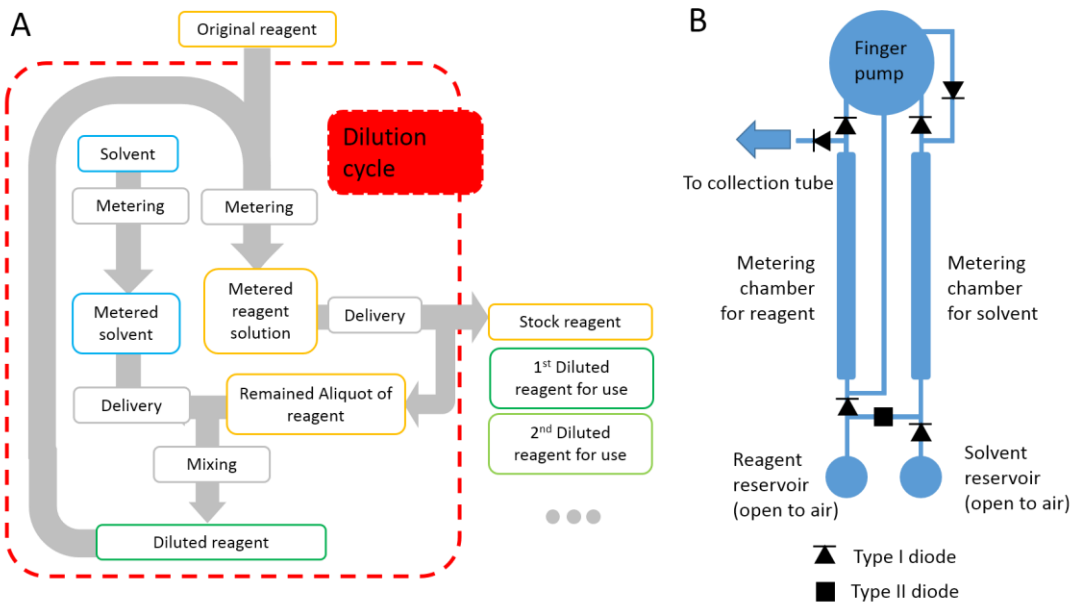

Figure 3-14. Serial diluter from concept to design. (A) Concept of the serial dilution procedure and (B) the design of a finger driven serial diluter based on the concept of serial dilution, containing two set of MaD circuits for the solvent and the reagent solution respectively.

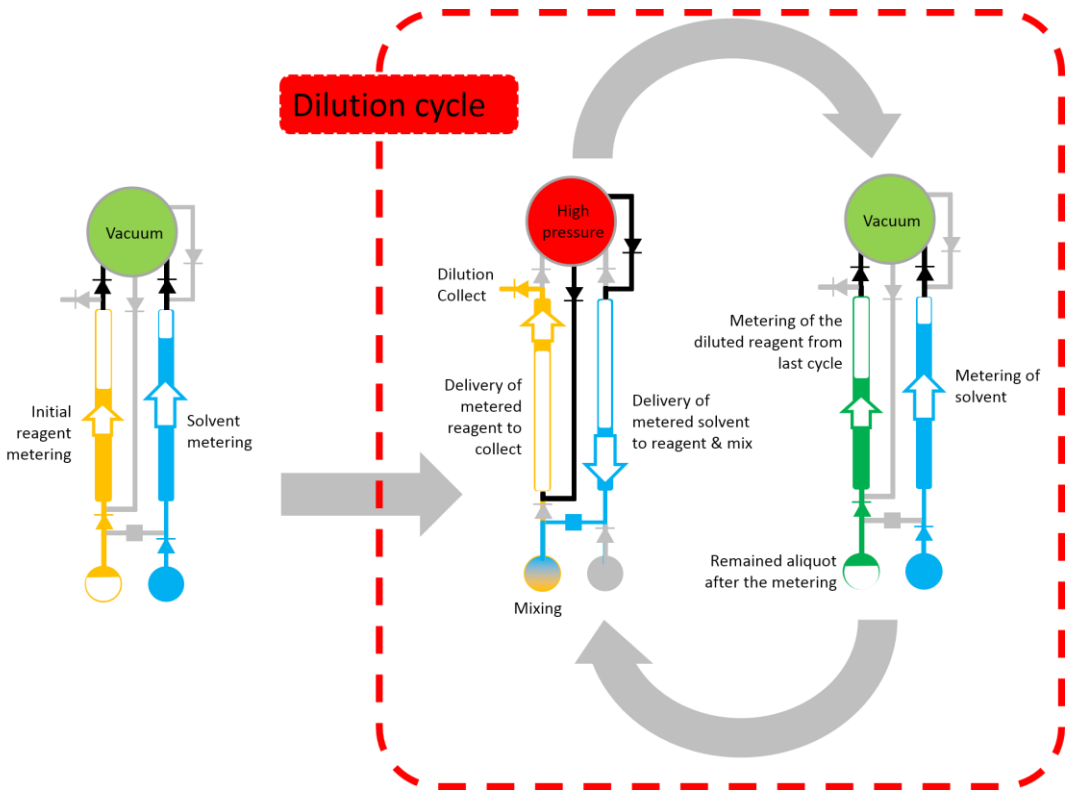

Figure 3-15. The diagram showing the process of serial dilution on the finger-driven microdevice. The path of the reagent solution is in yellow or green; the path of the solvent is in blue; and the air path is shown in black. The closed pathway is in grey color.

The microdevice also features a sandwiched GPG structure and the fabrication process is similar to the previously described in section 3.2.1. The snapshots of the video of the finger-driven serial dilution using the microdevice is shown in **Figure 3-16.** Blue dye solution **(**erioglaucine) was used to show the progress of the dilution. It is obvious that the color is becoming lighter and lighter as the dilution process cycles though. Using the same method described in section 3.3.5 the accuracy of the finger-driven serial dilution is determined and the comparison of the result with that of the pipette-generated serial

dilution shows that the finger-driven serial dilution is comparable with pipette generated serial dilution (**Figure 3-17**).

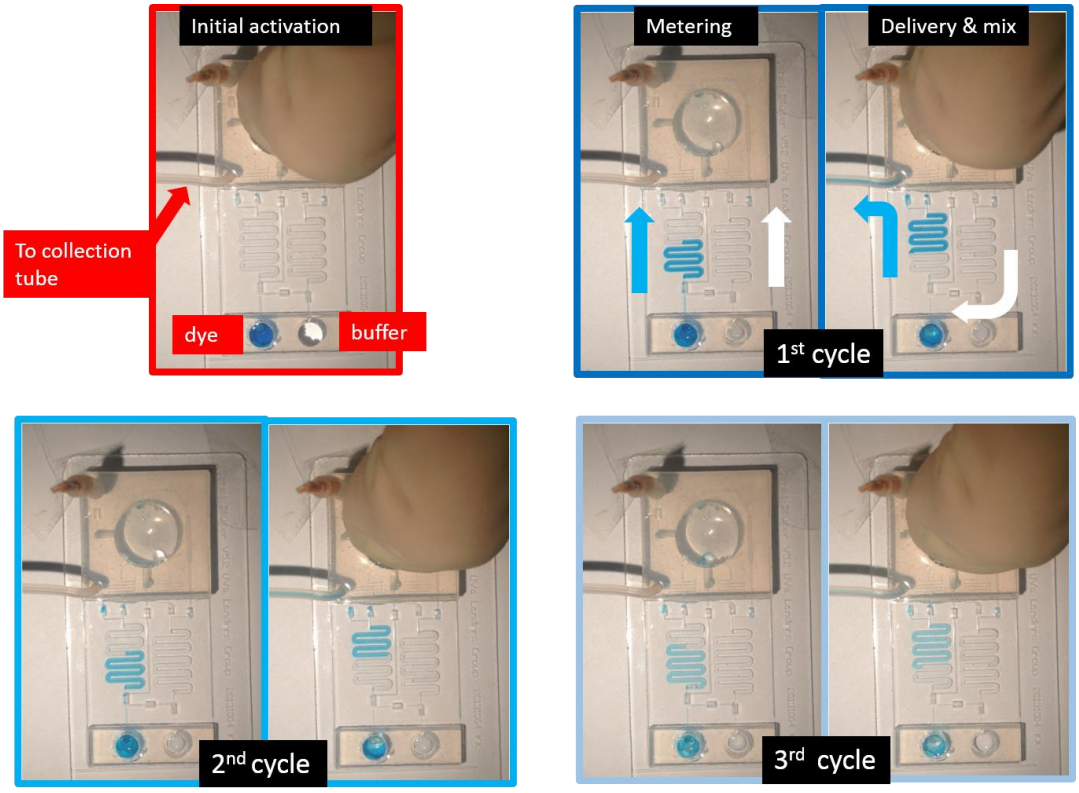

Figure 3-16. The snapshots of the video showing the functioning of the finger driven serial dilution. Three cycles of the dilution process are shown. The blue and white arrow in the first cycle indicate the direction of the flows of the dye solution and the buffer solution, respectively.

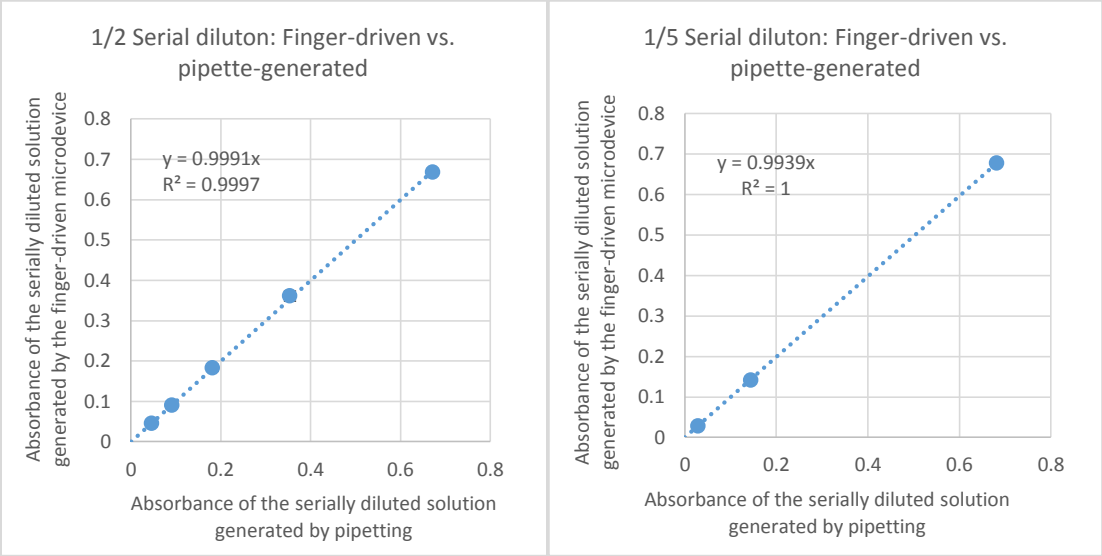

Figure 3-17. Comparison between finger driven serial dilution and pipette-generated serial dilution (n=3). The serial dilution is performed at diluting ratio of 1:2 (left) and 1:5 (right) using same design of the microdevice. Until the most diluted concentration of the dye can't be detected in the spectrometer 4 cycles of dilution have been performed in the 1:2 serial dilution and 2 cycles of the dilution have been performed in the 1:5 serial dilution.

3.4 Summary

We used CO_2 laser ablation to assist the fabrication of the flap structure of glass-PDMS-glass (GPG) hybridized fluidic diode. The flap membrane was created by laser ablation in commercial PDMS thin films with controllable thickness, which circumvented the time-consuming spin-coating/curing procedures that are commonly used in the fabrication of PDMS membrane. A novel finger-driven microdevice that can meter and deliver multiple solutions is constructed based on the passive flow control of the fluidic diodes, and the accuracy of the *MaD* on chip was proven to be comparable with pipetting. Its utility was demonstrated through preparation of a simple colorimetric test for protein

quantitation, and preparing a master PCR mix from four essential reagents. The basic structure of the *MaD* circuit can be easily multiplexed to achieve the *MaD* of a number of reagents without additional manual operation. Also the *MaD* structure can be used to construct a finger-driven serial diluter which can conduct serial dilution at arbitrary diluting ratios with comparable performance versus pipetting. Our prototype provides a manually drivable, highly portable and precise reagent dispensing platform for potential use in point-of-care applications.

3.5 Acknowledgements

I would like to thank Prof. Matthew R. Begley *(Department of Mechanical Engineering and Materials, University of California, Santa Barbara)* for the resources and advice provided by him and his research group and the NIBIB [5R01EB011591-04] for the funding that supported these efforts.

I would like to thank Prof. N. Zhang *(Department of Mechanics, Shanghai University)* for inspiring discussions on the characterization of the fluidic diode.

3.6 Reference

[1] M. A. Unger, H.-P. Chou, T. Thorsen, A. Scherer, and S. R. Quake, "Monolithic Microfabricated Valves and Pumps by Multilayer Soft Lithography," *Science.*, vol. 288, no. 5463, pp. 113–116, Apr. 2000.

[2] W. H. Grover, A. M. Skelley, C. N. Liu, E. T. Lagally, and R. A. Mathies, "Monolithic membrane valves and diaphragm pumps for practical large-scale integration into glass microfluidic devices," *Sensors Actuators B Chem.*, vol. 89, no. 3, pp. 315–323, Apr. 2003.

[3] T. Thorsen, S. J. Maerkl, and S. R. Quake, “Microfluidic large-scale integration.,” *Science*, vol. 298, no. 5593, pp. 580–4, Oct. 2002.

[4] E. T. Lagally, J. R. Scherer, R. G. Blazej, N. M. Toriello, B. A. Diep, M. Ramchandani, G. F. Sensabaugh, L. W. Riley, and R. A. Mathies, “Integrated portable genetic analysis microsystem for pathogen/infectious disease detection.,” *Anal. Chem.*, vol. 76, no. 11, pp. 3162–70, Jun. 2004.

[5] C. J. Easley, J. M. Karlinsey, J. M. Bienvenue, L. A. Legendre, M. G. Roper, S. H. Feldman, M. A. Hughes, E. L. Hewlett, T. J. Merkel, J. P. Ferrance, and J. P. Landers, “A fully integrated microfluidic genetic analysis system with sample-in-answer-out capability.,” *Proc. Natl. Acad. Sci. U. S. A.*, vol. 103, no. 51, pp. 19272–7, Dec. 2006.

[6] C. H. Ahn, J.-W. Choi, G. Beaucage, J. Nevin, J.-B. Lee, a. Puntambekar, and R. J. Y. Lee, “Disposable Smart Lab on a Chip for Point-of-Care Clinical Diagnostics,” *Proc. IEEE*, vol. 92, no. 1, pp. 154–173, Jan. 2004.

[7] D. Duffy, H. Gillis, and J. Lin, “Microfabricated centrifugal microfluidic systems: characterization and multiple enzymatic assays,” *Anal. Chem.*, vol. 71, no. 20, pp. 4669–4678, 1999.

[8] R. Johnson, I. Badr, G. Barrett, and S. Lai, “Development of a fully integrated analysis system for ions based on ion-selective optodes and centrifugal microfluidics,” *Anal. Chem.*, vol. 73, no. 16, pp. 3940–6, Aug. 2001.

[9] T.-S. Leu and P.-Y. Chang, “Pressure barrier of capillary stop valves in micro sample separators,” *Sensors Actuators A Phys.*, vol. 115, no. 2–3, pp. 508–515, Sep. 2004.

[10] H. Andersson, W. Van Der Wijngaart, P. Griss, and F. Niklaus, “Hydrophobic valves of plasma deposited octafluorocyclobutane in DRIE channels,” *Sensors Actuators B Chem.*, vol. 75, pp. 136–141, 2001.

[11] Y. Feng, Z. Zhou, X. Ye, and J. Xiong, “Passive valves based on hydrophobic microfluidics,” *Sensors Actuators A Phys.*, vol. 108, no. 1–3, pp. 138–143, Nov. 2003.

[12] Y. Ouyang, S. Wang, J. Li, P. S. Riehl, M. Begley, and J. P. Landers, “Rapid patterning of ‘tunable’ hydrophobic valves on disposable microchips by laser printer lithography.,” *Lab Chip*, vol. 13, no. 9, pp. 1762–71, May 2013.

[13] K. W. Oh and C. H. Ahn, “A review of microvalves,” *J. Micromechanics Microengineering*, vol. 16, no. 5, pp. R13–R39, May 2006.

[14] D. J. Laser and J. G. Santiago, “A review of micropumps,” *J. Micromechanics Microengineering*, vol. 14, no. 6, pp. R35–R64, Jun. 2004.

[15] S. Santra, P. Holloway, and C. D. Batich, “Fabrication and testing of a magnetically actuated micropump,” *Sensors Actuators B Chem.*, vol. 87, pp. 358–364, 2002.

[16] M. L. Adams, M. L. Johnston, A. Scherer, and S. R. Quake, “Polydimethylsiloxane based microfluidic diode,” *J. Micromechanics Microengineering*, vol. 15, no. 8, pp. 1517–1521, Aug. 2005.

[17] K. Iwai, A. T. Higa, R. D. Sochol, and L. Lin, “A Finger-Powered Cell Encapsulation System,” *Proc. 15th Int. Conf. Miniaturized Syst. Chem. Life Sci. (uTAS 2011)*, pp. 1182–1184, 2011.

[18] D. C. Leslie, C. J. Easley, E. Seker, J. M. Karlinsey, M. Utz, M. R. Begley, and J. P. Landers, “Frequency-specific flow control in microfluidic circuits with passive elastomeric features,” *Nat. Phys.*, vol. 5, no. 3, pp. 231–235, Feb. 2009.

[19] B. Mosadegh, C.-H. Kuo, Y.-C. Tung, Y.-S. Torisawa, T. Bersano-Begey, H. Tavana, and S. Takayama, “Integrated Elastomeric Components for Autonomous Regulation of Sequential and Oscillatory Flow Switching in Microfluidic Devices.,” *Nat. Phys.*, vol. 6, no. 6, pp. 433–437, Jun. 2010.

[20] J. K. Chang, H. Bang, S.-J. Park, S. Chung, C. Chung, and D. C. Han, “Fabrication of the PDMS microchip for serially diluting sample with buffer,” *Microsyst. Technol.*, vol. 9, no. 8, pp. 555–558, Oct. 2003.

[21] B. M. Paegel, W. H. Grover, A. M. Skelley, R. A. Mathies, and G. F. Joyce, “Microfluidic serial dilution circuit.,” *Anal. Chem.*, vol. 78, no. 21, pp. 7522–7, Nov. 2006.

[22] C.-W. Huang, S.-B. Huang, and G.-B. Lee, “A microfluidic device for precise pipetting,” *J. Micromechanics Microengineering*, vol. 18, no. 3, p. 035004, Mar. 2008.

[23] T. V Nguyen, P. N. Duncan, S. Ahrar, and E. E. Hui, “Semi-autonomous liquid handling via on-chip pneumatic digital logic.,” *Lab Chip*, vol. 12, no. 20, pp. 3991–4, Oct. 2012.

[24] E. C. Jensen, A. M. Stockton, T. N. Chiesl, J. Kim, A. Bera, and R. A. Mathies, “Digitally programmable microfluidic automaton for multiscale combinatorial mixing and sample processing.,” *Lab Chip*, vol. 13, no. 2, pp. 288–96, Jan. 2013.

[25] W. Li, T. Chen, Z. Chen, P. Fei, Z. Yu, Y. Pang, and Y. Huang, “Squeeze-chip: A finger controlled microfluidic flow network device and its application to biochemical assays,” *Lab Chip*, vol. 12, no. 9, 2012.

[26] C. K. Chung, H. C. Chang, T. R. Shih, S. L. Lin, E. J. Hsiao, Y. S. Chen, E. C. Chang, C. C. Chen, and C. C. Lin, “Water-assisted CO2 laser ablated glass and modified thermal bonding for capillary-driven bio-fluidic application.,” *Biomed. Microdevices*, vol. 12, no. 1, pp. 107–14, Feb. 2010.

[27] C. K. Chung, Y. S. Chen, and T. R. Shih, “Fabrication and flow test of long-term hydrophilic fluidic chip without using any surface modification treatment,” *Microfluid. Nanofluidics*, vol. 6, no. 6, pp. 853–857, Nov. 2008.

[28] H. Li, Y. Fan, R. Kodzius, and I. G. Foulds, “Fabrication of polystyrene microfluidic devices using a pulsed CO2 laser system,” *Microsyst. Technol.*, vol. 18, no. 3, pp. 373–379, Dec. 2011.

[29] H.-B. Liu and H.-Q. Gong, “Templateless prototyping of polydimethylsiloxane microfluidic structures using a pulsed CO2 laser,” *J. Micromechanics Microengineering*, vol. 19, no. 3, pp. 37002–37010, Mar. 2009.

[30] B. A. Fogarty, K. E. Heppert, T. J. Cory, K. R. Hulbutta, R. S. Martin, and S. M. Lunte, “Rapid fabrication of poly(dimethylsiloxane)-based microchip capillary electrophoresis devices using CO2 laser ablation.,” *Analyst*, vol. 130, no. 6, pp. 924–30, Jun. 2005.

[31] J. Huft, D. J. Da Costa, D. Walker, and C. L. Hansen, “Three-dimensional large-scale microfluidic integration by laser ablation of interlayer connections.,” *Lab Chip*, vol. 10, no. 18, pp. 2358–65, Sep. 2010.

[32] B. A. Fogarty, K. E. Heppert, T. J. Cory, K. R. Hulbutta, R. S. Martin, and S. M. Lunte, “Rapid fabrication of poly(dimethylsiloxane)-based microchip capillary electrophoresis devices using CO2 laser ablation.,” *Analyst*, vol. 130, no. 6, pp. 924–30, Jun. 2005.

[33] M. Li, S. Li, J. Wu, W. Wen, W. Li, and G. Alici, “A simple and cost-effective method for fabrication of integrated electronic-microfluidic devices using a laser-patterned PDMS layer,” *Microfluid. Nanofluidics*, vol. 12, no. 5, pp. 751–760, Dec. 2011.

[34] S. Xing, R. S. Harake, and T. Pan, “Droplet-driven transports on superhydrophobic-patterned surface microfluidics.,” *Lab Chip*, vol. 11, no. 21, pp. 3642–8, Dec. 2011.

[35] A. Chen and T. Pan, “Three-dimensional fit-to-flow microfluidic assembly.,” *Biomicrofluidics*, vol. 5, no. 4, pp. 46505–465059, Dec. 2011.

[36] D. C. Leslie, B. A. Melnikoff, D. J. Marchiarullo, D. R. Cash, J. P. Ferrance, and J. P. Landers, “A simple method for the evaluation of microfluidic architecture using flow quantitation via a multiplexed fluidic resistance measurement,” *Lab Chip*, vol. 10, no. 15, p. 1960, 2010.

[37] National Aeronautics and Space Administration, “Man-Systems Integration Standards,” vol. 1, no. 4.9.3.

[38] C. A. Burtis and E. R. Ashwood, Eds., *Tietz Textbook of Clinical Chemistry*, 3rd ed. W.B. Saunders Company, 1999.

[39] K. Lee, C. Kim, B. Ahn, R. Panchapakesan, A. R. Full, L. Nordee, J. Y. Kang, and K. W. Oh, “Generalized serial dilution module for monotonic and arbitrary microfluidic gradient generators.,” *Lab Chip*, vol. 9, no. 5, pp. 709–17, Mar. 2009.

[40] C. Kim, K. Lee, J. H. Kim, K. S. Shin, K.-J. Lee, T. S. Kim, and J. Y. Kang, “A serial dilution microfluidic device using a ladder network generating logarithmic or linear concentrations.,” *Lab Chip*, vol. 8, no. 3, pp. 473–9, Mar. 2008.

[41] S. Dertinger, D. Chiu, and N. Jeon, “Generation of gradients having complex shapes using microfluidic networks,” *Anal. Chem.*, vol. 73, no. 6, pp. 1240–1246, 2001.

[1] M. A. Unger, H.-P. Chou, T. Thorsen, A. Scherer, and S. R. Quake, “Monolithic Microfabricated Valves and Pumps by Multilayer Soft Lithography,” *Science.*, vol. 288, no. 5463, pp. 113–116, Apr. 2000.

[2] W. H. Grover, A. M. Skelley, C. N. Liu, E. T. Lagally, and R. A. Mathies, “Monolithic membrane valves and diaphragm pumps for practical large-scale integration into glass microfluidic devices,” *Sensors Actuators B Chem.*, vol. 89, no. 3, pp. 315–323, Apr. 2003.

[3] T. Thorsen, S. J. Maerkl, and S. R. Quake, “Microfluidic large-scale integration.,” *Science*, vol. 298, no. 5593, pp. 580–4, Oct. 2002.

[4] E. T. Lagally, J. R. Scherer, R. G. Blazej, N. M. Toriello, B. A. Diep, M. Ramchandani, G. F. Sensabaugh, L. W. Riley, and R. A. Mathies, “Integrated portable genetic analysis microsystem for pathogen/infectious disease detection.,” *Anal. Chem.*, vol. 76, no. 11, pp. 3162–70, Jun. 2004.

[5] C. J. Easley, J. M. Karlinsey, J. M. Bienvenue, L. A. Legendre, M. G. Roper, S. H. Feldman, M. A. Hughes, E. L. Hewlett, T. J. Merkel, J. P. Ferrance, and J. P. Landers, “A fully integrated microfluidic genetic analysis system with sample-in-answer-out capability.,” *Proc. Natl. Acad. Sci. U. S. A.*, vol. 103, no. 51, pp. 19272–7, Dec. 2006.

[6] C. H. Ahn, J.-W. Choi, G. Beaucage, J. Nevin, J.-B. Lee, a. Puntambekar, and R. J. Y. Lee, “Disposable Smart Lab on a Chip for Point-of-Care Clinical Diagnostics,” *Proc. IEEE*, vol. 92, no. 1, pp. 154–173, Jan. 2004.

[7] D. Duffy, H. Gillis, and J. Lin, “Microfabricated centrifugal microfluidic systems: characterization and multiple enzymatic assays,” *Anal. Chem.*, vol. 71, no. 20, pp. 4669–4678, 1999.

[8] R. Johnson, I. Badr, G. Barrett, and S. Lai, “Development of a fully integrated analysis system for ions based on ion-selective optodes and centrifugal microfluidics,” *Anal. Chem.*, vol. 73, no. 16, pp. 3940–6, Aug. 2001.

[9] T.-S. Leu and P.-Y. Chang, “Pressure barrier of capillary stop valves in micro sample separators,” *Sensors Actuators A Phys.*, vol. 115, no. 2–3, pp. 508–515, Sep. 2004.

[10] H. Andersson, W. Van Der Wijngaart, P. Griss, and F. Niklaus, “Hydrophobic valves of plasma deposited octafluorocyclobutane in DRIE channels,” *Sensors Actuators B Chem.*, vol. 75, pp. 136–141, 2001.

[11] Y. Feng, Z. Zhou, X. Ye, and J. Xiong, “Passive valves based on hydrophobic microfluidics,” *Sensors Actuators A Phys.*, vol. 108, no. 1–3, pp. 138–143, Nov. 2003.

[12] Y. Ouyang, S. Wang, J. Li, P. S. Riehl, M. Begley, and J. P. Landers, “Rapid patterning of ‘tunable’ hydrophobic valves on disposable microchips by laser printer lithography.,” *Lab Chip*, vol. 13, no. 9, pp. 1762–71, May 2013.

[13] K. W. Oh and C. H. Ahn, “A review of microvalves,” *J. Micromechanics Microengineering*, vol. 16, no. 5, pp. R13–R39, May 2006.

[14] D. J. Laser and J. G. Santiago, “A review of micropumps,” *J. Micromechanics Microengineering*, vol. 14, no. 6, pp. R35–R64, Jun. 2004.

[15] S. Santra, P. Holloway, and C. D. Batich, “Fabrication and testing of a magnetically actuated micropump,” *Sensors Actuators B Chem.*, vol. 87, pp. 358–364, 2002.

[16] M. L. Adams, M. L. Johnston, A. Scherer, and S. R. Quake, “Polydimethylsiloxane based microfluidic diode,” *J. Micromechanics Microengineering*, vol. 15, no. 8, pp. 1517–1521, Aug. 2005.

[17] K. Iwai, A. T. Higa, R. D. Sochol, and L. Lin, “A Finger-Powered Cell Encapsulation System,” *Proc. 15th Int. Conf. Miniaturized Syst. Chem. Life Sci. (uTAS 2011)*, pp. 1182–1184, 2011.

[18] D. C. Leslie, C. J. Easley, E. Seker, J. M. Karlinsey, M. Utz, M. R. Begley, and J. P. Landers, “Frequency-specific flow control in microfluidic circuits with passive elastomeric features,” *Nat. Phys.*, vol. 5, no. 3, pp. 231–235, Feb. 2009.

[19] B. Mosadegh, C.-H. Kuo, Y.-C. Tung, Y.-S. Torisawa, T. Bersano-Begey, H. Tavana, and S. Takayama, “Integrated Elastomeric Components for Autonomous Regulation of Sequential and Oscillatory Flow Switching in Microfluidic Devices.,” *Nat. Phys.*, vol. 6, no. 6, pp. 433–437, Jun. 2010.

[20] J. K. Chang, H. Bang, S.-J. Park, S. Chung, C. Chung, and D. C. Han, “Fabrication of the PDMS microchip for serially diluting sample with buffer,” *Microsyst. Technol.*, vol. 9, no. 8, pp. 555–558, Oct. 2003.

[21] B. M. Paegel, W. H. Grover, A. M. Skelley, R. A. Mathies, and G. F. Joyce, “Microfluidic serial dilution circuit.,” *Anal. Chem.*, vol. 78, no. 21, pp. 7522–7, Nov. 2006.

[22] C.-W. Huang, S.-B. Huang, and G.-B. Lee, “A microfluidic device for precise pipetting,” *J. Micromechanics Microengineering*, vol. 18, no. 3, p. 035004, Mar. 2008.

[23] T. V Nguyen, P. N. Duncan, S. Ahrar, and E. E. Hui, “Semi-autonomous liquid handling via on-chip pneumatic digital logic.,” *Lab Chip*, vol. 12, no. 20, pp. 3991–4, Oct. 2012.

[24] E. C. Jensen, A. M. Stockton, T. N. Chiesl, J. Kim, A. Bera, and R. A. Mathies, “Digitally programmable microfluidic automaton for multiscale combinatorial mixing and sample processing.,” *Lab Chip*, vol. 13, no. 2, pp. 288–96, Jan. 2013.

[25] W. Li, T. Chen, Z. Chen, P. Fei, Z. Yu, Y. Pang, and Y. Huang, “Squeeze-chip: A finger controlled microfluidic flow network device and its application to biochemical assays,” *Lab Chip*, vol. 12, no. 9, 2012.

[26] C. K. Chung, H. C. Chang, T. R. Shih, S. L. Lin, E. J. Hsiao, Y. S. Chen, E. C. Chang, C. C. Chen, and C. C. Lin, “Water-assisted CO2 laser ablated glass and modified thermal bonding for capillary-driven bio-fluidic application.,” *Biomed. Microdevices*, vol. 12, no. 1, pp. 107–14, Feb. 2010.

[27] C. K. Chung, Y. S. Chen, and T. R. Shih, “Fabrication and flow test of long-term hydrophilic fluidic chip without using any surface modification treatment,” *Microfluid. Nanofluidics*, vol. 6, no. 6, pp. 853–857, Nov. 2008.

[28] H. Li, Y. Fan, R. Kodzius, and I. G. Foulds, “Fabrication of polystyrene microfluidic devices using a pulsed CO2 laser system,” *Microsyst. Technol.*, vol. 18, no. 3, pp. 373–379, Dec. 2011.

[29] H.-B. Liu and H.-Q. Gong, “Templateless prototyping of polydimethylsiloxane microfluidic structures using a pulsed CO2 laser,” *J. Micromechanics Microengineering*, vol. 19, no. 3, pp. 37002–37010, Mar. 2009.

[30] B. A. Fogarty, K. E. Heppert, T. J. Cory, K. R. Hulbutta, R. S. Martin, and S. M. Lunte, “Rapid fabrication of poly(dimethylsiloxane)-based microchip capillary electrophoresis devices using CO2 laser ablation.,” *Analyst*, vol. 130, no. 6, pp. 924–30, Jun. 2005.

[31] J. Huft, D. J. Da Costa, D. Walker, and C. L. Hansen, “Three-dimensional large-scale microfluidic integration by laser ablation of interlayer connections.,” *Lab Chip*, vol. 10, no. 18, pp. 2358–65, Sep. 2010.

[32] B. A. Fogarty, K. E. Heppert, T. J. Cory, K. R. Hulbutta, R. S. Martin, and S. M. Lunte, “Rapid fabrication of poly(dimethylsiloxane)-based microchip capillary electrophoresis devices using CO2 laser ablation.,” *Analyst*, vol. 130, no. 6, pp. 924–30, Jun. 2005.

[33] M. Li, S. Li, J. Wu, W. Wen, W. Li, and G. Alici, “A simple and cost-effective method for fabrication of integrated electronic-microfluidic devices using a laser-patterned PDMS layer,” *Microfluid. Nanofluidics*, vol. 12, no. 5, pp. 751–760, Dec. 2011.

[34] S. Xing, R. S. Harake, and T. Pan, “Droplet-driven transports on superhydrophobic-patterned surface microfluidics.,” *Lab Chip*, vol. 11, no. 21, pp. 3642–8, Dec. 2011.

[35] A. Chen and T. Pan, “Three-dimensional fit-to-flow microfluidic assembly.,” *Biomicrofluidics*, vol. 5, no. 4, pp. 46505–465059, Dec. 2011.

[36] D. C. Leslie, B. A. Melnikoff, D. J. Marchiarullo, D. R. Cash, J. P. Ferrance, and J. P. Landers, “A simple method for the evaluation of microfluidic architecture using flow quantitation via a multiplexed fluidic resistance measurement,” *Lab Chip*, vol. 10, no. 15, p. 1960, 2010.

[37] National Aeronautics and Space Administration, “Man-Systems Integration Standards,” vol. 1, no. 4.9.3.

[38] C. A. Burtis and E. R. Ashwood, Eds., *Tietz Textbook of Clinical Chemistry*, 3rd ed. W.B. Saunders Company, 1999.

[39] K. Lee, C. Kim, B. Ahn, R. Panchapakesan, A. R. Full, L. Nordee, J. Y. Kang, and K. W. Oh, “Generalized serial dilution module for monotonic and arbitrary microfluidic gradient generators.,” *Lab Chip*, vol. 9, no. 5, pp. 709–17, Mar. 2009.

[40] C. Kim, K. Lee, J. H. Kim, K. S. Shin, K.-J. Lee, T. S. Kim, and J. Y. Kang, “A serial dilution microfluidic device using a ladder network generating logarithmic or linear concentrations.,” *Lab Chip*, vol. 8, no. 3, pp. 473–9, Mar. 2008.

[41] S. Dertinger, D. Chiu, and N. Jeon, “Generation of gradients having complex shapes using microfluidic networks,” *Anal. Chem.*, vol. 73, no. 6, pp. 1240–1246, 2001.

Chapter 4. Bead-Assisted Acoustic Differential Extraction of Sperm Cells in Dilute Samples for Potential Forensic Analyses

4.1 Introduction

Genetic analysis has been well established to be a powerful tool in human identification in terms of its high accuracy and specificity[1][2]. To obtain an unambiguous short tandem repeat (STR) profile, individual's biological sample has to be purified that avoids interference from other donor's DNA. In sexual assault (SA) cases evidence samples, usually in the form of vaginal swabs, contain both female epithelial cells and sperm cells. Accurate STR identification of male perpetrator requires separation of sperm cells from female DNA through differential extraction (DE), a commonly used technique in which female epithelial cells are first preferentially lysed while sperm cells remain intact due to their resilient membranes to proteinase, then separated from female DNA after several steps of wash, centrifugation and supernatant removal[3][4]. Although well-established, DE still remains one of the most time-consuming steps in the sample preparation of SA analysis, leading to significant backlog of SA evidence[5]. Extensive liquid handling in DE also hinders the automation of the procedure, raising the risk of human errors, contaminations and inefficient removal of female DNA.

Recent studies on microfluidic devices provided alternative methods for cell separation that lowered the burden of conventional centrifugation. Micro-fabricated filter or sieving structures in microfluidic device have been developed to separate particles above

certain cut-off size[6], [7] and these techniques have been applied to the separation of sperm cells from female epithelial cells[8]. However, clogging by large cells in the microstructures might reduce the recovery rate of filtrated cells of interest. Another type of passive cell separation techniques are based on hydrodynamic effects[9]–[13], however, the separation effect in these techniques requires strict flow rate conditions related to specific particles sizes, which makes these methods less flexible when applied towards various types of particles. In addition, these separation effects also requires a continuous flow through a relatively long, sometimes tandem-structured flow path which consumes significant space and efforts cost in microdevice design. Being a non-contact cell capture technique, dielectrophoresis (DEP) exploits electric field to trap dielectric particles or cells. Under a non-uniform electric field, a dipole moment will be induced in a dielectric particle and the DEP force acting on it will drive it to move[14]–[16]. However, to perform a desired trapping, a certain dielectric property of the buffer solution is required and should be adjusted prior to use, thus the compatibility of the method will be constricted by its working medium, especially when dealing with environment-sensitive biological samples.

In the last ten years, acoustic manipulation of particles in microfluidic flow has emerged as a promising new technology to enrich target microbes from diluted samples[17]. By exploiting acoustic waves generated by the high frequency vibration of a piezoelectric transducer (PZT), a well-defined pressure field distribution can be created within a microdevice, depending on the geometric features and mechanical properties of the microfluidic channel. In a sound-reflective cavity, the distribution of the resonating acoustic pressure field can be represented in the form of standing waves, created by the resonance of incident and reflected acoustic waves. The nodes of the standing waves

indicate the region of zero pressure gradient, in which particles are directed and trapped. Successful applications of acoustic trapping have been reported including the enrichment of yeast cells from water suspension[18], separation of blood cells from plasma[19] and online bioassay[20].

The power of acoustic trapping could also be exploited in the separation of sperm cells from female DNA. In our lab's previous work we have demonstrated the acoustic differential extraction (ADE) of sperm cells from mock sexual assault (SA) samples[21]. The concept of ADE has been proved highly efficient in terms of complete removal of female DNA and purified recovery of the sperm cells with complete, sole male STR profile obtained. However, this proof-of-principle procedure requires relatively high sample concentrations (~500 sperm cells/μL) and has a low processing throughput (1 μL/min), limiting its applicability to evidentiary samples that may contain less than 10 sperm cell/μL in a total volume of ≥100 μL. In this work, we investigated the efficiencies of acoustic trapping at a series of low concentrations of semen sample down to single cell per microliter. Trapping of such dilute semen sample was problematic because of insufficient aggregate formation. In order to retain the trapping efficiency at low cell concentration we use assisting polymeric beads to facilitate the formation of the trapping aggregate. The strategy of bead-assisted trapping was first developed by Hammarström et al. in the trapping of *E. coli,* a typical bacterial microbes that is otherwise too small to be trapped as an aggregate [22]. In this work we extended this strategy into the forensic field and proved its success in the separation of larger mammalian cells but in even more diluted concentration down to 1 cell per microliter.

4.2 Material and Methods

Unless otherwise specified, all reagents are purchased from Sigma Aldrich.

4.2.1 Simulation of the acoustic trapping

2D simulation of the acoustic resonance was conducted in COMSOL Multiphysics. A chamber was created consisting of a coupling layer in borosilicate glass, a fluid layer in water and a reflecting layer in borosilicate glass (**Figure** 4-4). The eigenfrequencies that enables the establishment of vertical nodal planes are recorded as the resonance frequencies.

4.2.2 Fabrication of ultrasonic transducer and glass-PDMS-glass (GPG) microdevice

Piezoelectric transducer assemblies were built from lead zirconate titanate (PZT) piezoelectric ceramic (SMD10T04F5000S111, Steiner and Martins Inc.) that was diced, scored, and then mounted and glued on a printed circuit board (PCB) using conductive epoxy. Channels were cut through a ~280 μm PDMS film (Roger HT-6240 solid silicone) using CO_2 laser ablation (VersaLaser 350, Universal Laser Systems) and then plasma bonded between two layers of ~180 μm cover glass (Fisher Scientific, PA). Access holes were cut through glass cover using laser ablation. Silicone tubings (IDEX) were glued with windshield glue on the surface of the glass to interface the polytetrafluoroethylene (PTFE) tubings (Cole-Parmer) and the microdevice (Figure 4-1).

A localized USW can be established in a glass-PDMS-glass (GPG) microfluidic resonator between the top and bottom glass layers[23]. The resonance frequency $\boldsymbol{f}$ of the USW was dependent on the height of the cavity $\boldsymbol{h}$ (i.e. the thickness of the PDMS layer),

as predicted by the 1D resonance approximation, $h=n\lambda/2=nv/2f$, (n=1,2,3...) where v is the speed of sound in water. The coupling layer, fluid layer and reflecting layer (**Figure** 4-1) were selected at thicknesses of 180 μm (cover glass), 280 μm (PDMS) and 180 μm (cover glass), respectively, in order to meet the requirement for the establishment of USW ($\lambda/4$ in coupling layer and reflecting layer; and $3\lambda/2$ in fluid layer)[17], [23].

Two types of resonator chips were used in this work. The first type has a simpler structure which only has a straight channel and two access holes (Figure 4-1); and the second type has a more complicated structure which enables on-chip fluidic switching of different reagents(**Figure** 4-3).

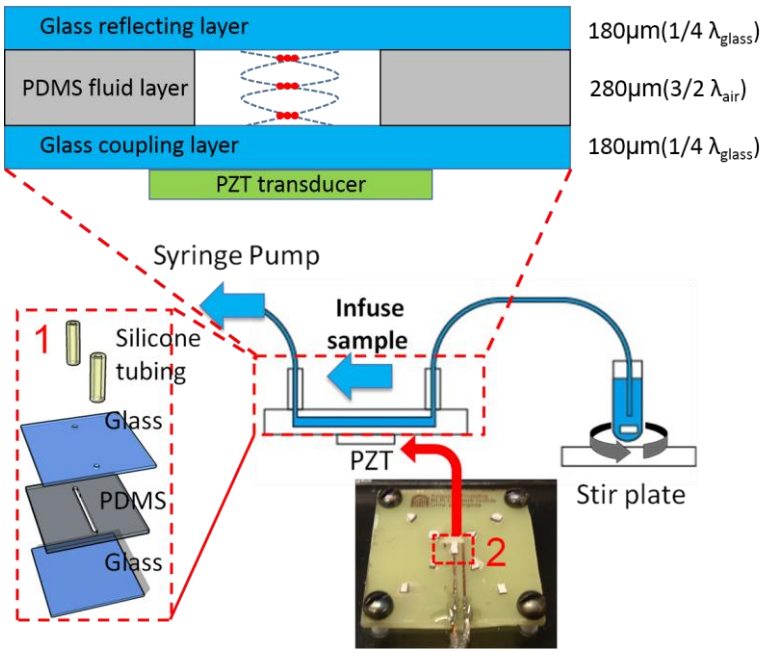

Figure 4-1. System of acoustic trapping. Simple Glass-PDMS-Glass (GPG) resonator chip (1) is fabricated by laser ablation and subsequent plasma bonding. Fluidic connections were made via PTFE tubing inserted into silicone tubing affixed with silicone adhesive. Completed GPG chip was clamped against a PZT transducer mounted on a printed circuit board (2).

4.2.3 Generation of the ultrasonic standing waves

During acoustic trapping the transducer was actuated near 8 MHz and ~12 V_{pp}. using a 20 MHz function generator (Agilent 33220A) and an in-house built amplifier.

4.2.4 Acoustic trapping and quantitation of sperm and fluorescent beads

Stock solution of 6 μm Yellow-Green fluorescent polystyrene beads (Polysciences) was diluted with 0.1% TWEEN 20 buffer solution creating a series of concentrations ranging from 10 to 800 per microliter

Neat semen samples were diluted with 0.1% TWEEN 20 buffer solution and labeled with 10 mM Syto 11 (Invitrogen), creating a series of concentrations ranging from 1 to 800 per microliter. Trapping was conducted at flow rate of 30 μL/min, f=8MHz and Vpp=12V.

The solution flowing through the acoustic trapping was collected and the concentration of the particles in it was quantitated using hemocytometer (Glasstic, KOVA slide II, Hycor Biomedical) under fluorescence microscope (excitation wavelength 488nm). The trapping efficiencies at different concentrations were calculated based on the quantitation result.

For semen samples at the concentration of ~1 cell per microliter, the trapping process was recorded by a CCD camera (Hitachi) mounted on the microscope and the trapping efficiency was obtained by direct counting of the trapped cells versus the total number of infused cells.

4.2.5 Bead-assisted trapping of sperm cells in mock SA sample

Neat semen samples were diluted with 0.01% TWEEN 20 and labeled with 10 mM Syto 11 (Invitrogen). The polymeric bead solution was prepared by diluting 6 μm violet polystyrene beads (Polysciences) in 0.1% TWEEN 20. Mixed samples were prepared by spiking calculated amount of diluted semen sample and bead solution into female standard DNA solution making a final mixture solution containing ~10 sperm cells/μL, ~400 beads/μL and 0.125 ng/μL female DNA (9947A female standard DNA, Promega). The ratio of female to male DNA concentration was about 5:1.

In order to perform the acoustic differential extraction (ADE) on the mocked sample a more complicated ADE microdevice was designed (**Figure** 4-3A). The flow switching of the ADE microdevice is achieved by actively controlled check valves (Figure 4-2). Briefly, the ADE microdevice has three branch channels that all connect to the resonator part, and each branch channel has a check valve to switch its open/closed state. The three branch channels correspond to three stages in ADE (Figure 4-3B): sample infusion/trapping, buffer wash and cell elution, with infusion of 300 μL mixture sample, 100 μL wash buffer and 50 μL elution buffer, respectively.

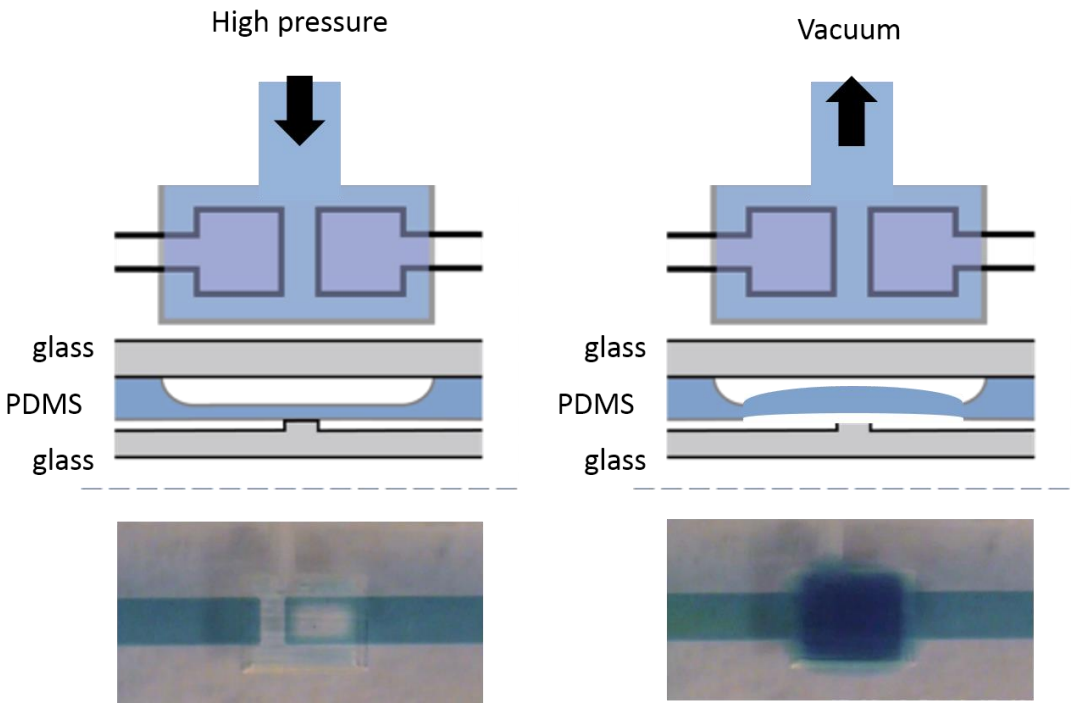

Figure 4-2. The schematics and real photos of the GPG check valve in closed (left panel) and open (right panel) states. Blue dye solution is used to fill the fluid channel for better visualization.

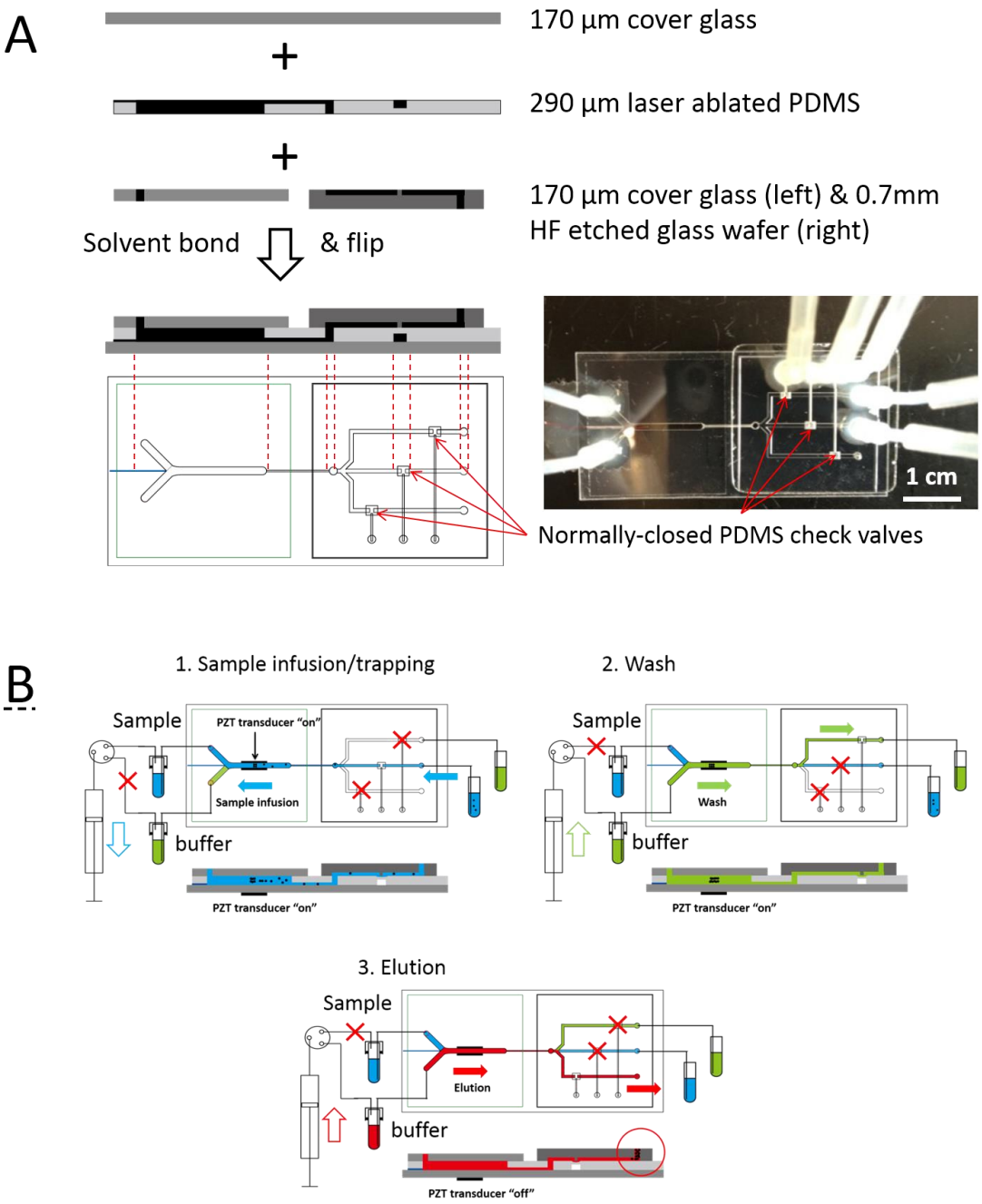

Figure 4-3. GPG integrated chip for the ADE of sperm cells from mixed sample. (A) Design and fabrication of the integrated GPG chip. The photo shows the real chip after bonding and connection with tubings. (B) The three stages of ADE showing the flow control: sample infusion and trapping, wash and elution.

4.2.6 DNA extraction and genotyping of the trapped sperm cells

DNA from cell samples was isolated via solid phase extraction (QIAmp DNA Mini Kit, Qiagen) followed by STR-PCR (AmpFLSTR Identifiler PCR Amplification Kit, Applied Biosystems). The amplified STR sequences were analyzed by multi-color capillary electrophoresis (ABI 310, Applied Biosystems).

4.3 Results and Discussion

4.3.1 Simulation and experimental validation of the trapping by USW

The simulation gives the resonance frequency at about 8 MHz, with 3 trapping nodes established in the vertical direction. The nodal planes in the simulation show lower sound pressure levels which means these regions are the local valleys of the energy landscape and particles will be accumulated in these regions.

The simulated acoustic trapping with three trapping nodes is validated by experimental results where the aggregates are being trapped in a GPG resonator at 8MHz, and upon being released and eluted by the flowing medium, due to the different fluidic velocities at multiple vertical positions, three layers of the aggregates are shifted apart and clearly observed.

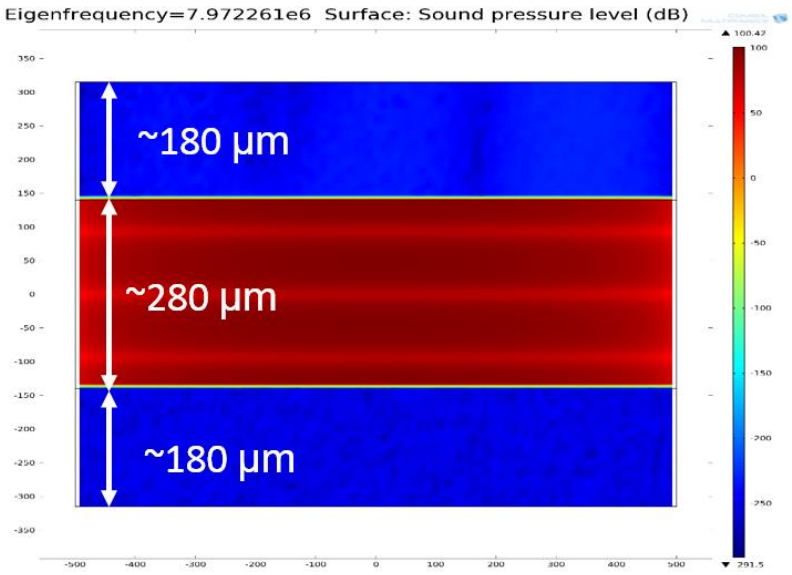

Figure 4-4. Simulation result of the ultrasonic standing waves at ~8MHz. The simulation shows three trapping nodes in the vertical direction

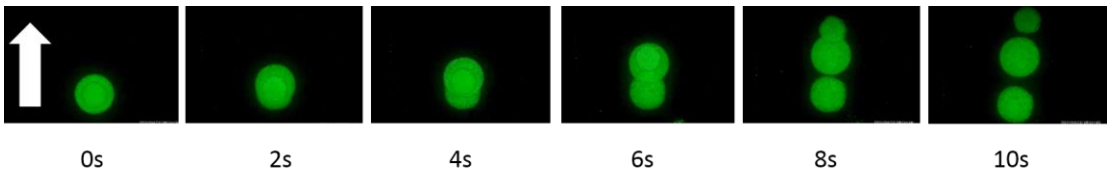

Figure 4-5. The shifting apart of the layers of aggregates of fluorescent beads upon releasing at 0s. Three layers of the aggregates can be clearly observed. The white arrow indicate the direction of the flow.

4.3.2 Resonance in GPG resonator

The resonance frequency of the acoustic trapping is found by finding the point where beads are best trapped. The theoretical resonance frequency of the acoustic trapping can be calculated by the height of the resonator:

$$f = \frac{v}{\lambda} = \frac{v}{\frac{2}{3}h} = \frac{3v}{2} \cdot \frac{1}{h}$$

where ***h*** is the height of the channel, and ***v*** is the speed of sound in water.

The experimental resonance frequency ***f*** is plotted versus **1/*h*** in **Figure** 4-6 and a proportional relationship is found by linear fitting, which is consistent with the theoretical calculation. The speed of sound in water is found to be 1517 m/s during the acoustic trapping, and by interpolate this value in the chart of water temperature-speed of sound relationship[24], the temperature of water is found to be 33-34 ℃, a mild level that is not harmful to human cells.

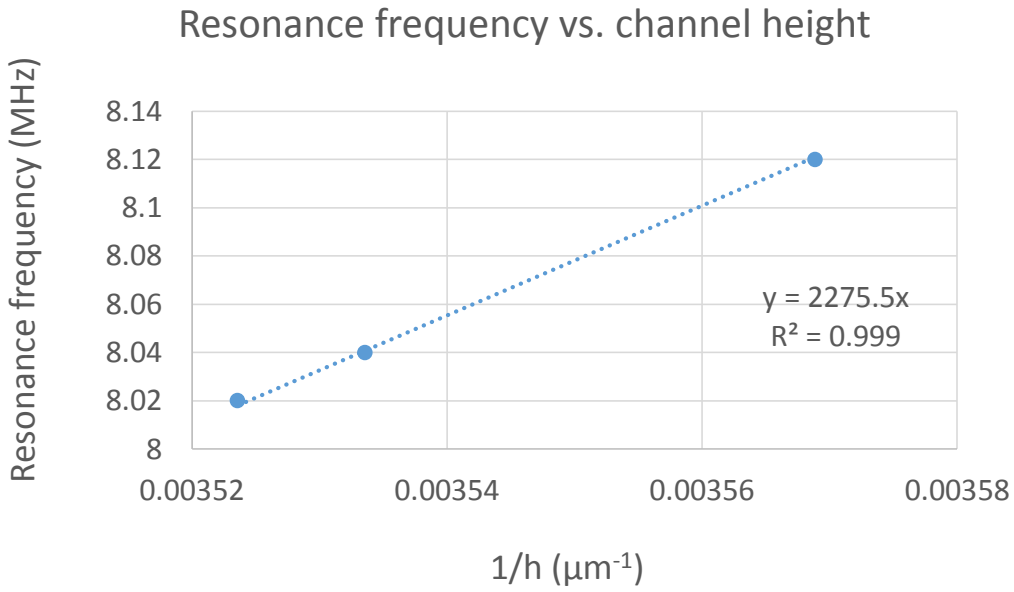

Figure 4-6. Resonance frequency f versus reciprocal of channel height (1/h) and fitted by linear regression.

4.3.3 Concentration dependent trapping efficiency

Trapping efficiency (number of retained particles / number of total infused particles ×100 %) decreases as the particle concentration drops (Figure 4-7). Both fluorescent beads and sperm cells can be trapped with efficiency over 80%, until the concentration decreases below 100 per microliter. The trapping efficiency drops sharply as the concentration decreases below 100 per micro liter, which reaches ~20% at the lowest concentration of ~10 particles per microliter.

The sharp decrease of trapping efficiency in dilute sample is attributed to the difficulties in aggregate formation[22]. The formation of aggregate in acoustic trapping mainly requires two sequential stages: (1) upon entering the acoustic field particles get slowed down by the primary radiation force (PRF) and recruited to the nodal plane of the USW; (2) when particles moves together and the interparticle distance is close enough, the secondary radiation force (SRF) rises and pull particles together to form a compact aggregate to resist the hydrodynamic drag to be captured[25]. Because the SRF is inversely proportional to $\boldsymbol{d^4}$ [25] ($\boldsymbol{d}$ is the interparticle distance), it diminishes drastically when the particles gets apart even by a small distance. As a result, SRF cannot hold particles together unless they are close enough.

To better show this unsuccessful trapping process due to enlarged inter-particle distance in dilute samples, we trafficked the trace of fluorescently labeled single cell at highly dilute concentration (1 per microliter) during acoustic trapping. Two cells have been recorded during a failed trapping process and their trajectories have been plotted in

Figure 4-8A. It shows that when two particles enter the acoustic field, they begin to slow down first and the inter-particle distance begins to decrease (Figure 4-8B). However, the inter-distance of the particle isn't close enough for the SRF to hold them together and they end up existing the acoustic field. The trapping efficiency of semen sample at 1 cell per microliter is only 18 ±3 % (n=3).

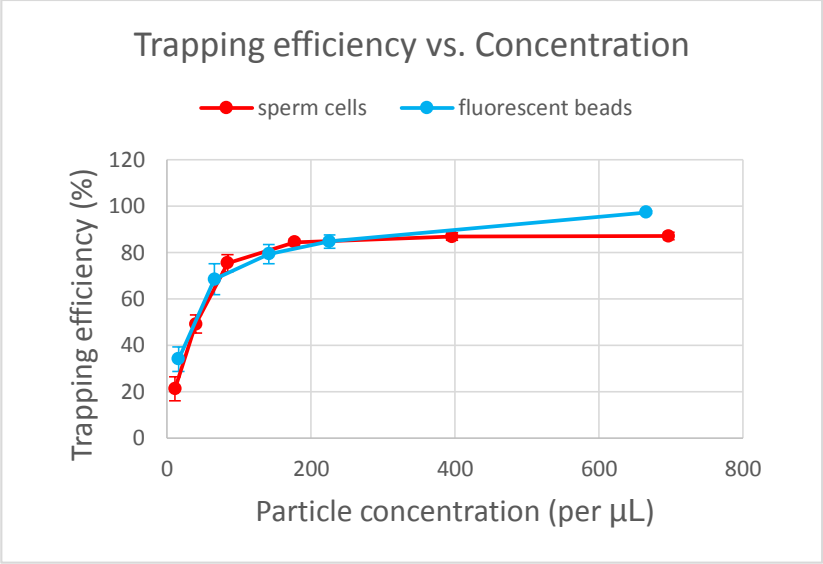

Figure 4-7. Dependence of trapping efficiency on particle concentration (n=3). Samples were infused at a flow rate of 30 µL/min and particles were quantitated via hemocytometer.

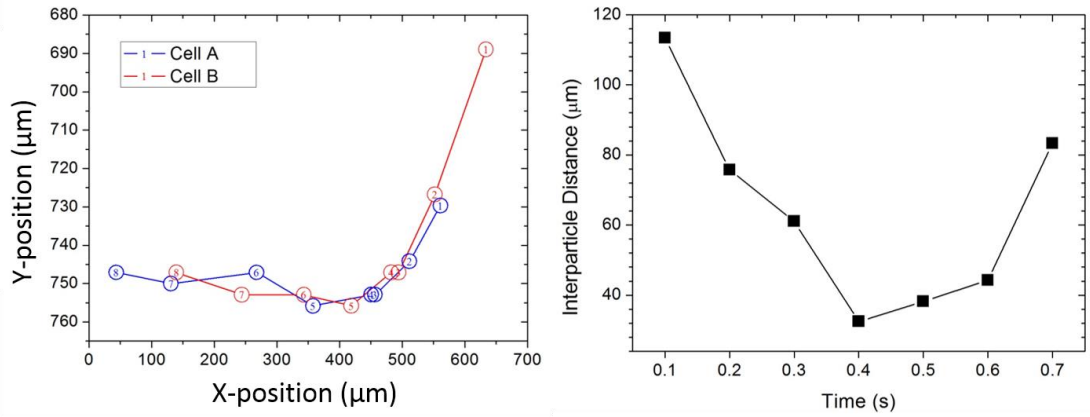

Figure 4-8. Trajectories and interdistance of two cells during a failed acoustic trapping process. (A) Step by step trajectories of two cells entering the acoustic field from 0 to 0.8s with time interval of 0.1s, labeled with order numbers. (B) Change of interdistance between cells.

4.3.4 Increase of trapping efficiency by bead-assisting strategy

The need of SRF in acoustic trapping requires the inter-particle distances to decrease fast enough when the particles travel through the acoustic field. Increasing the power of acoustic field can lead to stronger PRF and achieve that goal but the heat generation during trapping will also increase drastically and harm the sperm cells. Alternatively, because the 6 μm polymeric beads have similar dimensions with the sperm cells and show a similar trapping profile in **Figure** 4-6, we spike them into the dilute semen sample as "mimics" of the sperm cells to increase the total particle concentrations to assist trapping. The non-fluorescent violet beads shows significantly lower fluorescent intensity than the Syto 11-stained sperm cells (**Figure** 4-9) so it won't affect the monitoring of the sperm trapping under fluorescence microscopy while still being visible in bright-field microscopy.

After addition of the non-fluorescent polymeric beads, the dilute semen sample contains 1 cell and ~400 beads per microliter. Trapping under the same acoustic conditions is much more efficient than non-assisted one, with significant formation of aggregate consisting of beads and sperm cells (**Figure** 4-10). The efficiency of bead-assisted trapping is raised back to 85% ±4 % (n=3). The increased particle concentration reduces the inter-particle distance prior to the application of acoustic field and makes the particles get close quickly enough to let the SRF rise up and hold them together before brought away by the flowing medium. The effect of the bead-assisted strategy is consistent with previously reported "seeded" acoustic trapping[22].

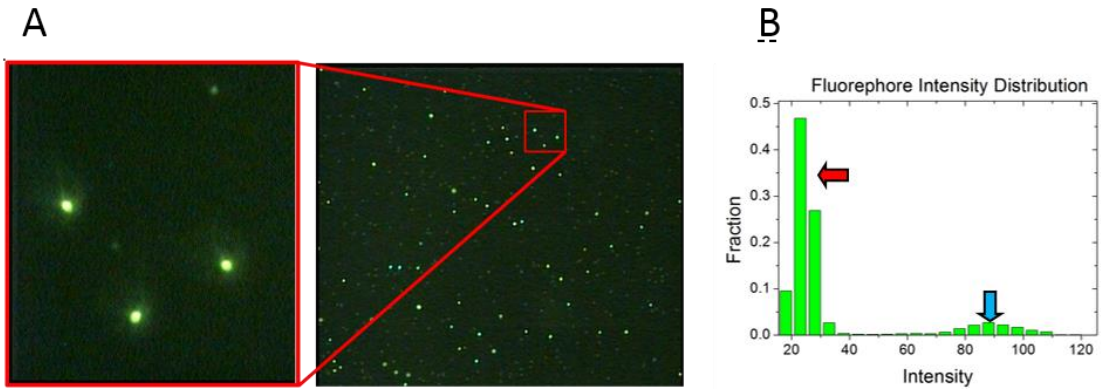

Figure 4-9. Comparison of fluorescence intensity of beads versus syto-11 stained sperm cells. (A) Fluorescence images and (B) fluorophore intensity distribution of the mixture of sperm cells (blue arrows) and polymeric beads (red arrows).

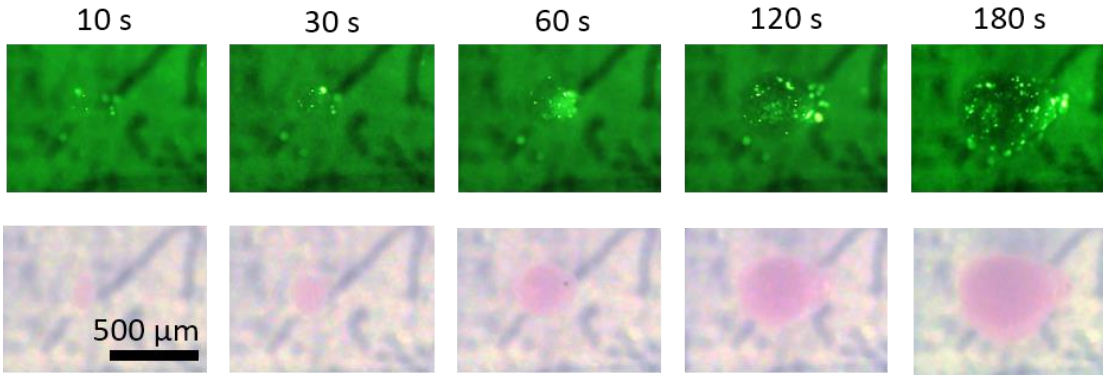

Figure 4-10. Visual monitoring of bead-assisted sperm trapping. Still images from video of a trapping experiment are shown at 10, 30, 60, 120, 180 seconds. The process was simultaneously monitored in fluorescence (upper row) and bright field (lower row) microscopy. The bright spots in the fluorescence images are fluorescently-stained sperm cells. Samples were infused at 30 µL/min for total volume of 100 µL.

4.3.5 Extraction of sperm cell and male DNA from mock SA sample

A test of bead-assisted ADE was performed on a sample containing ~10 sperm cells/µL, ~400 beads/µL and 0.125ng/µL standard female DNA. The whole process of trapping, washing and elution took about 17 min for a sample of 300 µL. The STR profiles of the mixed sample and female DNA are shown in Figure 4-11

The peaks from the female DNA obviously interfere the identification of the male profile. After ADE the full, purified STR profile of sperm cells with no detectable female peaks were obtained, indicating successful separation of the male and female components and negligible inhibition from the beads (Figure 4-12).

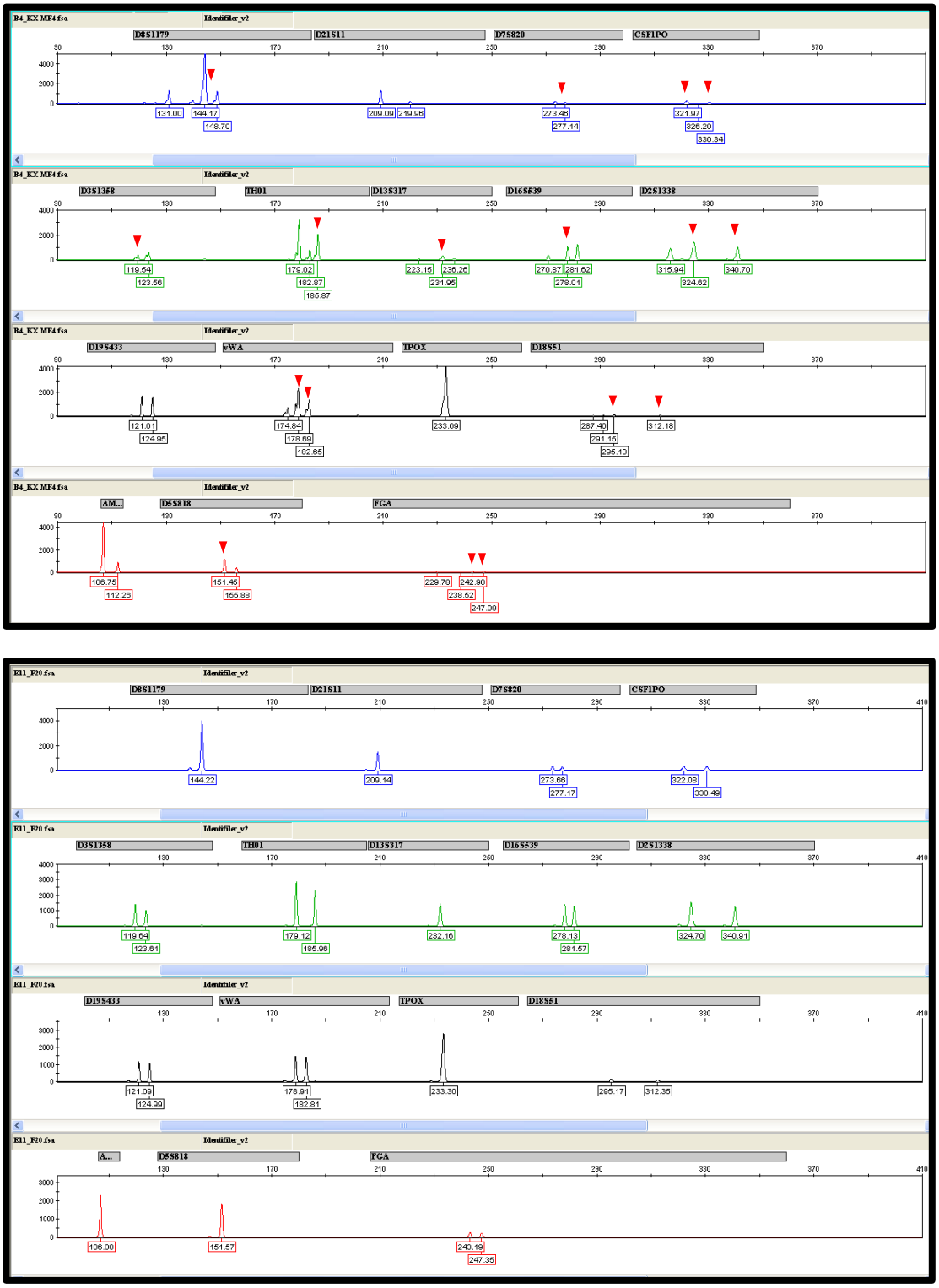

Figure 4-11. STR amplification of DNA in untreated mixed sample (top) and female profile (bottom). The interfering peaks from female profiles are pointed in the mixed sample's profile.

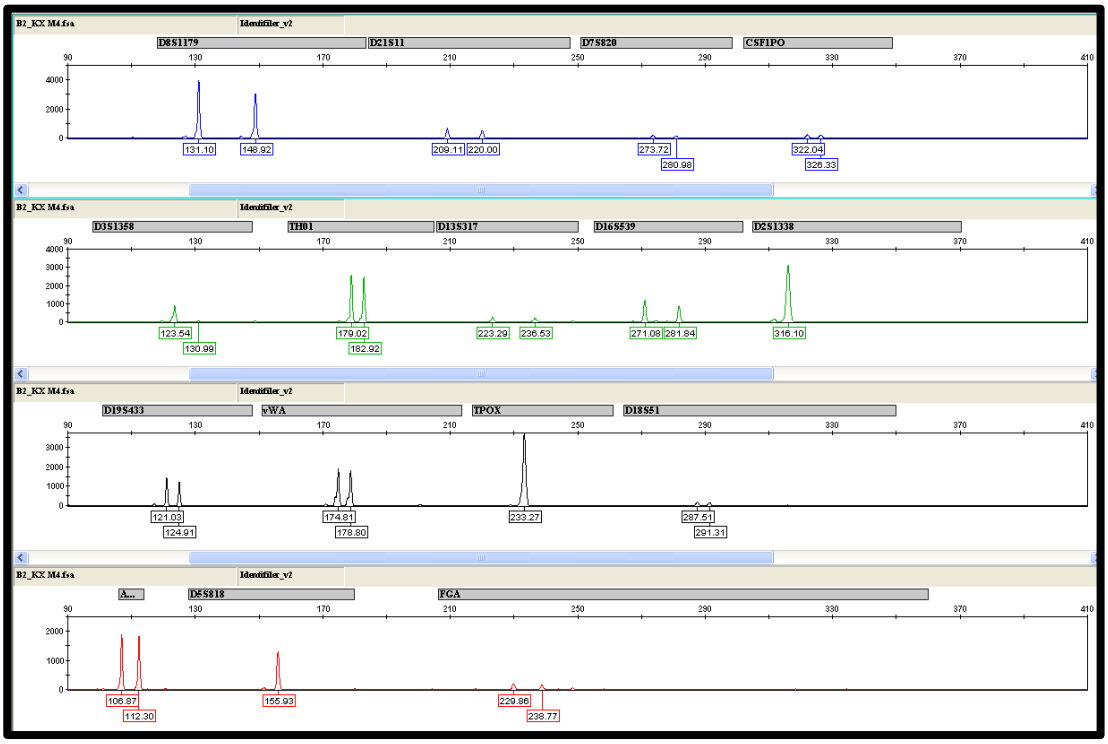

Figure 4-12. STR profile of purified sperm cells

4.3.6 Further development of the ADE system

In order to advance the current ADE system into a more portable, user-friendly method, further improvement and development have been implemented including (1) DNA extraction using EA1 enzyme; (2) improved manifold for the coupling of resonator and transducer; (3) smartphone camera monitored trapping and (4)design of disposable microdevices without tubing connections.

4.3.6.1 Liquid-based extraction of sperm DNA using EA1

In previous section 4.2.6, after the elution and collection of ADE, purified sperm cells are lysed by Proteinase K with the aid of reducing reagent dithiothreitol (DTT), followed by DNA extraction and purification using QIAmp DNA Mini kit. The whole

procedure of the DNA extraction is solid phase based and contains 16 steps of manual operations and a total processing time of 2 hours is required. The off-chip, post-trapping DNA extraction reduced the benefits of the automation and convenience brought by ADE, and the integration of the DNA extraction of the isolated sperm cells into the microdevice is highly desired in the future development. However, the integration of the solid phase extraction into the microdevice is not trivial[26], [27] in that : (1) consistent loading and filling of the solid phase column or bed on microdevice requires expertise, and (2) the pressure required for the fluid to flow through the solid-filled chamber is much higher than the liquid-filled channel because of the extremely high fluidic resistance.

In the further development a faster, more convenient DNA extraction method is needed with possibility of being integrated into the ADE system. Alternative to the solid phase extraction of DNA, liquid based DNA preparation using a neutral proteinase from an Antarctic *Bacillus* sp., EA1, has been developed[28] and applied in the treatment of forensic biological samples for STR analysis[29]. The enzyme EA1 can be used to lyse cells and degrade proteins including nucleases at 75 °C, while leaving the nucleic acids intact for subsequent PCR.

The efficiency of the EA1 on sperm cells was tested as follow: prior to the treatment by EA1, instead of using DTT, the sperm cells are pre-treated by another reducing reagent, tris(2-carboxyethyl)phosphine (TCEP) for its advantages of being odorless and more stable compared with DTT. The pre-treatment solution (pH 8.5) contains 10mM MES/Tris and 5mM TCEP. Neat semen sample was diluted in TCEP buffer (1μL of semen in 24μL of TCEP), and then pre-treated under 42 °C for 30min. 1μL of the pre-treated cell solution was added to the EA1 reaction mix to get further treatment, and after centrifugation of the

pre-treated cell solution, the supernatant is also collected for subsequent EA1 treatment to determine the loss rate of sperm cells by the undesired lysis during the pre-treatment. The pre-treated sperm cells and the supernatant were then treated by EA1-based DNA extraction kit (ZyGEM, New Zealand) following the extraction protocol for epithelial cells[29]. A control experiment was also done using 1X TE buffer for the pre-treatment step using the same protocols described above. The DNA concentration was determined by PicoGreen (Life Technologies) and the STR profile of the sperm cells are obtained by STR-PCR.

The results of the test are shown in Table 4-1. Obviously the TCEP pre-treatment has significantly increased the lysis of cells in the EA1 treatment compared with the control experiment, and the loss rate of the undesired lysis by the pre-treatment is low enough to be acceptable.

Table 4-1. The liquid phase extraction of the DNA of sperm cells using TCEP and EA1 (n=3)

	DNA from isolated cells (%)	DNA from supernatant (%)
Pretreatment by TCEP	80±6	9±2
Pretreatment by TE (control)	26±17	7±1

The full STR profile of the male DNA was successfully obtained (**Figure** 4-13), proving that the TCEP-EA1 extracted DNA is compatible with the STR PCR.

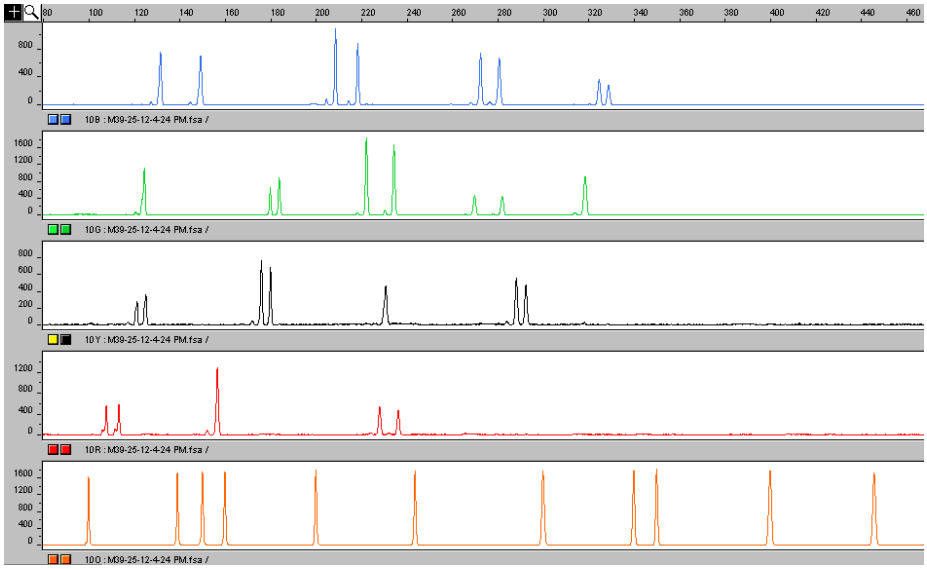

Figure 4-13. The full STR profile of the male DNA extracted by TCEP-EA1 protocol

4.3.6.2 Redesigned manifold for microdevice/transducer coupling

In the old design of the manifold for resonator-transducer coupling we used screws to tighten and add pressure onto the microdevice-transducer assembly. The biggest disadvantages of this type of design are: (1) the force is not uniformly nor consistently applied on to the assembly which causes cracking of the GPG microdevice and (2) each time to fasten the manifold multiple nuts (>4) need to be screwed in one by one which adds unnecessary manual operation.

To have a more convenient, more consistent and safer-to-chip coupling method we designed a new manifold to eliminate these disadvantages. The basic pressing force for microdevice-transducer coupling is provided by the repulsive forces between the same

polarities of two sets of face-to-face aligned magnets, and the major components of the manifold includes two sets of assembly each contains one upper plate and one lower plate, and can be operated independently(**Figure** 4-14 and **Figure** 4-15):

(1) One set for chip-transducer coupling and optical monitoring

(2) One set for fluidic connection and connected with syringe pumps or solenoid valves

In addition, to avoid cross-contamination between samples we designed a new type of microdevice with 6 on-chip reservoirs. All the reagents needed (bead test solution, sample and wash buffer) are loaded onto the microdevice by pipetting and the flow is driven by syringe-pushed air through the O-ring-sealed, air-tight interface on the manifold, so no liquid will be touched by the tubings in the manifold thus no transfer of contamination among microdevices.

The basic procedure of microdevice loading is:

(1) Insert the microdevice underneath the manifold

(2) Place the two lower plates on top of the microdevice

(3) Flip down the upper plates and lock up its position by a latch.

The distance between the upper plates and lower plates can be adjusted and fixed so that each loading the pressure applied is consistent and uniform. The pressure increase is also mild so that it won't snap the microdevice abruptly

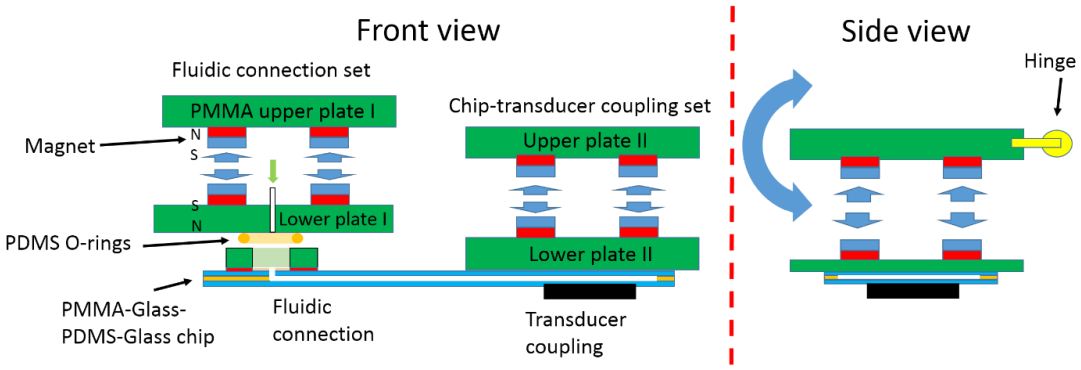

Figure 4-14. The schematic of the new manifold and chip.

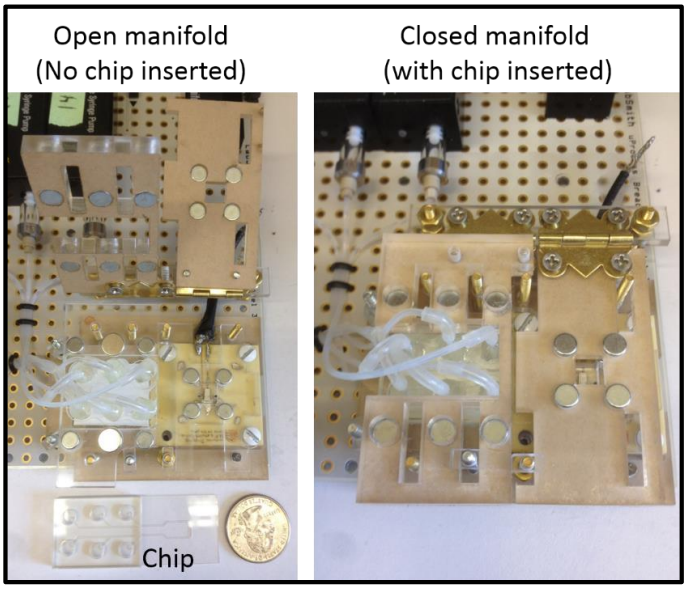

Figure 4-15. The actual photo of the manifold showing both the open state (idle) and closed state (working condition)

4.3.7 Smart phone camera-monitoring

A bulky part of the previous ADE system is the fluorescence microscope for the monitoring the trapping process. The miniaturization of the optical system for the monitoring of the trapping is still in progress. We used a smart phone camera coupled with

a laser pointer lens (**Figure** 4-16) to monitor the acoustic trapping. Formation and growing of the aggregates of yellow-green fluorescent beads (**Figure** 4-17) and Syto-11 stained sperm cells (**Figure** 4-18) has been clearly monitored.

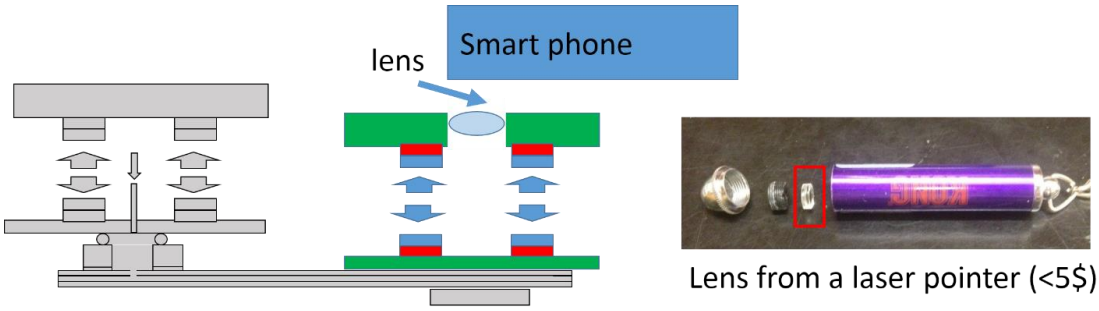

Figure 4-16: A laser pointer lens (in red nox) and the diagram of the smart phone-lens coupling through the manifold

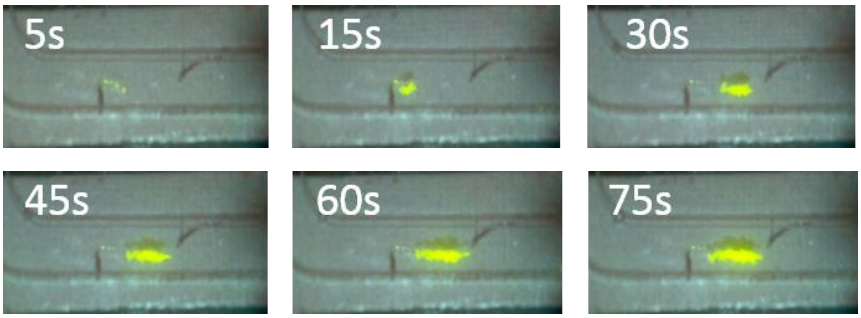

Figure 4-17: Video snapshots of 6µm fluorescent beads being trapped and recorded by a smart phone camera. Flow rate=30µL, frequency=8.1MHz, V_{pp}=12V

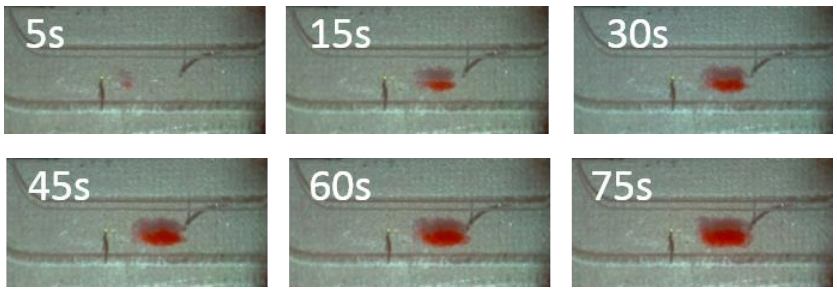

Figure 4-18: Video snapshots of 6µm Syto11-stained sperm cells being trapped and recorded by a smart phone. Flow rate=30µL, frequency=8.1MHz, V_{pp}=12V

4.3.7.1 Off-chip valving with 6-reservoir AGSiG microdevice

In previous design the ADE microdevice, part of the chip was HF-etched glass, which is not environmental friendly and consumes intensive labor and time. The current new design of the microdevice consists of three different materials: glass PDMS and PMMA and all the structures of the microdevice is fabricated by laser ablation which makes it truly low-cost and disposable.

The design of the 6-reservoir microdevice is shown in **Figure** 4-19 as well as the reagent assignment. The reservoir layer is made from PMMA so that the liquid can wet well on the wall of the reservoir, otherwise the solution will 'bead' a large droplet in the reservoir and touch the manifold causing contamination. The material used in the microdevice from the top to the bottom are: Polymethyl methAcrylate-Glass-PolydimethylSiloxane-Glass (AGSiG).

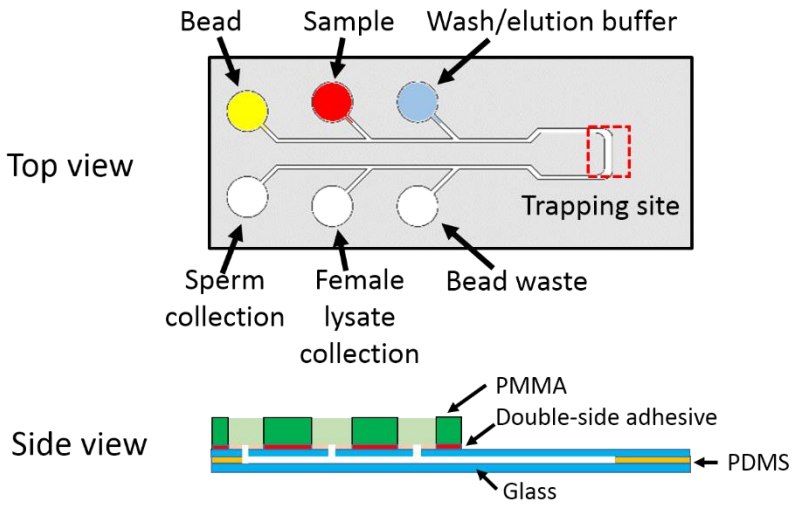

Figure 4-19: Structure of the PMMA-Glass-PDMS-Glass (AGSiG) chip

The off-chip valving procedure is shown in **Figure** 4-20 in which there are 5 steps in total:

(1) Add bead solution, sample solution and wash/elution buffer to R1, R2 and R3, respectively. Insert the microdevice underneath the manifold and close the manifold.

(2) Push bead solution from R1 to R4, close the other path (This is for the test trapping for the verification of microdevice's function)

(3) Push sample from R2 to R5, close the other path (sample trapping)

(4) Push wash/elution buffer from R3 to R5, close the other path (wash off the female lysate)

(5) Push wash/elution buffer from R3 to R6, close the other path (sperm cell elution)

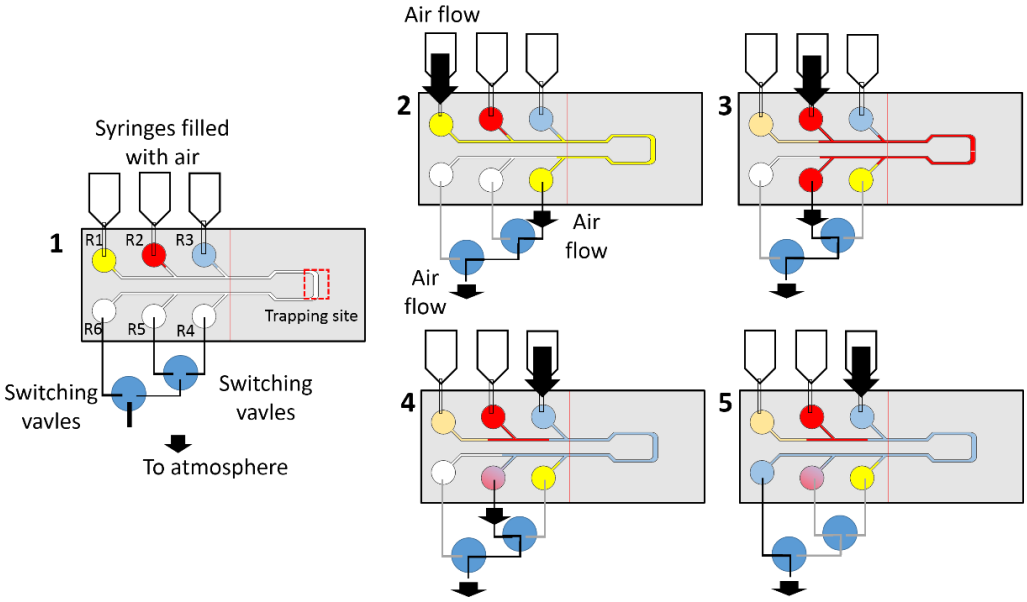

Figure 4-20: Valving operation and flow control procedure of the trapping and elution process.

Figure 4-21 shows the result of the demo fluidic manipulation, yellow dye, red dye and H_2O are used representing bead test solution, sample solution and wash/elution buffer, respectively. It is obvious that each solution goes into its designated target reservoir with only minor carry-over of undesired solutions, which verified that the new manifold and microdevice design is successful in airtightness and flow switching.

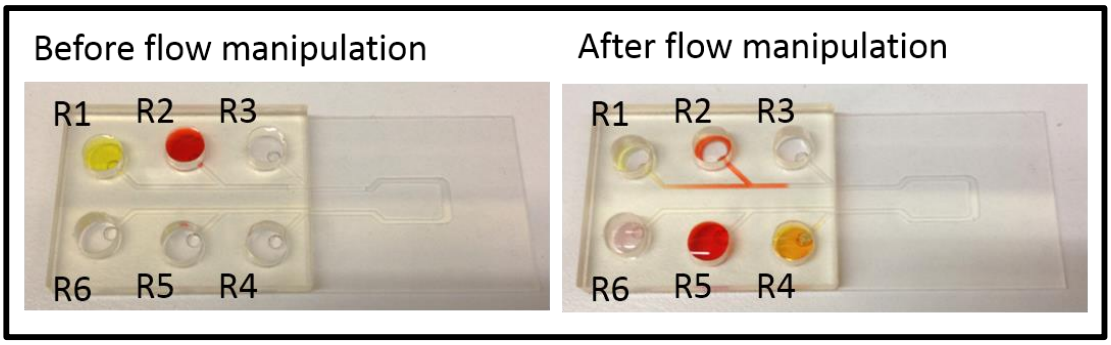

Figure 4-21: The solutions in the AGSiG chip before and after the flow test

4.4 Summary

In summary, we developed a GPG microdevice for the acoustic differential extraction of sperm cells from female DNA. Processing throughput is increased by 30 folds to 30 μL/min compared with our previous systems in 2009[21], and the trapping efficiency of highly dilute sample (~1 cell per microliter) was increased by nearly 5 folds using bead-assisted acoustic trapping. By using a laser-fabricated, integrated GPG microdevice and bead-assisted trapping strategy sperm cells are successfully separated and collected from female DNA even at the concentration as low as 10 cells/μL. A complete and cleaned STR profile of the male DNA is obtained, proving the success of the efficient recovery of the purified sperm cells from female DNA by microchip ADE, and the addition of the polymeric assisting beads is compatible with STR-PCR. Further development of the

ADE system into a commercial product is moving forward, and some preliminary progresses have been made including (1) the EA1 based liquid phase extraction of sperm DNA. (2) The re-designed manifold for better resonator-PZT coupling and smart phone camera-monitored trapping; (3) the redesigned, fully laser-fabricated disposable PMMA-glass-PDMS (AGSiG) microdevice and non-contact, contamination-free fluidic control. These initial tests of the newly developed system have been successful and will be a promising avenue toward expedited and lower cost processing of sexual assault forensic evidence in the future.

4.5 Acknowledgements

The author would like to thank Prof. Thomas. Laurell *(Department of Biomedical Engineering, Lund Universit)* for the resources and discussion provided by him and his research group on the basis of acoustic trapping.

The author would like to thank Dr. Brian L. Poe for the design and fabrication of the PZT transducers used in this Chapter.

The author would like to thank Dr. Orion N. Scott for the software control of the smartphone camera in section 4.3.7

4.6 References

[1] P. Gill, A. Jeffreys, and D. Werrett, “Forensic Application of DNA Fingerprints,” *Nature*, vol. 318, no. 6046, pp. 577–579, 1985.

[2] C. Comey, B. Koons, K. Presley, J. Smerick, C. Sobieralski, D. Stanley, and F. Baechtel, “Dna extraction strategies for amplified fragment length polymorphism analysis,” *J. Forensic Sci.*, vol. 39, no. 5, pp. 1254–1269, 1994.

[3] M. Iwasaki, S. Kubo, M. Ogata, and I. Nakasono, “A demonstration of spermatozoa on vaginal swabs after complete destruction of the vaginal cell deposits.,” *J. Forensic Sci.*, vol. 34, no. 3, pp. 659–664, 1989.

[4] P. Wiegand, M. Schurenkamp, and U. Schutte, “DNA extraction from mixtures of body fluid using mild preferential lysis,” *Int. J. Legal Med.*, vol. 104, no. 6, pp. 359–360, Nov. 1992.

[5] N. Lovich, GaffneyM., T. Pratt, C. Johnson, S. Lane, C. Asplen, L. Hurst, and T. Schellberg, “, 2004.,” *Atty. Gen. Rep. DNA Evid. Backlog*, 2004.

[6] L. Zhu, Q. Zhang, H. Feng, S. Ang, F. Chau, and W. Liu, “Filter-based microfluidic device as a platform for immunofluorescent assay of microbial cells,” *Lab Chip*, vol. 4, no. 4, pp. 337–341, 2004.

[7] S. K. Murthy, P. Sethu, G. Vunjak-Novakovic, M. Toner, and M. Radisic, “Size-based microfluidic enrichment of neonatal rat cardiac cell populations.,” *Biomed. Microdevices*, vol. 8, no. 3, pp. 231–7, Sep. 2006.

[8] R. Shaler, J. Chen, L. Kobilinsky, and D. Wolosin, “A physical method for separating spermatozoa from epithelial cells in sexual assault evidence A Physical Method for Separating Spermatozoa from Epithelial Cells in Sexual Assault Evidence,” *J. Forensic Sci.*, vol. 43, no. 1, pp. 114–118, 2015.

[9] J. V Green, M. Radisic, and S. K. Murthy, “Deterministic lateral displacement as a means to enrich large cells for tissue engineering.,” *Anal. Chem.*, vol. 81, no. 21, pp. 9178–82, Nov. 2009.

[10] M. Yamada, M. Nakashima, and M. Seki, “Pinched flow fractionation: Continuous size separation of particles utilizing a laminar flow profile in a pinched microchannel,” *Anal. Chem.*, vol. 76, no. 18, pp. 5465–5471, 2004.

[11] M. Yamada and M. Seki, “Hydrodynamic filtration for on-chip particle concentration and classification utilizing microfluidics.,” *Lab Chip*, vol. 5, no. 11, pp. 1233–9, Nov. 2005.

[12] A. J. Mach, J. H. Kim, A. Arshi, S. C. Hur, and D. Di Carlo, “Automated cellular sample preparation using a Centrifuge-on-a-Chip.,” *Lab Chip*, vol. 11, no. 17, pp. 2827–34, Sep. 2011.

[13] J. Sun, M. Li, C. Liu, Y. Zhang, D. Liu, W. Liu, G. Hu, and X. Jiang, “Double spiral microchannel for label-free tumor cell separation and enrichment.,” *Lab Chip*, vol. 12, no. 20, pp. 3952–60, Oct. 2012.

[14] H. Shafiee, J. L. Caldwell, and R. V. Davalos, “A Microfluidic System for Biological Particle Enrichment Using Contactless Dielectrophoresis,” *J. Assoc. Lab. Autom.*, vol. 15, no. 3, pp. 224–232, Jun. 2010.

[15] R. Pethig and Y. Huang, “Positive and negative dielectrophoretic collection of colloidal particles using interdigitated castellated microelectrodes,” *J. Phys. D. Appl. Phys.*, vol. 25, no. 5, pp. 881–888, 1992.

[16] R. Pethig, “Review article-dielectrophoresis: status of the theory, technology, and applications.,” *Biomicrofluidics*, vol. 4, no. 2, Jan. 2010.

[17] T. Laurell and J. Nilsson, “Cell and Particle Separation and Manipulation Using Acoustic Standing Waves in Microfluidic Systems,” in *Handbook of Capillary and Microchip Electrophoresis and Associated Microtechniques*, 3rd ed., J. P. Landers, Ed. Boca Raton, FL, USA: CRC Press, Inc., 2008, p. 1229.

[18] M. S. Limaye, J. J. Hawkes, and W. T. Coakley, “Ultrasonic standing wave removal of microorganisms from suspension in small batch systems,” *J. Microbiol. Methods*, vol. 27, no. 2–3, pp. 211–220, 1996.

[19] C. M. Cousins, P. Holownia, J. J. Hawkes, M. S. Limaye, C. P. Price, P. J. Keay, and W. T. Coakley, “Plasma preparation from whole blood using ultrasound,” *Ultrasound Med. Biol.*, vol. 26, no. 5, pp. 881–888, 2000.

[20] M. Evander, L. Johansson, T. Lilliehorn, J. Piskur, M. Lindvall, S. Johansson, M. Almqvist, T. Laurell, and J. Nilsson, “Noninvasive acoustic cell trapping in a microfluidic perfusion system for online bioassays.,” *Anal. Chem.*, vol. 79, no. 7, pp. 2984–91, Apr. 2007.

[21] J. V. Norris, M. Evander, K. M. Horsman-Hall, J. Nilsson, T. Laurell, and J. P. Landers, “Acoustic differential extraction for forensic analysis of sexual assault evidence.,” *Anal. Chem.*, vol. 81, no. 15, pp. 6089–95, Aug. 2009.

[22] B. Hammarström, T. Laurell, and J. Nilsson, “Seed particle-enabled acoustic trapping of bacteria and nanoparticles in continuous flow systems.,” *Lab Chip*, vol. 12, no. 21, pp. 4296–304, Oct. 2012.

[23] J. Hultström, O. Manneberg, K. Dopf, H. M. Hertz, H. Brismar, and M. Wiklund, “Proliferation and viability of adherent cells manipulated by standing-wave ultrasound in a microfluidic chip,” *Ultrasound Med. Biol.*, vol. 33, no. 1, pp. 145–151, 2007.

[24] N. Bilaniuk, “Speed of sound in pure water as a function of temperature,” *J. Acoust. Soc. Am.*, vol. 93, no. 3, p. 1609, 1993.

[25] S. M. Woodside, B. D. Bowen, and J. M. Piret, “Measurement of Ultrasonic Forces for Particle-Liquid Separations,” *AIChE J.*, vol. 43, no. July, 1997.

[26] K. A. Hagan, W. L. Meier, J. P. Ferrance, and J. P. Landers, “Chitosan-coated silica as a solid phase for RNA purification in a microfluidic device.,” *Anal. Chem.*, vol. 81, no. 13, pp. 5249–56, Jul. 2009.

[27] L. A. Legendre, J. M. Bienvenue, M. G. Roper, J. P. Ferrance, and J. P. Landers, “A simple, valveless microfluidic sample preparation device for extraction and amplification of DNA from nanoliter-volume samples.,” *Anal. Chem.*, vol. 78, no. 5, pp. 1444–51, Mar. 2006.

[28] D. Moss, S. A. Harbison, and D. J. Saul, “An easily automated, closed-tube forensic DNA extraction procedure using a thermostable proteinase,” *Int. J. Legal Med.*, vol. 117, no. 6, pp. 340–349, 2003.

[29] J. A. Lounsbury, N. Coult, D. C. Miranian, S. M. Cronk, D. M. Haverstick, P. Kinnon, D. J. Saul, and J. P. Landers, “An enzyme-based DNA preparation method for application to forensic biological samples and degraded stains.,” *Forensic Sci. Int. Genet.*, vol. 6, no. 5, pp. 607–15, Sep. 2012.

Chapter 5. Self-partitioned Droplet Array on Laser-patterned Superhydrophilic Glass Surface for Wall-less, Cell-array-based Bioassay Development

5.1 Overview and Introduction

One of the most significant advances brought about by the evolution of Micro-Total Analysis Systems (μTAS) is miniaturizing the size of assays to the micro- and nano-liter scale, thus enabling thousands or even millions of chemical/biological assays that are separately controlled but simultaneously interrogatable in a single experiment. This has led to the increased analytical throughput and data acquisition in various fields of study, including single-cell phenotyping[1]–[3] and genotyping[4]–[7], drug screening[8]–[11] and cell transfection studies[12]–[15]. Microdevices for high-throughput bioassays require arrays of spatially-resolved experimental sites, often created by inkjet printing[16]–[18], soft lithography[19], subdivision in micro-chamber/wells[20][21] or self-patterning[22].

Among these methods, inkjet printing is the fastest, most automated approach for generating microarrays with a range of desired chemical concentrations. However, in order to be printed by the inkjet properly, the solution's surface tension and viscosity need to be adjusted by adding additive reagent prior to the printing. The surfactant based additive reagent might affect some of the biomacromolecule's activity[23]. Besides, another concern is the risk of damage of the biomacromolecule by the shear forces when jet though

the nozzle[24]. On the other hand, soft lithography has been proved capable of making large scale of chamber or well array[25] which allow for the creation of integrated microfluidic circuit arrays for high-throughput bioassays [20] or micro well array based single cell analysis[26]. However, the molding and curing of stamp structures is rather time-consuming and labor-intensive[27].

As an emerging arraying technique, surface tension-based self-patterning of liquid solutions has drawn increasing attention, primarily due to its simple, power-free and equipment-independent nature[22][28]. In an array where superhydrophilic patches are patterned on a hydrophobic background, free-moving liquid (usually aqueous solutions) is retained in superhydrophilic regions and repulsed by the surrounding hydrophobic regions, which results the rapid self-partitioning of solution into an array of droplets defined by the array pattern of superhydrophilic patches. Numerous methods on the fabrication of the superhydrophlic-hydrophobic patterns have been reported, and these methods can be categorized into two types: (1) differential surface treatment (UV, plasma, chemical deposition etc.) on a mask-mounted or molded substrate where the patterns are laid on the substrate by the features of the physical mask [7][29]–[33] or (2) direct printing of superhydrophlic substances onto a hydrophobic substrate[34]–[37]. The mask or mold based patterning procedure requires additional cost and operations in the fabrication and alignment of the mask or mold and the fast change of the desired pattern in prototyping stage becomes rather inconvenient. On the other hand, most of the direct patterning approaches require multiple layers of deposition of chemicals and their corresponding treatments. Both types of methods are associated with challenges in the promotion of the microarray-based applications due to insufficient flexibility and considerable complexity.

In this work, we present a simple, mask-less approach for the fabrication of superhydrophilic-hydrophobic patterns using CO_2 laser. CO_2 laser patterned hydrophilic spots array against a hydrophobic background has been previously reported but on the surface of wax paper where the surface of paper substrate is exposed after removal of the wax coating[38]. However in that work an additional step of surface treatment of the exposed paper after laser cleaning is required, in which the silica particles are deposited on the exposed paper surfaces to increase their hydrophilicity so that the exposed spots array can trap liquid droplets.

In our work, by exploiting the ability of CO_2 lasers to 'clean' the glass surfaces and facilitate the removal of organic contaminants [39], we demonstrate their effectiveness in directly removing the hydrophobic coatings on a pre-dip-coated glass surface. Since the surface of glass, or silica, is already exposed by laser treatment, no post-laser surface modification is needed anymore and the cleaned surface of the glass already becomes superhydrophilic. If the glass is cleaned in a pattern of array, the sharp contrast of the wettability between the superhydrophilic laser-cleaned glass surface and untreated hydrophobic areas will enable the self-partitioning of aqueous liquid into an array of droplets. Besides, compared with paper substrate, another distinct advantage of the glass substrate is that it is transparent, which allows fluorescent detection and measurement even if the droplet arrays are sandwiched between two surfaces. This advantage opened the door for long term cell culturing in droplet array since the evaporation of the droplet needs to be minimized by this sandwiched structure. We illustrate the utility of this rapid self-patterning system with an array-based mapping of the culturing conditions for GFP expression in bacteria cells.

5.2 Materials and methods

Unless otherwise indicated, all chemicals are purchased from Sigma-Aldrich (Oakville, ON)

5.2.1 Preparation of hydrophobic glass surface

Commercial borosilicate cover glass (Fisher Scientific, Pittsburgh, PA) was briefly cleaned by nitrogen purging and then dip-coated in Sigmacote® and air dried in the hood. The coated glass was stored in a desiccator for future use.

5.2.2 Laser cleaning of glass

The pattern to be cleaned out was designed in a commercial graphic designing software, CorelDRAW 10.0 (Corel Corporation, Ottawa, Canada), and then printed by VersaLaser VLS 3.50 with 50W CO_2 laser source (Universal Laser System Inc.) on the coated glass surfaces. The laser was in raster mode with power level at 5.5%, speed level at 16% and image density level at 6. The cleaned glass surface was briefly purged by nitrogen flow and ready to be used.

5.2.3 Contact angle measurement

The contact angles of the Sigmacote® coated glass surface before and after cleaning were taken by a Canon EOS Rebel T1i camera (Canon Inc., Tokyo, Japan) and analyzed in ImageJ. For the comparison of the recovery of the surface wettability, the piranha-cleaned, plasma-cleaned and laser cleaned glass surfaces are stored in a covered petri-dish

and the contact angle on each surface is measured at the time point of the 0, 1, 2, 4, and 7th days after cleaning.

Preparation of piranha cleaned glass surface: hydrophobic cover glass prepared in section 5.2.1 was treated by piranha solution [30% H_2O_2 (Avanter Performance Materials, Center Valley, PA) and 98% sulfuric acid (Fisher Scientific, Pittsburgh, PA)] that was freshly mixed upon use in volume ratio of 3:7 for 30 min to remove any possible coating or contaminations. After thorough wash of di-H2O the glass cover was air dried in the hood and stored in a desiccator.

Preparation of plasma cleaned glass surface: hydrophobic cover glass prepared in section 5.2.1 was treated by air plasma for 60 sec and stored in a desiccator.

For the study of the preservation of the superhydrophilicity, the laser cleaned glass surface was stored in a sealed petri-dish (Fisher Scientific, Pittsburgh, PA) with soaked cotton to create a saturated humidity under room temperature. The glass was taken out at the 0, 1, 2, 4, 7, 14 and 28th day after the laser cleaning for the measurement of the contact angles. Laser cleaned glass surface stored in a covered dry petri-dish was also taken out at the 0, 1, 2, 4, 7, 14 and 28th day after the laser cleaning for the measurement of the contact angles as a control.

5.2.4 Examination of the surface structures

The coated glass and laser-cleaned glass was examined by the Environmental Scanning Electron Microscope (ESEM) to reveal their surface structures. Images were obtained by FEI Quanta 650 Scanning Electron Microscope (FEI Company, Hillsboro, OR)

5.2.5 Determination of the volume of the droplets

The volumes of the droplets were determined by the self-partitioning of a solution of 6 μm yellow-green fluorescent beads (Spherotech, Lake Forest, IL) with a known concentration. The beads in each self-patterned droplet was counted under Axio Scope.A1 fluorescence microscope (ZEISS, Jena, Germany) and the volume of the droplet was back-calculated using the beads concentration and the counted number in each droplet.

5.2.6 Design of the cell array and cell culture

E. coli HCB1 (wildtype) [40]were genetically tagged with green fluorescent protein (pGLO bacterial transformation kit, Bio-Rad, Hercules, CA). Culturing medium was prepared by adding 0.50 g tryptone (Bacto™, BD, Franklin Lakes, New Jersey), 0.25 g NaCl (Fisher Scientific, Pittsburgh, PA) into 50 mL diH_2O followed by autoclaving. The frozen stock of GFP-encoded *E. coli* HCB1 was thawed at room temperature and a 100 μL aliquot of the stock added into the 50 mL of medium and suspended by vortexing. 10 μL of 100 mg/mL ampicillin and 1 mL of 100 mg/mL L-(+)-arabinose were added into HCB1's growth medium to provide selective pressure for plasmid-containing, fluorescing bacteria.

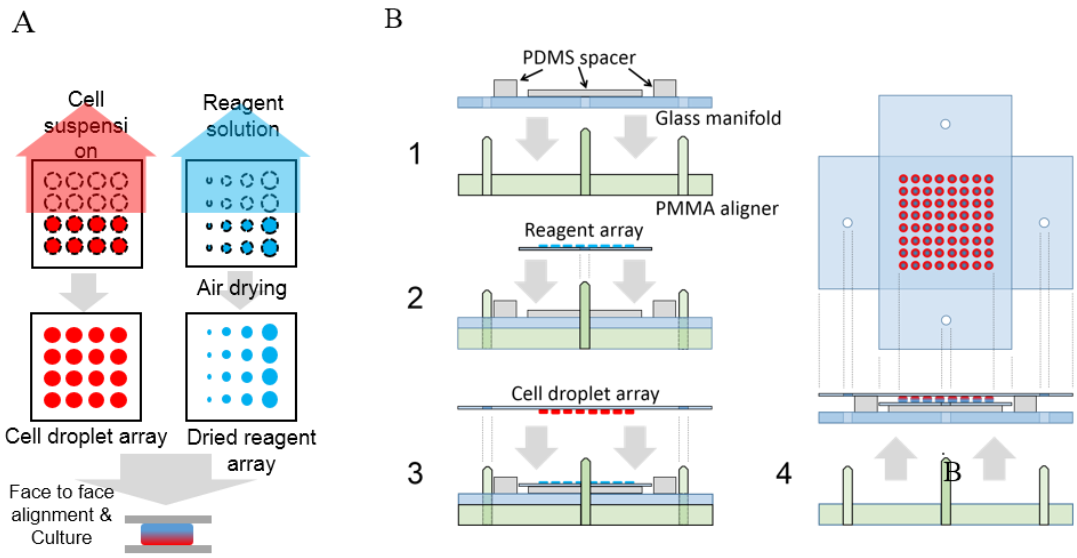

Figure 5-1. Assembly of dip-chip cell droplet array. (A) The conceptual illustration of the creation of cell array under various reagent concentrations. (B) The stepwise assembling of cell array facilitated with the manifold and aligner. (1) A glass manifold with PDMS spacer is inserted onto the PMMA aligner; (2) insert the dried reagent array onto the aligner facing up; (3) insert the cell droplet array onto the aligner facing the reagent array; (4) the glass covers are reversible bonded with the PDMS and the two-array assembly can be lift off from the aligner and ready for cell culture.

In the construction of the cell array an in-house constructed glass-PDMS manifold and PMMA aligner was used to facilitate the alignment of the arrays (**Figure 5-1**). Briefly, one surface of glass was prepared by CO_2 laser to form an array with different spot sizes of 0.24, 0.48, 0.72, 0.96 and 1.2 mm in diameters, and total of 96 (12 by 8) spots were arrayed in a 12 by 18mm area. 1mL of the solution of L-(+)-arabinose is added over the array, and then the excessive solution is absorbed away by a folded Kimwipe™ tissue wiper (Kimberly-Clark, Dallas, TX). The L-(+)-arabinose sampled array (reagent array) is dried and attached to the manifold by the reversible bonding between the back of the cover glass and the PDMS spacer.

The bacterial suspension is patterned into an array of droplet on another surface of glass using the same procedure described above, except that the sizes of the spots are uniform with a diameter of 1.2mm. The cell-suspension sampled array was immediately combined face-to-face with the reagent array. The double-layered manifold-cover glass assembly was put in a sealed petri-dish with soaked cotton and cultured overnight in 30 ℃. The array was then examined under Axio Scope.A1 fluorescence microscope (ZEISS, Jena, Germany) and the images were taken by a CCD camera. The RFU of the droplet array was measured using ImageJ.

5.3 Results and Discussion

5.3.1 Superhydrophilic-hydrophobic patterning of glass

Converting the hydrophilic nature of a glass surface to one that is hydrophobic by 'coating' the exposed silanols is not a new concept. The functionalization of silanol groups with some form of organosilane was seminal to the creation of reverse phase chromatography in the 1970's[41]. It was also exploited to hydrophobically-coat the glass plates used for electrophoretic gel sequencing, a must to assure that, post-separation, the thin sequencing gels could be removed intact for processing. Sigmacote® was a common glass 'silanizing' reagent used for this purpose, and by simply 'dipping' the glass plate in this reagent, the hydrophilic glass surface was converted to one that was hydrophobic. This is illustrated in **Figure 5-2** with images of the treated and untreated surfaces for contact angle and by scanning electron micrographs (SEM). The untreated hydrophobic surface yields a contact angle >90° (Figure 5-2A), while the contact angle of the laser-treated

surface has been reduced to ~13° (Figure 5-2B). The increased wettability of the surface might be attributed to either the laser (i) simply cleaning the surface via decomposition and evaporation of hydrophobic polymer[39] or (ii) texturizing the glass surface in a manner that exposes more silanol groups [42][43]. The SEM images of the Sigmacote®-treated glass surface before and after the laser cleaning are shown in Figure 5-2C and D, respectively. It is clear that the surface of the glass is well cleaned by the laser treatment, and most of the features attributed to the coating have been removed, which implies that the increased wettability is due to the simple cleaning of the glass surface rather than creating textures. The power and the speed of the laser was carefully adjusted so that there was no detectable damage to the glass, e.g., cracking or peeling, the undesired effects that have been reported when applying a CO_2 laser to glass[44].

At power level of 5.5%, different levels of the scan speed are tested in order to investigate the relationship between laser energy and the cleaning effect. Increasing the speed of the raster of the laser beam will decrease the energy applied in unit area on the surface, thus weaker cleaning effect is resulted, reflected by the less-reduced contact angles after laser cleaning (Figure 5-3). At the power level of 5.5%, 16% is found to be lowest speed level that can be used in the laser cleaning beyond which the cracking or peeling rate of the surface will increase significantly.

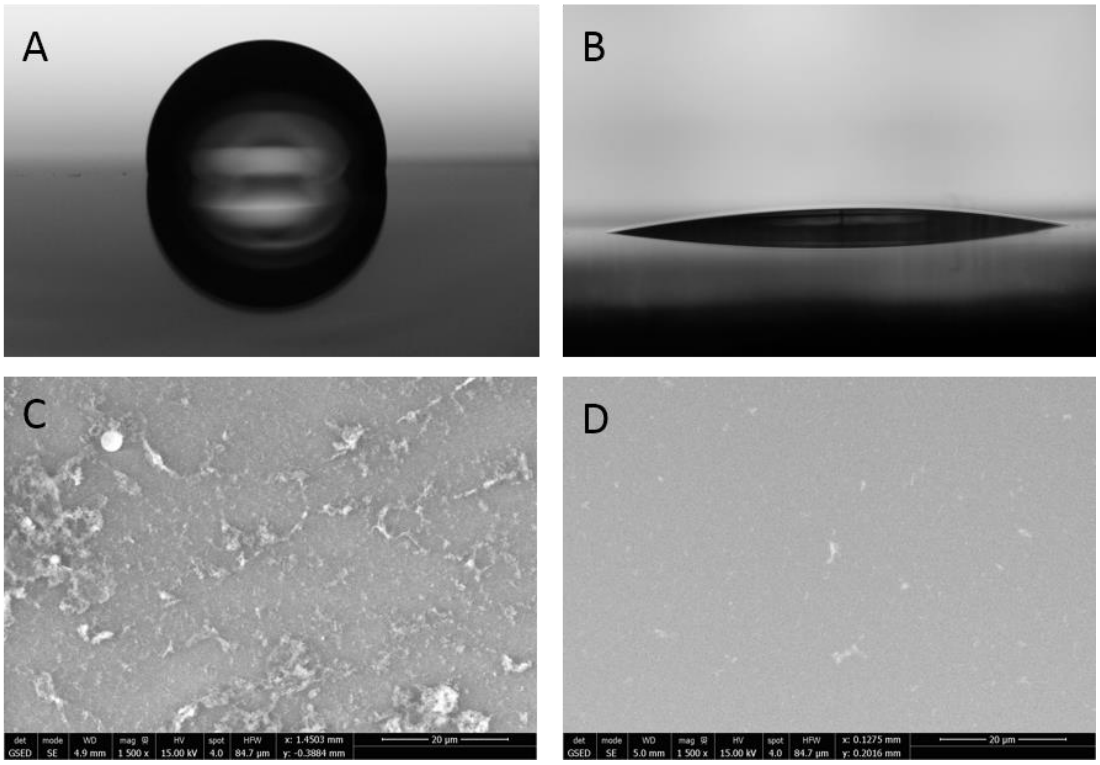

Figure 5-2. The wettability of coated glass surface before and after laser cleaning. The contact angle of a droplet of water on the surface of Sigmacote®-treated glass (A) before and (B) after laser ablation, together with the SEM images of their microstructures

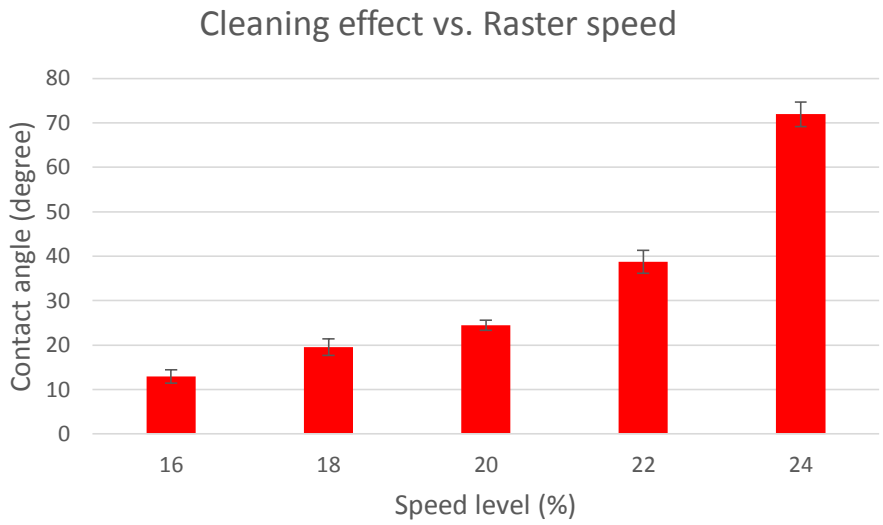

Figure 5-3. The contact angle after laser cleaning using different scanning speed

Takeda et al. demonstrated that the cleaned surface of glass will lose its hydrophilicity in open air as a result of the re-adsorption of atmosphereric contaminants[45]. We compared the laser-cleaned glass surface with two of the most commonly used glass-cleaning methods – plasma oxidation and treatment by 'piranha' solution. The change of the contact angles after the treatment of these three cleaning methods over time was plotted in Figure 5-4A. In comparison with the commonly used methods, cleaning with CO_2 laser is slightly less effective than plasma oxidation (implied by the higher initial contact angle), which may be explained by incomplete dissociation of coating residue from the ablated surface.

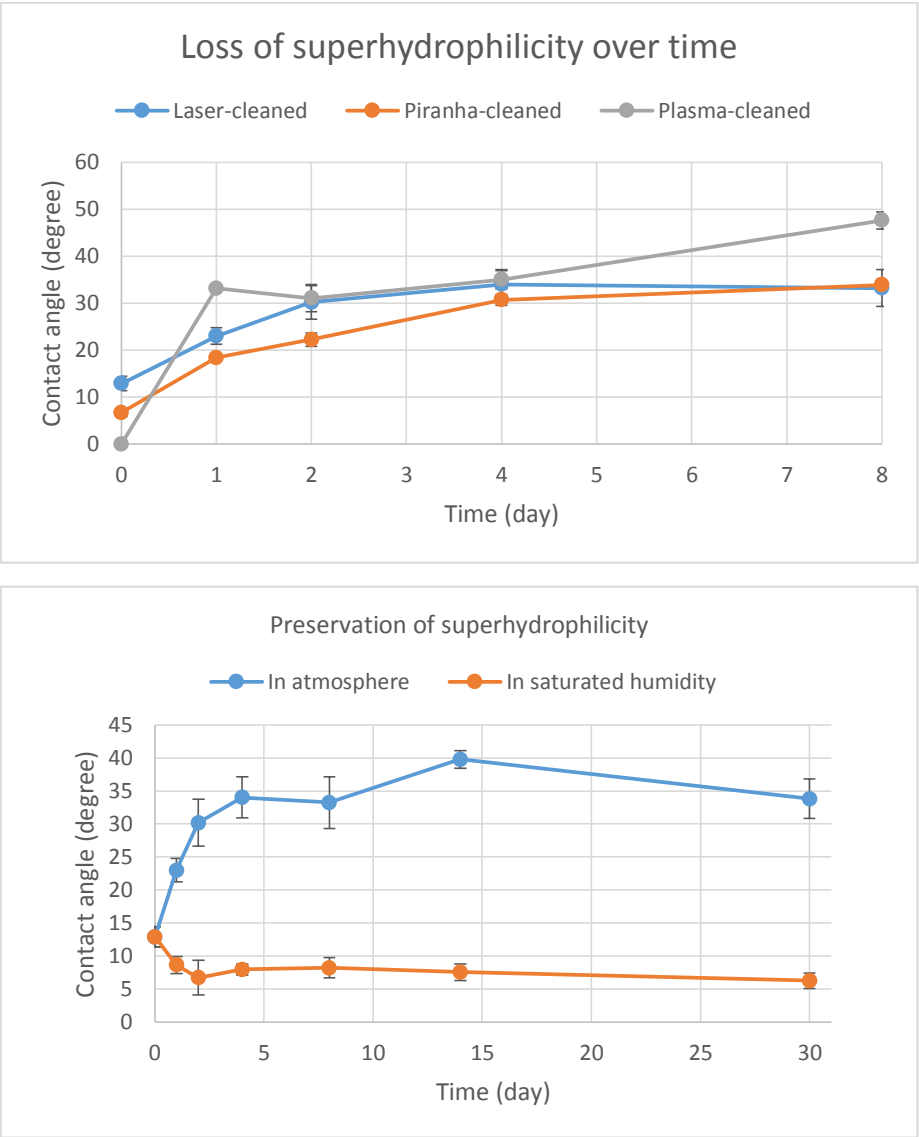

Figure 5-4. The loss and preservation of the superhydrophilicity of the laser-cleaned glass surface. (A) Comparison of the recovery of the surface wettability by different cleaning methods(n=3). (B) The preservation of superhydrophilicity in saturated humidity in a month (n=3).

Patel et al. reported that the wettability of cleaned glass could be preserved in a high humidity environment [46]. Figure 5-4B shows that storage of the laser-cleaned surface under high humidity conditions allowed for the superhydrophilicity to be

maintained with a corresponding contact angle <13° for as long as a month; this result indicates that the recovery to a hydrophobic state at a rate slower that in dry air by almost an order of magnitude. The prolonged preservation of superhydrophilicity might be attributed to the adsorption of water molecules on the surface[47], thus affording some level of protection against the adsorption of atmospheric contaminants.

5.3.2 Self-partitioning of liquid into a droplet array

With laser treatment of the glass surface, arrays of superhydrophilic spots with the highest spatial resolution of 1000 spots per 2 cm^2 can be created in only a few minutes without the requirement for any subsequent treatment, and the size/spacing of the spots can be conveniently and quickly modified in a commercial graphic design software (CorelDRAW) and transferred onto glass by laser in several minutes. With the contrast in wettability of the cleaned regions relative to untreated Sigmacote®-coated areas, aqueous solution rapidly self-patterns into the superhydrophilic regions by either trapping down from the moving liquid or even by dipping the glass into the solution (Figure 5-5). A laser-patterned cover glass with resolution of 0.5mm per spot was dipped in dye solution and the resultant droplet array shown in **Figure 5-6**.

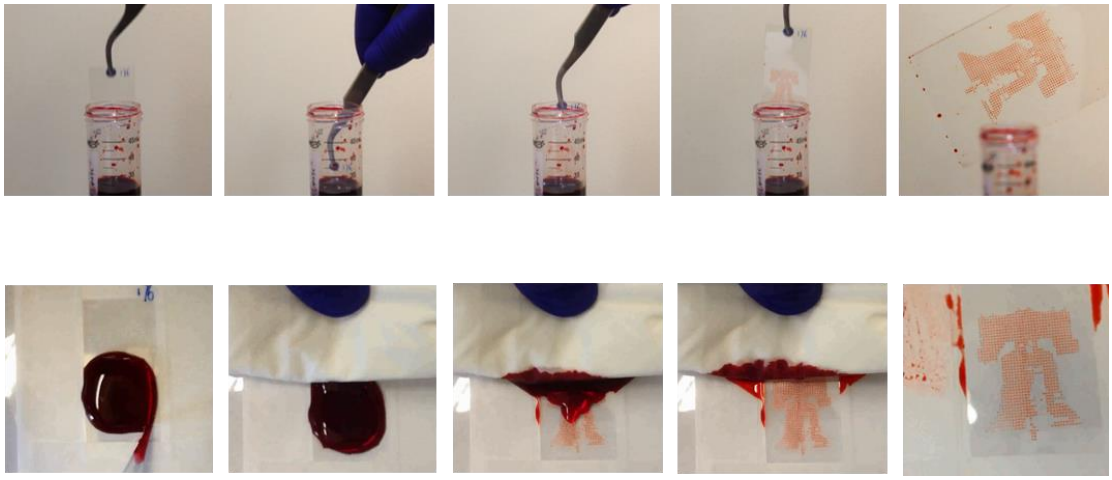

Figure 5-5. Two different methods for the patterning of droplets on the glass: (Top) dipping & pulling. (Bottom) placing a large droplet of the solution over the patterned array and absorbing away excess solution (bottom)

Figure 5-6. A pixelized pattern transferred via CO2 laser etching from a stamp onto a glass dipped in dye solution (32 mM Allura red in 1:1 glycerol-water solvent).

To measure the volumes of the droplets, a bead solution with a fixed concentration was patterned in the hydrophilic region, and the number of the beads counted to back-calculate the volume. The number of the beads in each droplet follows a Poisson distribution[31], as shown in Figure 5-7A. The mean volume is denoted by the

characteristic parameter of the Poisson distribution, λ, which was obtained by nonlinear curve fitting of the data.

Supposing each bead was encapsulated into each droplet with a consistent probability, and the event of the encapsulation of each of the beads are identical and independently distributed, then in each droplet the number of the encapsulated beads, *x*, follows Poisson distribution,

$$f_X(x) = \frac{\lambda^x}{x!} e^{-\lambda}$$

The mean and the variance of the sampling distribution of x are:

$$\mu = \lambda;\ \sigma^2 = \lambda.$$

The mean and the variance of the sampling distribution of the mean, $\bar{x}$:

$$\mu_m = \lambda;\ \sigma_m^2 = \frac{\lambda}{n},$$

where n is the number of replicates.

μ_m and σ_m^2 can be estimated by the sample mean $\bar{x}$ and the sample variance s^2, respectively. To reduce the relative standard deviation (RSD) of the mean of the volume measurement below 10%, the number of replicates, n, needs to be set accordingly based on the estimated mean of the measurement which satisfies:

$$\sqrt{\lambda n} > 10$$

For example the smallest droplet (d=0.3mm) has an average of about 1-2 beads per droplet so that at least 100 replicates are need to achieve RSD <10%. We used 760 droplets to estimate λ.

The volumes of the droplets are, therefore, determined and plotted versus diameter (Figure 5-7B). The volume (V, in nL) of the droplet is dependent on the diameter of the laser-cleaned spot (d, in mm) with a relationship of $V=32.9d^{2.44}$. However, if all droplets are assumed to have the same geometry (spherical crowns), the volume should be proportional to r^3. The difference between the ideal and experimentally-determined factor stems from a non-proportional increase in the droplet height as the base radius increases. The effect of gravity on the liquid-air interface of the droplet 'pulls down' as it becomes larger, so less liquid is retained.

A B

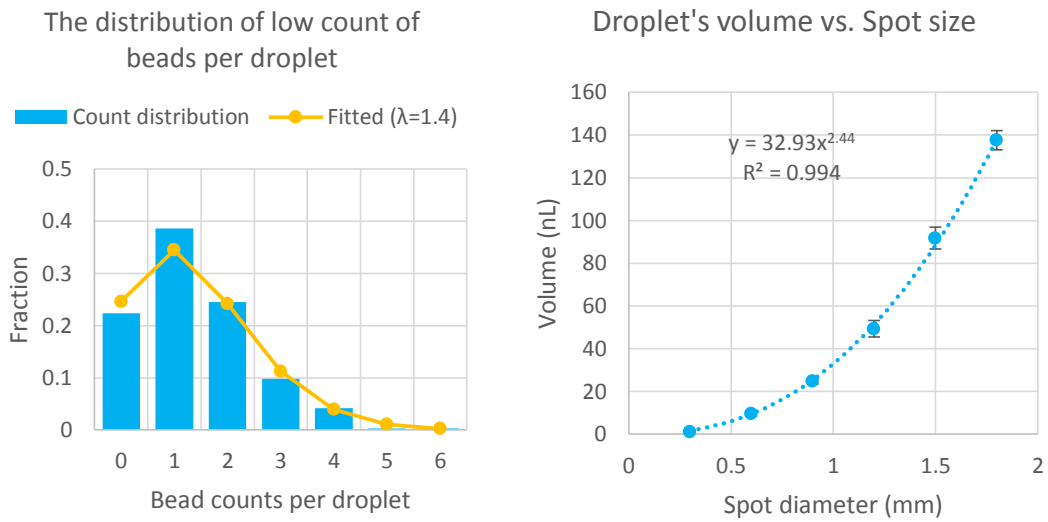

Figure 5-7. The volume of self-partitioned droplets. (A) The distribution of bead counts per droplet in an array of 760 droplets partitioned into 300 µm superhydrophilic spots. (B) The spot size determined volume of droplets (n>10).

5.3.3 Precise Alignment in of array plates

The volume-spot size relationship described earlier (Figure 5-7) suggests a simple and convenient method for sampling nanoliter-scale volumes of liquid reagent and, where reagent concentrations or other variables need to be evaluated, can be exploited for array-based high throughput bioassays. The basic procedure illustrated in **Figure 5-1** has two laser-cleaned pattern arrays dipped into different reagents/solutions for droplet loading with volumes specified by the hydrophilic spot sizes. One of the arrays is allowed to dry (e.g., the reagent array) prior to sandwiching, in a mirror image fashion, with an array surface containing droplets (e.g., cell suspension); this fuses the dried reagents to the droplets in a spatially-controlled manner. The reason for the reagent array being dried is

that it will not affect the total volume of the droplet after combining with the cell suspension droplet array. In order for this to be achieved accurately without droplet-to-droplet contamination, the inter-droplet spacing and glass-glass distance needed to be defined.

A

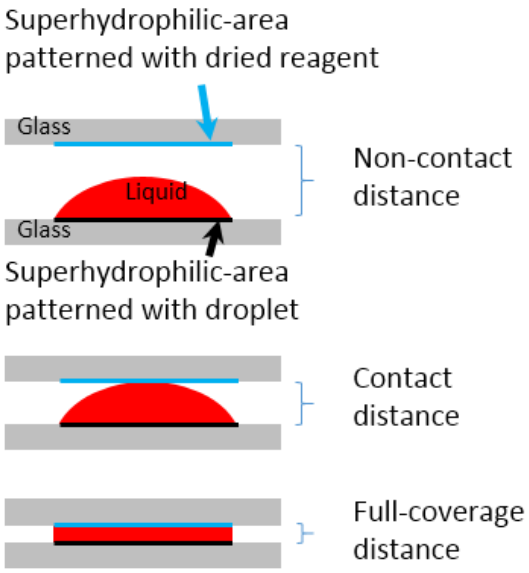

B

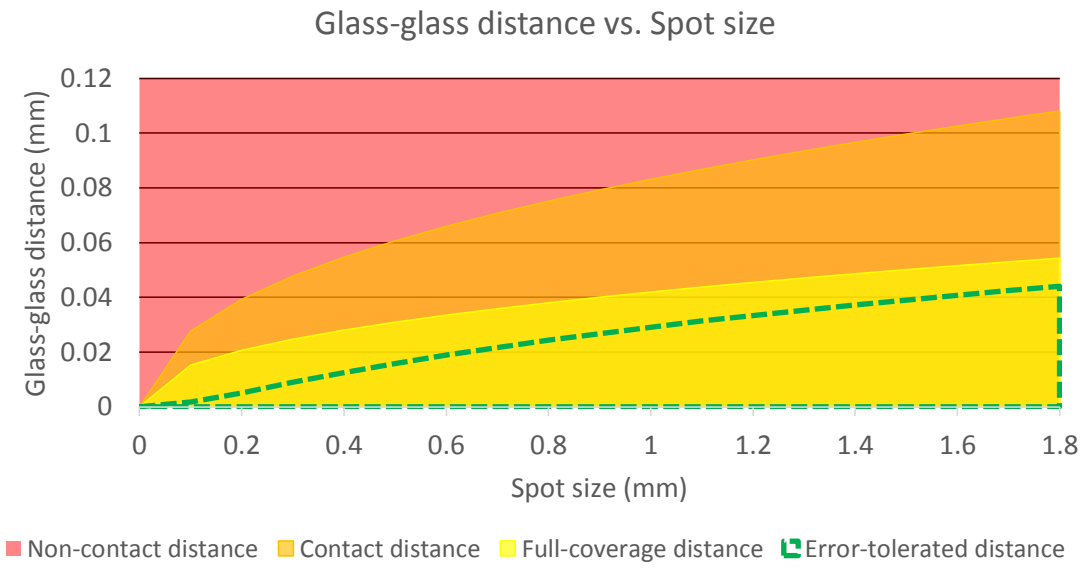

Figure 5-8. Precise alignment for spatial coupling of droplet/reagents between two laser-patterned surfaces. (A) The illustrative definition of non-contact distances, contact distance and full-coverage distance. (B) The relationship between glass-glass distance and spot diameters.

As illustrated in Figure 5-8, the glass-to-glass 'contact' distance is critical, as this determines when the droplets are in close enough proximity to have the top of a single droplet (cell suspension in this case) reach the surface loaded with reagent. Following droplet fusion, the glass-glass distance is narrowed to the point that the boundary of the sandwiched droplet is in intimate contact with the hydrophobic part of the surface. This ensures that the liquid-solid interfaces experience an inward surface tension – from a top view, this results in a regular round-shaped droplet. This distance, defined as the 'full-coverage' distance, is the point at which the liquid disk between the two surfaces of the glass fully covers the superhydrophilic area.

Based on the volume and the base area of the droplet (described in section 3.2), we calculated the minimum contact distance (the borderline between the red and the orange areas in Figure 5-8B) and the maximum full-coverage distance (the borderline between the orange and the yellow area in Figure 5-8B) at a given radius of the base area. The desired glass-glass distance and the diameter of spot size were then determined using Figure 5-8B and adjusted by the bonding to the manifold the PDMS film spacer with appropriate thickness.

Given a spot size, the maximum full-coverage distance can be conveniently found in Figure 5-8B by setting a vertical line from the given diameter d and the intersecting points with the yellow boundary will be the maximum full-coverage distance, h_{max}. However this value only gives the upper bound of the glass-glass distance and the optimized distance h_{opt} should be further determined at some value below the maximum distance.

In actual assembling of the cell droplet array, due to the accuracy of the assembling manifold we allow for a ±0.1mm tolerance of the alignment. So we need the liquid in a spot region with diameter *d* to be able to cover a spot region with diameter *d*+0.2mm. Therefore the optimized distance is:

$$h_{opt} = h_{max} \times \frac{d^2}{(d + 0.2mm)^2}$$

So if the given spot has *d*=1.2mm the optimized distance is:

$$h_{opt} = h_{max} \times \frac{1.2^2}{1.4^2} = 0.735 h_{max}$$

The h_{max} for d=1.2mm spot is founded to be 45 μm from Figure 5-8B so the h_{opt} is 33 μm.

5.3.4 Cell culture

As one of the most canonical model microbes in biology, *Escherichia coli* has been well studied, at least in part, because its genome could be manipulated robustly with current molecular biology and bioengineering techniques. A common approach for studying gene expression, is the introduction of the green fluorescent protein (GFP) reporter gene to the bacterial genome, with the expression level of GFP quantitatively regulated by L-(+)-arabinose.

To show proof of feasibility for the laser-patterned superhydrophilic arrays, we cultured a GFP reporter gene encoded *E. coli* strain (HCB1) [40] that uses L-(+)-arabinose

as the inducing reagent for the expression of the encoded gene. The L-(+)-arabinose concentration-dependent induction profile was reported in the expressing of the encoded gene[48]. The *E. coli* cells are cultured in the droplet arrays with varying concentrations of L-(+)-arabinose and the fluorescence intensity of GFP is used as indicator of the expression level. After overnight culture of the cell array in a sealed petri-dish there is no observable change in either the size or the shape of the droplets. The *E. coli* array cultured under different L-(+)-arabinose concentrations shows a gradient of fluorescence intensity (

Figure 5-9A and C), which confirms the L-(+)-arabinose-dependent expression of GFP. The trend of the expression level versus concentration (

Figure 5-9B) is consistent with reported data[48]–[50], showing a non-linear, exponential rising curve versus the logarithm of the arabinose concentration. The reason for this non-linear rising curve is the mechanism of the autocatalytic induction, in which the transporter of the inducing reagent is up-regulated by the inducing reagent itself. This feedback causes the accumulation of the inducing reagent in already induced cells and an all-or-none induction in each cell [43]. So the whole population of the *E. coli* contains two sub-population, the already induced and un-induced[49]. As the concentration of the arabinose increase, the fraction of the induced population increases making the fluorescence intensity of the droplet increase. The agreement between the results shown here and the reported response further validates this method as a potential tool for quantitative array-based bioassay.

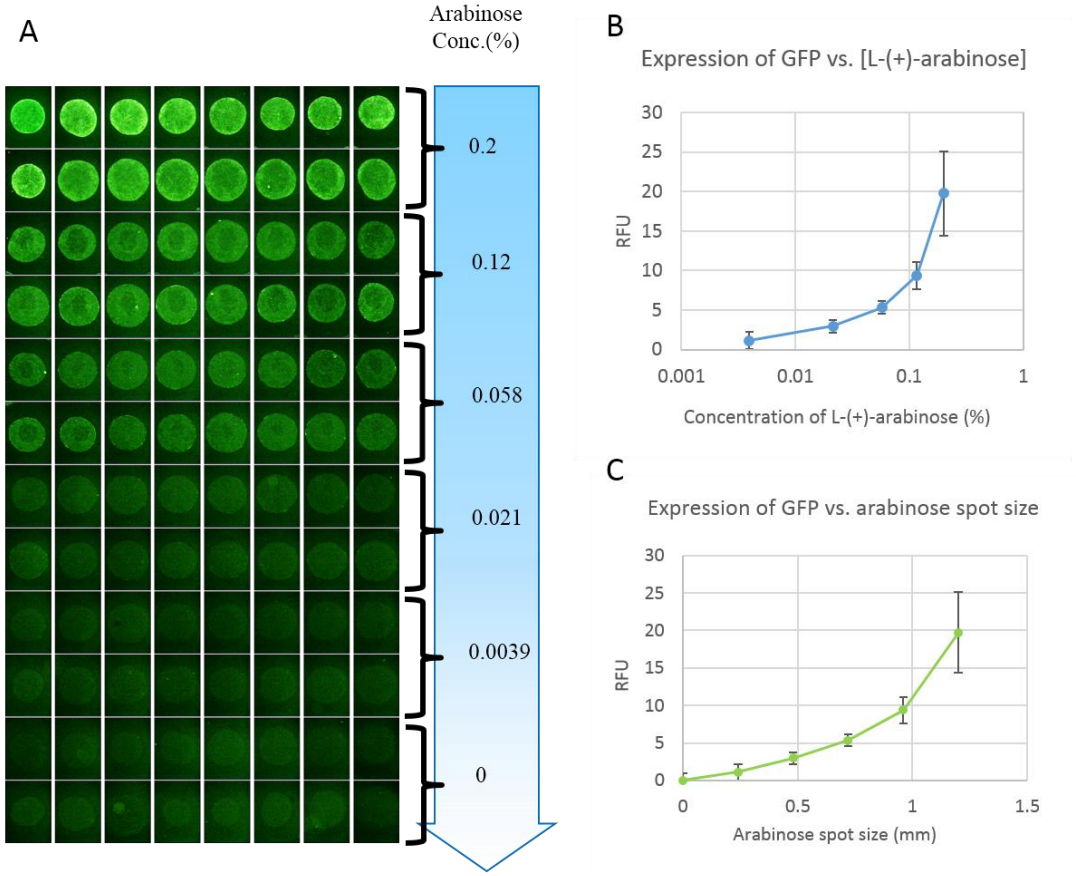

Figure 5-9 Array of E. coli cultured under different concentrations of L-(+)-arabinose. (A) The fluorescent images of a 12 by 8 array of E. coli at 6 different arabinose concentrations. (B) The relationship between the expression level of GFP (in RFU) and the concentrations of L-(+)-arabinose (n=16). (C) The expression level of GFP versus the spot size of arabinose droplet.

5.4 Summary

In summary, we developed a simple method for the fabrication of superhydrophilic-hydrophobic patterns on a coated glass surface using CO_2 laser patterning. The method requires only two simple steps: (1) dip-coating of glass into a silanization reagent (hydrophobic coating), and (2) direct writing of the desired pattern by laser ablation of the

hydrophobic coating, without any masking, lithography or molding procedures. The pre-coated cover glass in (1) can be conveniently prepared in large quantities and stored for future use upon request, so that the creation of the hydrophilic patterns actually only requires one single step of the laser cleaning in several minutes without any required post-treatment/fabrication, which is much shorter than all the previously reported hours-taking methods. The superhydrophilicity of the laser-ablated surface slowly reverts within a week, but this can be preserved by storage in a humidity-saturated environment. The volumes of the self-patterned droplets can be tuned by the size of the superhydrophilic pattern and, thus, provides a quantitative sampling technique with volumes ranging from couple of nanoliters to a few hundreds of nanoliters. Long-term stability of the droplet array with negligible evaporation in saturated humidity enables the culturing of cells while simultaneously exposing them to a variety of reagents, reagent concentrations or culturing conditions. The reported method demonstrates a fast, convenient and low-cost approach to construct spatially-resolved sub-colonies of cell cultures, which could provide a much more accessible and cost-effective array-based platform for bioassays.

5.5 Acknowledgements

The author would like to thank Prof. Roseanne. M. Ford *(Department of Chemical Engineering, University of Virginia)* for the resources provided by her research group.in the cell culture assay.

5.6 Reference

[1] D. Di Carlo, N. Aghdam, and L. P. Lee, "Single-cell enzyme concentrations, kinetics, and inhibition analysis using high-density hydrodynamic cell isolation arrays.," *Anal. Chem.*, vol. 78, no. 14, pp. 4925–30, Jul. 2006.

[2] R. Iino, K. Hayama, H. Amezawa, S. Sakakihara, S. H. Kim, Y. Matsumono, K. Nishino, A. Yamaguchi, and H. Noji, "A single-cell drug efflux assay in bacteria by using a directly accessible femtoliter droplet array.," *Lab Chip*, vol. 12, no. 20, pp. 3923–9, Oct. 2012.

[3] R. Iino, Y. Matsumoto, K. Nishino, A. Yamaguchi, and H. Noji, "Design of a large-scale femtoliter droplet array for single-cell analysis of drug-tolerant and drug-resistant bacteria.," *Front. Microbiol.*, vol. 4, no. October, p. 300, Jan. 2013.

[4] E. A. Ottesen, J. W. Hong, S. R. Quake, and J. R. Leadbetter, "Microfluidic digital PCR enables multigene analysis of individual environmental bacteria.," *Science.*, vol. 314, no. 5804, pp. 1464–7, Dec. 2006.

[5] X. Shi, L.-I. Lin, S. Chen, S.-H. Chao, W. Zhang, and D. R. Meldrum, "Real-time PCR of single bacterial cells on an array of adhering droplets.," *Lab Chip*, vol. 11, no. 13, pp. 2276–81, Jul. 2011.

[6] J. Wang, H. C. Fan, B. Behr, and S. R. Quake, "Genome-wide single-cell analysis of recombination activity and de novo mutation rates in human sperm.," *Cell*, vol. 150, no. 2, pp. 402–12, Jul. 2012.

[7] F. L. Geyer, E. Ueda, U. Liebel, N. Grau, and P. A. Levkin, "Superhydrophobic-superhydrophilic micropatterning: towards genome-on-a-chip cell microarrays.," *Angew. Chem. Int. Ed. Engl.*, vol. 50, no. 36, pp. 8424–7, Aug. 2011.

[8] D. A. Brafman, S. Chien, and K. Willert, "Arrayed cellular microenvironments for identifying culture and differentiation conditions for stem, primary and rare cell populations.," *Nat. Protoc.*, vol. 7, no. 4, pp. 703–17, Apr. 2012.

[9] G. Arrabito, C. Galati, S. Castellano, and B. Pignataro, "Luminometric sub-nanoliter droplet-to-droplet array (LUMDA) and its application to drug screening by phase I metabolism enzymes.," *Lab Chip*, vol. 13, no. 1, pp. 68–72, Jan. 2013.

[10] G. Du, J. Pan, S. Zhao, Y. Zhu, J. M. J. Den Toonder, and Q. Fang, "Cell-Based Drug Combination Screening with a Microfluidic Droplet Array System," *Anal. Chem.*, vol. 85, pp. 6740–6747, 2013.

[11] L. Mugherli, O. N. Burchak, L. a Balakireva, A. Thomas, F. Chatelain, and M. Y. Balakirev, "In situ assembly and screening of enzyme inhibitors with surface-

tension microarrays.," *Angew. Chem. Int. Ed. Engl.*, vol. 48, no. 41, pp. 7639–44, Jan. 2009.

[12] S. Baghdoyan, Y. Roupioz, A. Pitaval, D. Castel, E. Khomyakova, A. Papine, F. Soussaline, and X. Gidrol, "Quantitative analysis of highly parallel transfection in cell microarrays.," *Nucleic Acids Res.*, vol. 32, no. 9, p. e77, Jan. 2004.

[13] H. Erfle, B. Neumann, U. Liebel, P. Rogers, M. Held, T. Walter, J. Ellenberg, and R. Pepperkok, "Reverse transfection on cell arrays for high content screening microscopy.," *Nat. Protoc.*, vol. 2, no. 2, pp. 392–9, Jan. 2007.

[14] J. K. Rantala, R. Mäkelä, A.-R. Aaltola, P. Laasola, J.-P. Mpindi, M. Nees, P. Saviranta, and O. Kallioniemi, "A cell spot microarray method for production of high density siRNA transfection microarrays.," *BMC Genomics*, vol. 12, no. 1, p. 162, Jan. 2011.

[15] A. Roguev, D. Talbot, G. L. Negri, M. Shales, G. Cagney, S. Bandyopadhyay, B. Panning, and N. J. Krogan, "Quantitative genetic-interaction mapping in mammalian cells.," *Nat. Methods*, vol. 10, no. 5, pp. 432–7, May 2013.

[16] I. Barbulovic-Nad, M. Lucente, Y. Sun, M. Zhang, A. R. Wheeler, and M. Bussmann, "Bio-microarray fabrication techniques--a review.," *Crit. Rev. Biotechnol.*, vol. 26, no. 4, pp. 237–59, 2006.

[17] C. Hu, X. Bai, Y. Wang, W. Jin, X. Zhang, and S. Hu, "Inkjet printing of nanoporous gold electrode arrays on cellulose membranes for high-sensitive paper-like electrochemical oxygen sensors using ionic liquid electrolytes," *Anal. Chem.*, vol. 84, no. 8, pp. 3745–3750, 2012.

[18] G. C. Jensen, C. E. Krause, G. A. Sotzing, and J. F. Rusling, "Inkjet-printed gold nanoparticle electrochemical arrays on plastic. Application to immunodetection of a cancer biomarker protein.," *Phys. Chem. Chem. Phys.*, vol. 13, no. 11, pp. 4888–4894, 2011.

[19] R. S. Kane, S. Takayama, E. Ostuni, D. E. Ingber, and G. M. Whitesides, "Patterning proteins and cells using soft lithography.," *Biomaterials*, vol. 20, no. 23–24, pp. 2363–76, Dec. 1999.

[20] T. Thorsen, S. J. Maerkl, and S. R. Quake, "Microfluidic large-scale integration.," *Science.*, vol. 298, no. 5593, pp. 580–4, Oct. 2002.

[21] J. W. Hong and S. R. Quake, "Integrated nanoliter systems.," *Nat. Biotechnol.*, vol. 21, no. 10, pp. 1179–83, Oct. 2003.

[22] E. Ueda and P. A. Levkin, “Emerging applications of superhydrophilic-superhydrophobic micropatterns.,” *Adv. Mater.*, vol. 25, no. 9, pp. 1234–47, Mar. 2013.

[23] S. Di Risio and N. Yan, “Piezoelectric ink-jet printing of horseradish peroxidase: Effect of ink viscosity modifiers on activity,” *Macromol. Rapid Commun.*, vol. 28, no. 18–19, pp. 1934–1940, 2007.

[24] G. M. Nishioka, A. A. Markey, and C. K. Holloway, “Protein damage in drop-on-demand printers,” *J. Am. Chem. Soc.*, vol. 126, no. 50, pp. 16320–16321, 2004.

[25] J. M. K. Ng, A. D. Stroock, and G. M. Whitesides, “Review Components for integrated poly (dimethylsiloxane) microfluidic systems,” *Electrophoresis*, pp. 3461–3473, 2002.

[26] Y. Wang, P. Shah, C. Phillips, C. E. Sims, and N. L. Allbritton, “Trapping cells on a stretchable microwell array for single-cell analysis,” *Anal. Bioanal. Chem.*, vol. 402, no. 3, pp. 1065–1072, 2012.

[27] D. Qin, Y. Xia, and G. M. Whitesides, “Soft lithography for micro- and nanoscale patterning.,” *Nat. Protoc.*, vol. 5, no. 3, pp. 491–502, 2010.

[28] X. Yao, Y. Song, and L. Jiang, “Applications of bio-inspired special wettable surfaces.,” *Adv. Mater.*, vol. 23, no. 6, pp. 719–34, Feb. 2011.

[29] Y. Zhang and T.-H. Wang, “Full-Range Magnetic Manipulation of Droplets via Surface Energy Traps Enables Complex Bioassays.,” *Adv. Mater.*, pp. 2903–2908, Mar. 2013.

[30] X. Liu, Q. Wang, J. Qin, and B. Lin, “A facile ‘liquid-molding’ method to fabricate PDMS microdevices with 3-dimensional channel topography.,” *Lab Chip*, vol. 9, no. 9, pp. 1200–5, May 2009.

[31] L.-I. Lin, S.-H. Chao, and D. R. Meldrum, “Practical, microfabrication-free device for single-cell isolation.,” *PLoS One*, vol. 4, no. 8, p. e6710, Jan. 2009.

[32] A. I. Neto, C. A. Custódio, W. Song, and J. F. Mano, “High-throughput evaluation of interactions between biomaterials, proteins and cells using patterned superhydrophobic substrates,” *Soft Matter*, vol. 7, no. 9, p. 4147, 2011.

[33] B. Gumuscu, J. G. Bomer, A. van den Berg, and J. C. T. Eijkel, “Large scale patterning of hydrogel microarrays using capillary pinning,” *Lab Chip*, vol. 15, no. 3, pp. 664–667, 2015.

[34] Y. Lu, B. Lin, and J. Qin, “Patterned paper as a low-cost, flexible substrate for rapid prototyping of PDMS microdevices via ‘liquid molding’.,” *Anal. Chem.*, vol. 83, no. 5, pp. 1830–5, Mar. 2011.

[35] L. Zhang, H.-Y. Si, and H.-L. Zhang, “Highly ordered fluorescent rings by ‘breath figures’ on patterned substrates using polymer-free CdSe quantum dots,” *J. Mater. Chem.*, vol. 18, no. 23, p. 2660, 2008.

[36] J. S. Li, E. Ueda, A. Nallapaneni, L. X. Li, and P. A. Levkin, “Printable superhydrophilic-superhydrophobic micropatterns based on supported lipid layers.,” *Langmuir*, vol. 28, no. 22, pp. 8286–91, Jun. 2012.

[37] U. Manna, A. H. Broderick, and D. M. Lynn, “Chemical patterning and physical refinement of reactive superhydrophobic surfaces.,” *Adv. Mater.*, vol. 24, no. 31, pp. 4291–5, Aug. 2012.

[38] G. Chitnis, Z. Ding, C.-L. Chang, C. A. Savran, and B. Ziaie, “Laser-treated hydrophobic paper: an inexpensive microfluidic platform.,” *Lab Chip*, vol. 11, no. 6, pp. 1161–1165, 2011.

[39] Y. Ye, X. Yuan, X. Xiang, X. Cheng, and X. Miao, “Laser cleaning of particle and grease contaminations on the surface of optics,” *Opt. - Int. J. Light Electron Opt.*, vol. 123, no. 12, pp. 1056–1060, Jun. 2012.

[40] A. J. Wolfe, M. P. Conley, T. J. Kramer, and H. C. Bergt, “Reconstitution of Signaling in Bacterial Chemotaxis,” *J. Bacteriol.*, vol. 169, no. 5, pp. 1878–1885, 1987.

[41] I. Molnár and C. Horváth, “Reverse-phase chromatography of polar biological substances: separation of catechol compounds by high-performance liquid chromatography.,” *Clin. Chem.*, vol. 22, no. 9, pp. 1497–502, Sep. 1976.

[42] T. Chang, T. Tsai, H. Yang, and J. Huang, “Microelectronic Engineering Effect of ultra-fast laser texturing on surface wettability of microfluidic channels,” *Microelectron. Eng.*, vol. 98, pp. 684–688, 2012.

[43] J. Canning, H. Weil, and M. Naqshbandi, “Laser tailoring surface interactions, contact angles, drop topologies and the self-assembly of optical microwires,” *Opt. Mater. Express*, vol. 3, no. 2, pp. 4059–4063, 2013.

[44] Z. K. Wang and H. Y. Zheng, “Investigation on CO2 laser irradiation inducing glass strip peeling for microchannel formation.,” *Biomicrofluidics*, vol. 6, no. 1, pp. 12820–12831, Mar. 2012.

[45] S. Takeda, K. Yamamoto, Y. Hayasaka, and K. Matsumoto, “Surface OH group governing wettability of commercial glasses,” *J. Non. Cryst. Solids*, vol. 249, no. 1, pp. 41–46, Jul. 1999.

[46] P. Patel, C. K. Choi, and D. D. Meng, “Superhydrophilic Surfaces for Antifogging and Antifouling Microfluidic Devices,” *J. Assoc. Lab. Autom.*, vol. 15, no. 2, pp. 114–119, Apr. 2010.

[47] Y.-W. Chen and H.-P. Cheng, “Interaction between water and defective silica surfaces.,” *J. Chem. Phys.*, vol. 134, no. 11, p. 114703, Mar. 2011.

[48] L. M. Guzman, D. Belin, M. J. Carson, and J. Beckwith, “Tight Regulation , Modulation , and High-Level Expression by Vectors Containing the Arabinose P BAD Promoter,” *J. Bacteriol.*, vol. 177, no. 14, pp. 4121–4130, 1995.

[49] A. Khlebnikov, O. Risa, T. Skaug, T. A. Carrier, and J. D. Keasling, “Regulatable arabinose-inducible gene expression system with consistent control in all cells of a culture.,” *J. Bacteriol.*, vol. 182, no. 24, pp. 7029–34, Dec. 2000.

[50] D. A. Siegele and J. C. Hu, “Gene expression from plasmids containing the araBAD promoter at subsaturating inducer concentrations represents mixed populations.,” *Proc. Natl. Acad. Sci. U. S. A.*, vol. 94, no. 15, pp. 8168–8172, 1997.

[51] A. Novick and M. Weiner, “Enzyme induction as an all-or-none phenomenon,” *Proc. Natl. Acad. Sci. USA*, vol. 43, pp. 553–566, 1957.

Chapter 6. Conclusions and Future Directions

6.1 Concluding remarks

The microdevices and related techniques described in this dissertation demonstrated the versatility of laser-assisted fabrication in various applications. The laser fabrication techniques have enabled fast, inexpensive prototyping of microdevice due to its broad selection of materials and micromachining ability directly from design to reality, especially in the early stage of development when enormous details of the microdevice need to be tested.

Specifically, **Chapter 2** as a beginning chapter, has provided a low-cost and convenient scanner-based profiling technique that answered the questions about the quality of laser ablated microstructures. The reported technique provides a low-cost, non-contact profilometry method that is able to detect the profile of elastic surfaces and an already enclosed microstructures with resolution of 2 μm. The qualities of the laser ablated PDMS surface and laser-fabricated PeT chambers have been quantitatively determined.

Chapter 3 explored the power of laser ablation in the fabrication of layered PDMS structures that is used in microfluidic check valves, an essential part in almost all microfluidic devices that needs flow control. The laser-ablated fluidic diode (one-way check valve) shows comparable performance with those made by conventional soft-lithography but requires much less labor and time cost to fabricate. A finger driven metering and delivery (*MaD*) fluidic circuit has been developed and modularized into a structurally stackable unit. By multiplexing the *MaD* unit two different functions can be performed solely by finger pressing in two different designs of the microdevices:

(1)simultaneous metering and delivery of 4 reagents at desired ratio with a simple demonstrative application in the preparation of the STR-PCR mix; (2) microfluidic circuit that can perform serial dilution at arbitrary diluting ratios. Being highly portable and minimum demanding in equipment and operating skills without compromise to its accuracy, the finger driven microfluidic device provides a promising liquid handling platform in the field of point of care (PoC) diagnostics.

In **Chapter 4**, laser-fabricated glass-PDMS-glass (GPG) integrated microdevices show potentials in forensic applications by enabling acoustic trapping and separation of sperm cells with high trapping efficiency. The acoustic differential extraction (ADE) system automated the isolation, purification and collection of sperm cells from female lysate. With the assistance of polymeric beads sperm cells in dilute sample can be trapped with trapping efficiency as high as that in concentrated samples, and the STR-PCR result shows the complete and purified profile of male DNA which proved the success of the ADE system. The acoustic trapping technique not only provides a collection method for sperm cells but also the capability of cell retention in flowing medium, which enables the convenient continuous switching of solutions in multi-step treatment of the cells. Such capability is the foundation of the further integration of even more steps into the microdevice such as post-trapping lysis of the sperm cells and will further increase the automation level of the ADE process. The current ADE system is a promising platform that has many possibilities to be extended and developed into a product that can serve real forensic labs.

In **Chapter 5**, laser cleaned glass surface has shown superhydrophilic properties that allows fast partitioning of aqueous liquid into droplet array which enables high throughput

cell assays. The laser-cleaning process in producing the superhydrophilic surface outpaces other techniques in the saving of both time and labor. A demonstrative droplet array-based cell assay revealed the inducing effect of L-(+)-arabinose on the gene expression of bioengineered *E. coli*. The results obtained from the droplet array based cell assay is in agreement with previously reported findings through conventional methods, which proved the biocompatibility and capability of the self-partitioned droplet array in high throughput quantitative bioassay. The arraying glass, manifolds, and protocol developed in this work may be adapted for other biological systems and mapping tasks in the future.

Laser–assisted fabrication has opened a door to a more automated, less laborious and low-cost process in the development of microfluidic devices. In addition, as a fabrication method that is applicable to a wide range of disposable, polymeric materials, laser-assisted fabrication and manufacturing will play a significant role in the rising-up trend of the commercialization of lab-on-a-chip microdevices and more laser-fabricated products are expected to emerge in both academic and industrial field in the future.

6.2 Future work

Future work mainly includes:

(1) Extend the droplet array based bioassay to more biological problems and systems such as mammalian cells and develop the whole methods in to a more general tool for biological study.

(2) Further development of the ADE system into a portable prototype that can be used to deal with real sexual assault sample in real forensic labs.